

SPIN-ANYON DUALITY AND \mathbb{Z}_2 TOPOLOGICAL ORDER

Dissertation

zur Erlangung des akademischen Grades
Doctor of Philosophy (Ph. D.)

vorgelegt

der Fakultät Physik
Bereich Mathematik und Naturwissenschaften
der Technischen Universität Dresden

von

PENG RAO, M. Sc.

geboren am 03.07.1993 in Guangdong, China



MAX PLANCK INSTITUTE
FOR THE PHYSICS OF COMPLEX SYSTEMS

Max-Planck-Institut für Physik komplexer Systeme
Dresden, 2022

Wissenschaftlicher Betreuer:
Prof. Roderich Moessner und Prof. Inti Sodemann

Eingereicht am 06.09.2022

Gutachter:

1. Prof. Dr. Roderich Moessner
2. Prof. Dr. Inti Sodemann
3. Prof. Dr. Matthias Vojta

Abstract

In this thesis we consider the properties of a class of \mathbb{Z}_2 topological phases on a two-dimensional square lattice. The ground states of \mathbb{Z}_2 topological order are generally degenerate on a periodic lattice, characterized by certain global \mathbb{Z}_2 quantum numbers. This property is important for application in quantum computing as the global quantum numbers can be used as protected qubits. It is therefore instrumental to construct and study \mathbb{Z}_2 topological order from a general framework.

Our results in this thesis provide such a framework. It is based on the simplest and most illustrative \mathbb{Z}_2 topological order: the Toric Code, which contains static and non-interacting anyonic quasiparticles e , m and ε . Building on this interpretation, in the first part of the thesis two exact mappings are presented from the spin-1/2 Hilbert space to the Hilbert space of (e, m) and (e, ε) . The mappings are derived on infinite, open, cylindrical and periodic lattices respectively. Mutual anyonic statistics as well as the effect of the global \mathbb{Z}_2 quantum numbers are taken into account. Due to the mutual anyonic statistics of the elementary excitations, the mappings turn out to be highly non-local. In addition, it is shown that the (e, ε) -duality can be carried over directly to the honeycomb lattice, where e , ε are the π -vortices (visons) and Majorana fermions in the Kitaev honeycomb model.

The mappings allow one to rewrite any spin Hamiltonians as Hamiltonians of anyons. In the second part of the thesis, we construct a series of spin models which are mapped to Hamiltonians of free m and ε , and static e -particles. In particular, a series of \mathbb{Z}_2 topological phases ‘enriched by lattice translation symmetry’ are constructed which contain superconducting ε -fermions. Their properties can be analyzed generally using the (e, ε) -duality and then the theory of topological superconductivity. In particular, their ground state degeneracy on a periodic lattice may depend on lattice size. For these phases a $\mathbb{Z} \times (\mathbb{Z}_2)^3$ classification scheme is proposed, which generalizes classification by the integer Chern number C . Some of the conclusions are then verified directly by exact solutions on the spin lattice.

The emergent anyon statistics of e -particles in these phases is also analyzed by computing numerically the Berry phase of their motion on top of the superconducting vacua. For phases with $C = 0$ yet still topologically non-trivial, we discover examples of ‘weak symmetry breaking’: the e -lattice splits into two inequivalent sublattices which are exchanged by lattice translations. The e -particles on the two sublattices acquire mutual anyonic statistics. In topological phases with non-zero C , the mutual braiding of e is confirmed explicitly. In addition, the Berry phase due to background flux of each square unit cell is 0 or π depending on the underlying topology of the phases. This quantity is related to properties of the vison band in Kitaev materials.

Lastly, the $\mathbb{Z}_N (N > 2)$ extension of \mathbb{Z}_2 topological order is discussed. Constructing the duality to ‘parafermions’ in this case is much more complex. The difficulties of deriving such a mapping are pointed out and we only present exact solutions to certain Hamiltonians on the spin lattice.

Acknowledgement

I would like to, foremost, express my gratitude to my doctoral supervisor Prof. Inti Sodemann, who introduced me to several fascinating and diverse areas in condensed matter theory, for his academic guidance and support and for giving me the rare opportunity to work at the frontier of that field, and to Prof. Roderich Moessner for his considerate and generous leadership of the condensed matter division at MPI-PKS.

I am fortunate to have also worked with Dr. Francesco Piazza and Dr. Andres Schliefl on exciting topics in field theory. In particular, I am grateful for Francesco's patience and kindness in our daily interactions and during our collaboration. And I have benefited enormously from Andres' deep and vast scientific expertise as well as professional advice both during our brief collaboration and after. The numerous and candid advices by Panagiotis Giannakeas are also instrumental in helping me navigate the field. In addition, Aniket Patra, Margarita Davydova and Junkai Dong also share with me their resolute commitment to knowledge. With them I had many interesting and illuminating discussions on many diverse physics problems. These conversations constitute, professionally and scientifically, some of the happiest moments of my PhD. Their determination in pursuing understanding regardless of direct relevance to their own work helps me recover that early promise of happiness and truth in physics, which had drawn us in as students but is sometimes forgotten along the way.

Of course, my PhD would have been impossible without the support of my family and friends, as well as the obscure cult sitcom 'Community'. Due to the pandemic, I could not visit my family nearly as much as I hoped during my PhD. Thus the sacrifice behind this PhD is as much theirs as mine. My friends are too numerous to list here but I hold dear in my memory every moment I have spent with them. As I have only belatedly and gradually come to understand, it is an incredible fortune and luxury to have known such groups of people. I hope that in the future I can pass on to others the same kindness that they have shown me.

Finally, I would like to thank the entire non-scientific staff of PKS and the Covid response team, whose labour, perhaps more than that of everyone else, is indispensable in maintaining the scientific atmosphere and collective working environment at MPI-PKS, and has shielded us, like Archimedes preoccupied with his mathematical drawings, from the profound consequences created by the pandemic and vicissitudes of the outside world.

Contents

1	Introduction	9
1.1	The Toric Code - Exact Solutions	13
1.2	The Toric Code - Elementary Excitations	14
1.3	\mathbb{Z}_2 Lattice Theories with e - and m -bosons	16
1.4	The ε -fermions	19
1.5	Outline of the Thesis	21
2	Duality between spins and quasiparticles on \mathbb{Z}_2 lattices	23
2.1	Mapping between spins and e -, m -bosons	24
2.1.1	Open Lattice	24
2.1.2	Periodic Lattice	26
2.2	Mapping between spins and e -boson and ε -fermions	30
2.2.1	Open Lattice	30
2.2.2	Periodic Lattice	32
2.2.3	Equivalence to the Honeycomb lattice	35
3	Example: Bosonic \mathbb{Z}_2 Lattice Theory as two-dimensional Ising Model and Confinement of e-bosons	37
4	\mathbb{Z}_2 vortices in an ideal gas of anyons with $U(1)$ global symmetry	39
4.1	Static e -vortices in an ideal m -boson gas	39
4.2	Static e -vortices in an ideal ε -fermion gas	42
5	\mathbb{Z}_2 Topological Order of Superconducting ε-fermions Enriched by Lattice Translation Symmetry	47
5.1	Relation between \mathbb{Z}_2 Topological Order and Topological Superconductivity	47
5.2	Model	50
5.2.1	Phase Diagram	51
5.2.2	Atomic Insulator phases (AI)	52
5.2.3	Weak Topological Superconductor phases (KW)	52
5.2.4	Phases with non-zero Chern number	57
5.2.5	Bulk-Edge Correspondence	57
5.3	Equivalence to the Kitaev Honeycomb Model	59
6	Berry phase and Emergent Anyon Statistics from Motion of e-bosons	61
6.1	Weak Symmetry Breaking in KW phases	62
6.2	Berry phase and Emergent Anyon Statistics in phases with non-zero Chern number	67
6.2.1	$C = \pm 1$ phases	68
6.2.2	$C = -2$ phase	72
6.3	Discussion of Results and Experimental Relevance	73

7	\mathbb{Z}_N Topological Order	75
7.1	Definitions and Elementary Excitations	75
7.2	Duality Mapping	77
7.3	Parafermion Operators	80
7.4	Exact Solutions on Periodic Spin Lattices	83
8	Conclusions	86
Appendix A	Cylindrical lattices and independence of local parity operators	88
Appendix B	Free electrons in the field of a point vortex	91
Appendix C	Topological Superconductivity	95
Appendix C.1	Classification by Chern Number	95
Appendix C.2	Classification by Ground State Fermion Number	99
Appendix D	KW phases corresponding to diagonal stacking of Kitaev Wires	101
Appendix E	BCS ground state wave-function without translational symmetry	103
Appendix E.1	The first excited state of a BdG Hamiltonian with odd ground state parity	106
Appendix F	Matrix Elements between BCS ground states	107

Notation

Unless specified otherwise, the notation in this thesis is:

Matrix elements:

Pauli matrices σ_x , σ_y and σ_z defined on each edge on the \mathbb{Z}_2 spin lattice are written as X , Y and Z . In all figures, edges multiplied by X are shown in red whereas those multiplied by Z are shown in blue.

τ_i^α , σ_i^α are the σ_x and σ_z matrices in the doublet of local occupation number of α -anyon $|n_i^\alpha\rangle$ at the i -th site. Here $\alpha = e, m, \varepsilon$, $n_i^\alpha = 0, 1$.

The ground state is written as $|0\rangle$.

Operators:

The creation and annihilation operators for m -bosons on plaquette p are a_p^\dagger , a_p . For e -bosons on vertex v : b_v^\dagger , b_v .

The creation and annihilation operators for ε -fermions on plaquette p : c_p^\dagger , c_p . They are related to Majorana operators γ_p , γ'_p as follows:

$$\gamma_p = c_p + c_p^\dagger, \quad \gamma'_p = -i(c_p - c_p^\dagger).$$

In the functional integration formalism, we use \bar{c} instead of c^\dagger for the fermionic field variable.

Parafermion operators on plaquette p are η_p , η'_p .

Commutators and anti-commutators between two operators are:

$$[f, g] = fg - gf, \quad \{f, g\} = fg + gf.$$

Units:

We use *natural units* in which $\hbar = c = 1$.

The Boltzmann constant $k_B = 1$, so temperature is given in energy unit.

The lattice constants are always taken unity.

List of Figures

1	Toric Code and the Kitaev Honeycomb model.	11
2	Topological operators in the Toric Code on the periodic lattice.	14
3	Nearest neighbour pair-creation operators and loop motion for elementary excitations e and m	15
4	Binding convention and local operators for ε -fermions.	20
5	Open lattice geometry and non-local single-boson creation operators for e - and m -particles.	24
6	Non-local pair-creation operators and anyonic statistics for e - and m -bosons.	28
7	Jordan-Wigner transformation for ε -fermions on open lattices.	31
8	Topological operators for ε -fermions and Jordan-Wigner transformation on periodic lattices.	33
9	Equivalence of duality on square lattice to the honeycomb lattice.	36
10	Energy of an e -vortex in an ideal gas of ε -fermions.	44
11	Change in particle number of ideal gas of ε -fermions due to an e -vortex.	45
12	Phase diagram for the Hamiltonian (5.8).	51
13	Majorana coupling in KW_x phases.	53
14	Edge mode dispersions for the Hamiltonian (5.8) on a cylindrical lattice.	58
15	Equivalence of Majorana modes on the square lattice to the honeycomb lattice.	59
16	Weak Symmetry Breaking in KW_x phases.	63
17	Reduction of the KW_x phases to the Toric Code.	65
18	Ground state parity and energy of the effective Kitaev honeycomb model with a pair of e -vortices.	69
19	Berry phase of e -vortex motion.	70
20	Levin-Wen protocol for anyon braiding.	71
21	Coupling terms for the Hamiltonian with $C = -2$	73
22	Operator definitions for \mathbb{Z}_N theories.	76
23	Pair-creation and Wilson operators for parafermions and duality mapping.	80
A.24	Cylindrical lattice and global topological operators.	89
B.25	Energy and number differences for ε -fermions with and without an e -vortex.	93
B.26	Fermion density near the vortex.	94
C.27	Topology of superconducting phases on two-dimensional Brillouin zone.	96
D.28	Emergent anyon statistics in KW_{x+y} phases.	102

1 Introduction

One of the cornerstones of theoretical condensed matter physics is the concept of order parameter, proposed by L.D. Landau [1]. It characterizes a wide range of different phases by their symmetry groups, and describes quantitatively the thermodynamics and kinetics of second order phase transitions.

According to the theory of second order phase transitions, a phase can be characterized by a symmetry group G and a certain local function $\eta(\mathbf{r})$ called the ‘order parameter’. Consider a three-dimensional magnet. The order parameter η is a vector function taken to be the averaged local spontaneous magnetization \mathbf{M} . In the paramagnetic phase at high temperatures, $\mathbf{M} = 0$ and the symmetry group $G = SO(3)$ corresponds to rotational invariance of the system. As the temperature is lowered, a second order phase transition occurs at a given critical temperature T_c at which \mathbf{M} starts to develop continuously from zero. The magnet then enters a ferromagnetic state in which \mathbf{M} is non-zero and the symmetry group is lowered to $H = SO(2)$, since the system is invariant only under rotations with the axis along \mathbf{M} . More generally, the state of a system with symmetry group G is described by the thermodynamic potential $\Omega[\eta]$, which is a functional of η and invariant under transformation of η under certain representation of G . For simplicity we neglect fluctuations. Then the ‘symmetric phase’ with full symmetry G corresponds to $\bar{\eta} = 0$ being the minimum of $\Omega[\eta]$. The emergence of a non-zero $\bar{\eta}$ at thermal equilibrium spontaneously breaks G into a subgroup H : $\bar{\eta}$ is invariant under H which characterizes the ‘asymmetric’ phase.

Using symmetry to classify and study phases is extremely powerful, as it describes widely different phases under a unified framework even if the phase transition is absent or not second order. Apart from the previous example of magnets, this ranges from classifying crystals using space groups, to a quantitative description of superconductors and superfluids where the order parameters are the condensate wave-functions of Cooper pairs and Helium atoms respectively [2]. Furthermore, breaking of the full symmetry group G of the system by the non-zero averaged order parameter in the ‘asymmetric phase’ determines, automatically, the low-energy dynamics of the system (the Goldstone theorem and Higgs mechanism); c.f. Ref. [3]. The concept of symmetry is also central in a field-theoretical framework in the study of critical phenomena and high-energy physics. For an overview in field theory but mainly concerned with critical phenomena, see Ref. [4].

However with the discovery of the fractional quantum Hall effect (FQHE) more than thirty years ago, it was realized that not all phases can be described by the Landau paradigm, due to the absence of a local order parameter in FQHE. This gave rise to the concept of topological order, which was introduced in the context of FQHE [5] and spin liquids in the theory of high-temperature superconductivity [6, 7]. Since then it has come to describe a large number of both theoretical and physical phases which cannot be captured by the usual Landau theory of phase transitions, namely they are characterized by neither local order parameters nor symmetry; see Ref. [8] and references therein. For *gapped* topological order, such phases usually have long-range entanglement at zero temperature [9, 10], ground state degeneracy on closed manifolds (i.e. a torus) [7, 11–13], fractionalization and anyons in the excitation spectrum [7]. Phases belonging to different topological orders cannot be adiabatically

ically transformed into each other without gap closing.¹ Here the phases are ‘topological’ in the sense of long-range entanglement. The term apparently originated from low-energy description of chiral spin liquids by theories of Chern-Simons types, i.e. topological quantum field theories [15]; see (1.13) below. This is to be distinguished from a different class of systems which are also called ‘topological’ in the literature, because their eigenstates or field configurations admit invariants that can be classified by homotopy groups from algebraic topology. Instantons in quantum field theory and topological band theory are some of the prominent examples in this group. These phases do not constitute topological order.

Among the topologically ordered phases, \mathbb{Z}_2 topological order is of particular importance [3, 16]. In addition to the preceding properties, its ground state degeneracy on torus is characterized by \mathbb{Z}_2 quantum numbers of non-local operators. That these \mathbb{Z}_2 invariants are global necessarily means that the ground state degeneracy is stable against local perturbations, which makes these systems ideal as protected qubits for quantum computing [13]. Therefore, from both theoretical and practical points of view, it is important to develop and study models of \mathbb{Z}_2 topological order that illustrate all the essential properties, but are nonetheless simple enough to be implemented in an experimental setting.

One of the simplest and most illustrative examples of \mathbb{Z}_2 topological order is given by the Toric Code [13]. Since it forms the conceptual foundation for the class of models of \mathbb{Z}_2 topological order in this thesis, let us describe its properties in some detail. Consider a square lattice with spin-1/2 degrees of freedom on the edges and periodic boundary conditions (B.C.s). We shall write X , Y and Z for Pauli matrices σ_x , σ_y and σ_z defined on each edge. Then the Toric Code Hamiltonian is given by [13]:

$$H_{\text{TC}} = - \sum_v A_v - \sum_p B_p, \quad (1.1)$$

where the summation is taken over all vertices v and plaquettes p of the lattice. For a given vertex v , A_v consists of X operators on the four edges that join at the vertex. Similarly, B_p has Z operators on four edges of the plaquette p . They are written explicitly as:

$$A_v = \prod_{i \in v} X_i, \quad B_p = \prod_{i \in p} Z_i. \quad (1.2)$$

In Fig. 1, the operators in Eq. (1.2) are shown visually on the lattice.

The Hamiltonian (1.1) can be solved exactly [13], and has the important property that its eigenstates are ‘topological’ in the following sense: due to the underlying geometry of the torus, each eigenstate carries two global ‘topological quantum numbers’ with eigenvalues ± 1 . Eigenstates differing only in those two topological quantum numbers are degenerate. Therefore, each energy level is at least four-fold degenerate. In particular, the ground

¹There are additionally gapped phases with symmetries and short-range entanglement but no bulk topological order, i.e. topological insulators. They are called ‘symmetry protected topological order’ (SPT) [14]. In this case, if deformation of the Hamiltonian preserves the symmetry then gap closing is necessary for phase transition. Otherwise such a transition might occur without gap closing.

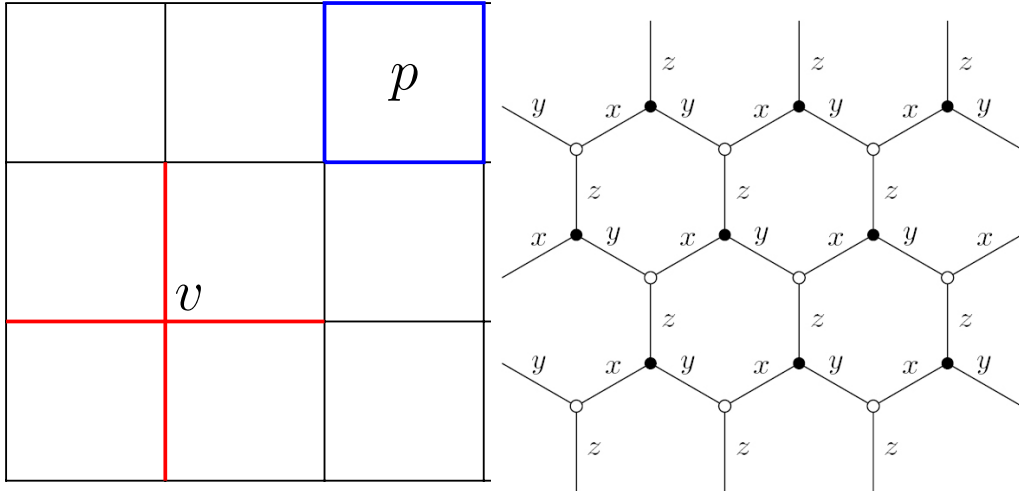


Figure 1: Left: A_v and B_p operators on a square lattice. An edge is multiplied by X (Z) if it is shown in red (blue). This color convention is used for all figures for spin operators in this thesis. Right: the honeycomb lattice where the x -, y - and z -links for the honeycomb model (1.3) are shown explicitly.

states are gapped and four-fold degenerate. This fact makes them stable with respect to local perturbations which cannot induce a global change of the system. Additionally, the spectrum of (1.1) contains two types of static and non-interacting quasiparticles e and m with mutual abelian anyon statistics. They also form a bound-state of ε -fermions. These properties are reviewed in Secs. 1.1 and 1.2 below.

Two considerations arise from the discussions so far. On the one hand, it is clear that the Toric Code can be generalized to a series of \mathbb{Z}_2 models on the spin lattice in which e - and m -particles, or e - and ε -particles, can acquire dynamics and interact. Given that these models are on the periodic lattice and can be interpreted in terms of anyons, at least some of them give further examples of \mathbb{Z}_2 topological order. The question naturally arises of developing a systematic method to study these phases directly in the anyonic degrees of freedom, and of clarifying their relationships to \mathbb{Z}_2 topological order. On the other hand, the Hamiltonian (1.1) contains only four-spin operators and seems unlikely to be realized in a conventional platform. However, it turns out that the Toric Code can be derived as a specific limit in the parameter space (J_x, J_y, J_z) of the following ‘Kitaev honeycomb model’ [17]:

$$H = -J_x \sum_{x\text{-links}} X_i X_j - J_y \sum_{y\text{-links}} Y_i Y_j - J_z \sum_{z\text{-links}} Z_i Z_j, \quad (1.3)$$

defined on a honeycomb lattice and the summation is over the x -, y - and z -links of the honeycomb edges, as is shown in Fig. 1. The model (1.3) contains free Majorana fermions and static bosonic π -vortices (‘visons’) which are also mutual anyons. The honeycomb model is considerably more physical in comparison to the Toric Code, since the Hamiltonian (1.3) consists of two-spin operators only. This fact motivates extensive theoretical and experimental research into its realization in the so-called candidate ‘Kitaev materials’ in which additional spin interactions (i.e. Heisenberg terms) are inevitably present in the

Hamiltonian, α -RuCl₃ being a notable example [18–22]. From a theoretical perspective, the dynamical properties of the Majorana fermions and visons and possible experimental signature of the spin liquid are also problems of intense interests [18, 23–27]. For a review, see Ref. [28].

Many methods have been developed to solve similar problems to those stated above in different contexts, by mapping local spin operators directly to the underlying quasiparticle fields [10, 17, 29–44]. In the case of anyons, fictitious degrees of freedom are usually introduced to deal with the non-local nature of anyon statistics. The final results are then projected back into the physical sector of the Hilbert space. Apart from the additional complexity that such a local extension of the Hilbert space produces, it also obscures the connection between anyonic excitations and periodicity of the spin lattice, i.e. the global \mathbb{Z}_2 quantum numbers. In this thesis, we derive *exact* dualities between spin operators on the square lattice and field operators of e -, m -particles or e - and ε -particles. Since no additional degrees of freedom are introduced and the mappings are between spin and anyon Hilbert spaces, it allows one to construct and study a series of \mathbb{Z}_2 topological phases directly and systematically in terms of anyons. It also shows unambiguously the interrelation between global \mathbb{Z}_2 invariants and certain properties of the systems. At the same time, it turns out that (e, ε) -duality on the square lattice can be carried over directly to the honeycomb, where e and ε naturally become the visons and Majorana fermions in the honeycomb model (1.3). Therefore, both \mathbb{Z}_2 models as generalizations of the Toric Code and extensions of the Kitaev honeycomb model for physical systems ² can be studied under a unified theoretical framework.

This thesis focuses on constructing the aforementioned spin-anyon dualities, and their application to a series of spin models. These models are mapped to quadratic anyonic Hamiltonians interacting via Chern-Simons type vector potentials in a specific gauge. However, after the mapping, the Hamiltonians are usually highly non-local. This makes exact solutions difficult to obtain even numerically, since the motion of one group of anyons strongly affects all anyons of the other group in the system. To simplify the problem, we shall always take e -bosons to be static. Consequently solutions to these models can be approached from both the perspective of \mathbb{Z}_2 topological order on the spin lattice and directly in terms of quasiparticles. For example, the most important lattice spin models that we consider have superconducting ε -fermions and static e -bosons. The underlying \mathbb{Z}_2 topological order ‘enriched by translation symmetry’ [45–47] (symmetry-enriched topological order has both topological order and symmetries; compare with SPT in the first footnote) can then be analyzed and classified by using the theory of topological superconductivity [48–61]. Many other results, i.e. confinement properties of e -particles, and the low-energy emergent anyon statistics in topological superconducting phases, are also obtained using the duality which are otherwise impossible on the spin lattice. Given the importance of the spin-anyon dualities for preceding considerations, in the rest of the introduction we shall discuss the essential ideas behind it.

²This assumes that the low-energy states of such models are not completely altered by additional spin-interactions so that their description in terms of visons and Majorana fermions still makes sense.

1.1 The Toric Code - Exact Solutions

Since the eigenstates of Toric Code (1.1) are used as basis for the quasiparticle Hilbert space, let us first outline the solution of Toric Code and prove its ground state degeneracy.

Operators A_v and B_p in Eq. (1.2) can take eigenvalues ± 1 since $A_v^2 = B_p^2 = 1$, and are the so-called ‘ \mathbb{Z}_2 operators’. Furthermore, they commute with each other and, as a result, also commute with the Hamiltonian (1.1). Thus each eigenstate is characterized by the set of eigenvalues $A_v = \pm 1$, $B_p = \pm 1$ on the lattice. In particular, the ground states have $A_v = B_p = 1$. Since on a periodic lattice there are $2L_x L_y$ number of edges, where L_x and L_y are the side lengths of the lattice (the lattice constant is taken unity), the $2L_x L_y$ number in total of A_v and B_p operators would suggest that the Hilbert space is completely described by the eigenvalues of A_v and B_p , and the ground state is unique. However, not all of A_v , B_p are independent, due to the constraints from periodic boundary conditions:

$$\prod_{v \in \text{lattice}} A_v = 1, \quad \prod_{p \in \text{lattice}} B_p = 1; \quad (1.4)$$

the product is taken over all vertices and plaquettes in the lattice. The two constraints in Eq. (1.4) mean that only $2L_x L_y - 2$ degrees of freedom are specified by the eigenvalues of A_v and B_p . The remaining two degrees of freedom can be accounted for by the eigenvalues of the following ‘Wilson loop’ operators:

$$W_x^{\text{TC}} = \prod_{i \in \gamma_x} X_i, \quad W_y^{\text{TC}} = \prod_{i \in \gamma_y} X_i; \quad [W_x^{\text{TC}}, W_y^{\text{TC}}] = 0. \quad (1.5)$$

The paths $\gamma_{x,y}$ are on the upper row and right column respectively, and traverse the lattice along the x - and y -directions; see Fig. 2. It will be proven at the end of this section that $W_{x,y}^{\text{TC}}$ are indeed independent degrees of freedom. For now we note that they commute with A_p and B_p , and do not enter into the Hamiltonian (1.1). Accordingly the Hilbert space is divided into $2^2 = 4$ degenerate ‘super-selection’ sectors specified by the eigenvalues of $\{W_x^{\text{TC}}, W_y^{\text{TC}}\}$ ($W_{x,y}^{\text{TC}} = \pm 1$). In particular, the ground states are four-fold degenerate.

Transitions between different super-selection sectors are given by the ‘t’Hooft’ operators $T_{x,y}^{\text{TC}}$ which anticommute with $W_{y,x}^{\text{TC}}$ and hence change their eigenvalues, but commute with A_v and B_p :

$$T_x^{\text{TC}} = \prod_{i \in \gamma'_x} Z_i, \quad T_y^{\text{TC}} = \prod_{i \in \gamma'_y} Z_i; \quad \{T_x^{\text{TC}}, W_y^{\text{TC}}\} = \{T_y^{\text{TC}}, W_x^{\text{TC}}\} = 0, \quad [T_x^{\text{TC}}, T_y^{\text{TC}}] = 0. \quad (1.6)$$

These operators are also shown in Fig. 2. We note that the choice of diagonalizing $W_{x,y}^{\text{TC}}$ to account for the four global degrees of freedom is purely conventional. For example, one can also characterize the system with eigenvalues of $T_{x,y}^{\text{TC}}$. In that case, $W_{y,x}^{\text{TC}}$ become the t’Hooft operators.

Finally, it should be emphasized that for the ground state, the specific forms of the contours in Eqs. (1.5) and (1.6) are immaterial. This is because a product of X or Z along any contours can be deformed by multiplying $A_v = 1$ or $B_p = 1$ (remember that

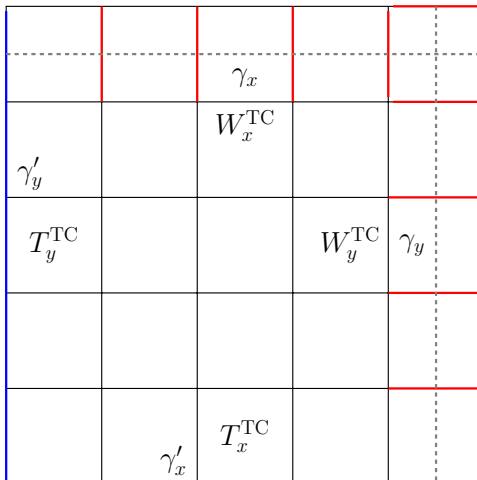


Figure 2: The global Wilson and t'Hooft operators given by Eqs. (1.5) and (1.6).

here we are concerned only with the ground state multiplets). More generally, any closed loops can be written as products of A_v or B_p ; see Eqs. (1.9) and (1.10) below. They are therefore ‘contractible’ to a point. But in $W_{x,y}^{TC}$ and $T_{x,y}^{TC}$, the contours traverse the lattice and cannot be deformed in this way into a point. These loops are ‘incontractible’ and are thus robust. This also proves the assertion that $W_{x,y}^{TC}$ and $T_{x,y}^{TC}$ cannot be expressed in terms of A_v and B_p . For excited states this deformation is problematic, because some A_v or B_p might have eigenvalue -1 , and $W_{x,y}^{TC}$ and $T_{x,y}^{TC}$ change sign after their contours sweep past the corresponding site. However, from the point of view of specifying the basis of the Hilbert space, it suffices to choose a specific path for each loop. The corresponding eigenvalues are then designated as the ones that characterize the state. We have chosen the particular paths in Eqs. (1.5) and (1.6) for later convenience.

1.2 The Toric Code - Elementary Excitations

The solution outlined in Sec. 1.1 admits the following physical interpretation. For a given eigenstate, on each vertex v we regard $A_v = -1$ as having an *elementary excitation* or *quasiparticle*³ (the e -particle) occupying that vertex, whereas $A_v = 1$ means that the vertex is empty. Analogously, $B_p = -1$ means that the plaquette p is occupied by an elementary excitation of a different kind (the m -particle). Thus each eigenstate is specified essentially by the local occupation numbers of e - and m -particles, as well as the eigenvalues of two commuting global operators which are taken to be $W_{x,y}^{TC}$. Here e - and m -particles are hardcore bosons because their occupation number at a given site cannot exceed unity. A_v and B_p then measure the parity of e - and m -particles on given sites. Since the ground states

³Sometimes in the literature, ‘elementary excitations’ refers exclusively to quasiparticles with bosonic statistics, while ‘quasiparticles’ is reserved for fermionic quasiparticles. In this thesis we use the two terms interchangeably which should not cause any confusion.

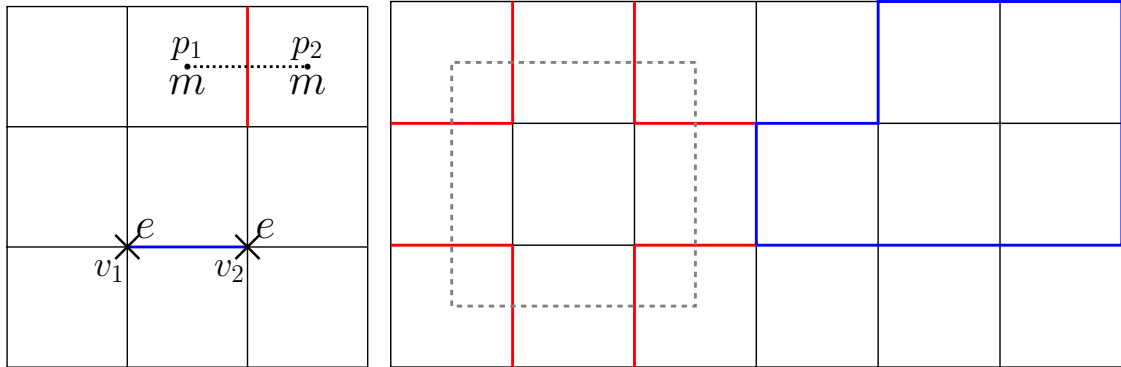


Figure 3: Left: examples of pair creation operators in Eqs. (1.7) and (1.8). Right: examples of loop motion of e - and m -bosons. The plaquettes in the product in (1.9) are contained by the blue line. The dotted gray line encloses all vertices on the right hand side of (1.10).

have $A_v = B_p = 1$, they can be naturally seen as the ‘vacuum states’ having no elementary excitations.

Following the same reasoning, we can also introduce pair-creation operators of e and m . For e -particles, such an operator that creates e -bosons on vertices v_1 and v_2 should anti-commute with A_{v_1} and A_{v_2} , but commute with other A_v and B_p . For two neighbouring vertices, we then have:

$$U_{v_1, v_2}^e = Z_{v_1 v_2}, \quad (1.7)$$

where $Z_{v_1 v_2}$ is the Z operator along the edge that connects v_1 and v_2 , as shown in Fig. 3. A pair of e -bosons can be created on arbitrary v_1 and v_2 by a product of Eq. (1.7), taken along any path that connects the two vertices. Any e -boson pair-creation operator thus defined satisfies the commutation requirements above. Similarly we can define nearest neighbour pair-creation operators for m -bosons:

$$U_{p_1, p_2}^m = X_{p_1 p_2}, \quad (1.8)$$

where $X_{p_1 p_2}$ is the X operator shared by the two plaquettes p_1 , p_2 ; see also Fig. 3. Pair-creation of m -bosons can also be written as a product of Eq. (1.8) over a path that connects p_1 and p_2 . Note that only pair-creation is possible on a torus, due to the constraints (1.4) which allow only even numbers of quasiparticles. Operators that create a single quasiparticle on an open lattice will be discussed in Sec. 2.1.

The physical meaning of the global degeneracy given by Eq. (1.5) now becomes clear. $W_{x,y}^{\text{TC}}$ simply correspond to creating a pair of m -bosons then moving one across the Torus along x - or y -direction to annihilate the other. The phases acquired are due to a ‘background’ flux which pierces through the torus. Accordingly $T_{x,y}^{\text{TC}}$ create a pair of e -bosons then annihilate them after moving one across the torus along x - or y -direction. These quantized phases characterize the underlying geometry of the lattice which results in the degeneracy.

It follows from Eqs. (1.7) and (1.8) that e - and m -bosons have mutual anyonic statistics. To see this, we create a pair of e -bosons on top of a given state then move one e -boson

around a closed loop which returns it to its original position. Multiplying Eq. (1.7) over a closed loop gives:

$$\prod_v Z_{v_1 v_2} = \prod_p B_p; \quad (1.9)$$

the product in v is taken over the closed string that transports the e -boson, and the product in p is taken over all plaquettes encircled by the loop; see Fig. 3. Thus in moving around one m -boson, the e -boson acquires a π -phase. Similarly by creating a pair of m -bosons and moving one around a closed loop, we have:

$$\prod_p X_{p_1 p_2} = \prod_v A_v; \quad (1.10)$$

see also Fig. 3. As a consequence of Eqs. (1.9) and (1.10), e - and m -bosons have mutual statistical angle $\pi/2$,⁴ so they are mutual semions or π -vortices. This also explains the previously mentioned fact that a contour that pair-creates e -bosons cannot be smoothly deformed through a plaquette p with $B_p = -1$. This is because the m -boson there acts as a point magnetic flux vortex for e -bosons so the contour will be pinned around it. The same holds for deforming a m -boson loop through vertices with e -bosons.

Finally, there is an additional type of elementary excitations. We can form a ‘composite’ ε -particle by binding an e -boson with another m -boson. In this thesis, we shall choose the binding convention as the following: an ε -particle defined on a plaquette p consists of an m -boson on plaquette p and an e -boson on the South-West vertex of p ; see Fig. 4 below. ε -particles are fermions with respect to themselves: exchanging a pair of ε -particles gives -1 , since each e (m) in one ε -particle acquires a factor of i from m (e) in the other ε -particle. Its mutual statistical angles with respect to e - and m -particles are $\pi/2$: they are still mutual semions or π -vortices.

We shall further investigate ε -fermions and their lattice operators in Sec. 1.4. Here we merely emphasize that the ‘compositeness’ of ε -fermions is in a sense artificial. For instance, one can alternatively regard e -bosons and ε -fermions as ‘elementary particles’, then m -bosons become bound states of e and ε .

1.3 \mathbb{Z}_2 Lattice Theories with e - and m -bosons

The physical arguments presented in Sec. 1.2 are not immediately related to the Hamiltonian (1.1) *per se*. More generally it suggests a rewriting of the spin-1/2 degrees of freedom along edges of the plaquettes in terms of two of the three quasiparticles e , m and ε on vertices and centers of plaquettes. Under such a duality between spin and quasiparticles, the Toric Code Hamiltonian (1.1) can be seen as a model with static and non-interacting quasiparticles e and m . By including pair-creation and parity operators, the elementary excitations can acquire dynamics and interact. In this thesis we construct a series of \mathbb{Z}_2

⁴The statistical angle θ between two anyons is half the phase acquired by one anyon after moving around the other, or the phase acquired by the wave-function after a pair permutation: $\Psi(x_1, x_2) = e^{i\theta} \Psi(x_2, x_1)$. For example, $\theta = \pi$ for fermions and $\theta = 0$ for bosons.

lattice theories that allow anyon dynamics and include the Toric Code (1.1) as the static limit, and study their \mathbb{Z}_2 topological order explicitly in the quasiparticle degrees of freedom. Of course, the utility of the method is restricted by that the spin models must physically make sense as models of anyons, which is generally not true for an arbitrary Hamiltonian.

What are the general features of such a mapping and the quasiparticle Hilbert space that it maps to? First the mapping must incorporate the effect of mutual anyonic statistics of the quasiparticles. Additionally, the quasiparticle Hilbert space should take into account the global \mathbb{Z}_2 indices (for example $W_{x,y}^{\text{TC}}$ and $T_{x,y}^{\text{TC}}$) due to periodicity of the spin lattice. Such dualities between lattice spins and two of the elementary excitations (e, m) or (e, ε) that satisfy these requirements are presented in Sec. 2, but their mappings are non-trivial. Therefore, let us first discuss the general physical considerations behind the mappings, and the restrictions imposed by the foregoing requirements which turn out to be quite strong.

In this section we shall discuss the simpler case of duality between spin and e - and m -bosons, and defer the more complex discussion of e - and ε -particles to Sec. 1.4. First, we consider the mapping on an infinite lattice. However, even in this case the mapping between spin and quasiparticle operators is not straightforward. At first sight, it seems that one can simply use the hardcore boson construction.⁵ For example, the parity operators A_v and B_p will become:

$$B_p \rightarrow \exp(i\pi a_p^\dagger a_p) = 1 - 2a_p^\dagger a_p, \quad A_v \rightarrow \exp(i\pi b_v^\dagger b_v) = 1 - 2b_v^\dagger b_v, \quad (1.11)$$

where a_p and b_v are annihilation operators of m - and e -particles on plaquette p and vertex v . As for the nearest neighbour pair-creation operators (1.7) and (1.8), the hardcore boson construction suggests:

$$X_{p_1 p_2} \rightarrow (a_{p_1}^\dagger + a_{p_1})(a_{p_2}^\dagger + a_{p_2}), \quad Z_{v_1 v_2} \rightarrow (b_{v_1}^\dagger + b_{v_1})(b_{v_2}^\dagger + b_{v_2}), \quad (1.12)$$

since $X_{p_1 p_2}$ changes the occupation numbers of m -bosons on plaquettes p_1 and p_2 and similarly for $Z_{v_1 v_2}$. Any spin operators can then be written as products of these ‘fundamental operators’. However, it can be immediately seen that Eq. (1.12) cannot be correct, because $X_{p_1 p_2}$ for two neighbouring plaquettes is defined on the same edge as $Z_{v_1 v_2}$ connecting the two vertices shared by the plaquettes: $X_{p_1 p_2}$ and $Z_{v_1 v_2}$ anticommute as a result, whereas field operators of different quasiparticles must commute. More fundamentally, Eq. (1.12) has not taken into account the mutual anyonic statistics of e - and m -bosons which follow from Eqs. (1.9) and (1.10).

Conventionally, the mutual statistics of abelian anyons in 2+1 dimensions are accounted for in a *local* theory by coupling quasiparticle momenta to $U(1)$ gauge fields a_μ^i with a ‘Chern-Simons’ action [62–65]. The corresponding Lagrangian density is:

$$\mathcal{L} = \frac{1}{4\pi} \sum_{i,j} e^{\mu\nu\lambda} K_{ij} a_\mu^i \partial_\nu a_\lambda^j - \sum_i j_\mu^i a^{i\mu}. \quad (1.13)$$

⁵For hardcore bosons defined on lattice sites, their creation and annihilation operators commute on different sites. On the same site they satisfy: $b_i^2 = b_i^{\dagger 2} = 0$, $\{b_i^\dagger, b_i\} = 1$. In the local basis of doublets of boson occupation number $|n_i\rangle$, $n_i = 0, 1$ on each site: $b_i = (\sigma_i^x + i\sigma_i^y)/2$.

Here i, j are indices for types of anyon, $e^{\mu\nu\lambda}$ is the Levi-Civita tensor, j_μ^i is the current for the i -th anyon and K_{ij} is an invertible, symmetric matrix that includes all information about the self- and mutual-statistics of anyons. It can be shown that for the i -th quasiparticle, a_μ^i then pins a point magnetic vortex to each anyon in accordance with their mutual- and self-anyonic statistics.

However, the description of anyon statistics in terms of local gauge fields a_μ^i contains a large degeneracy, since the Lagrangian (1.13) is invariant under a local $U(1)$ gauge transformation. In mapping from the spin lattice to such a theory, this necessitates a large degeneracy also on the lattice that is proportional to the system size, unless the Hilbert space is locally extended in the process. There are other ways to consider anyonic statistics, the parton construction on the Honeycomb lattice being one example [17]; see also the beginning of this section. Nevertheless in that case too, locality of the theory is only preserved after introducing fictitious Majorana fermions on each vertex of the Honeycomb, which also enlarges the Hilbert space. Hence it seems that in general, the long-range anyon statistics can only be described by a local theory with additional degenerate degrees of freedom which mediate this effect.

Such a large degeneracy generally does not exist in the spin lattice. Moreover, we want to study the effect of \mathbb{Z}_2 topological indices (1.5) and (1.6) on the quasiparticle Hilbert space on a finite, periodic lattice. For this reason, we do not wish to introduce redundant degrees of freedom, since they might make the connection obscure. Therefore, as is clear from discussions above, the mapping for hardcore boson pair-creations should correspond to a specific ‘gauge’ of π -vortices pinned to each e -boson for the m -bosons and vice versa, and the description should be *non-local*. The form of such a mapping on an infinite lattice can be directly inferred by considering operator commutation relations. Pair-creation operators $Z_{v_1 v_2}$ for e and $X_{p_1 p_2}$ for m commute with all B_p and A_v respectively, and change local anyon occupation numbers on adjacent sites by unity. This together with Eq. (1.11) suggests that their mapping to quasiparticle operators on an infinite lattice must be of the form:

$$X_{p_1 p_2} \rightarrow (a_{p_1}^\dagger + a_{p_1})(a_{p_2}^\dagger + a_{p_2}) \left(\prod_v e^{i\pi b_v^\dagger b_v} \right), \quad (1.14a)$$

$$Z_{v_1 v_2} \rightarrow (b_{v_1}^\dagger + b_{v_1})(b_{v_2}^\dagger + b_{v_2}) \left(\prod_p e^{i\pi a_p^\dagger a_p} \right). \quad (1.14b)$$

The non-local product of parity operators is naturally related to a specific ‘gauge convention’ for π -vortices of mutual-anyon statistics. For example, for each e -boson pair-creation operator, the m -parity terms give a additional -1 if one of the plaquettes included in the product is occupied. This means that a static m -boson extends a ‘branch-cut’ from its position whose form is determined by the plaquettes that enter into the parity product in Eq. (1.14). Upon crossing the branch-cut, the e -boson translation changes sign. Thus, after completing a closed loop around an m -boson, the e -boson must cross the branch-cut for an odd number of times and gain an additional π phase. The same also holds for m -bosons.

Any spin operator can be written as product of parity and pair-creation operators of e and m . Thus the problem of constructing the mapping from spin to quasiparticle Hilbert

spaces on an infinite lattice is reduced to finding the conventions of the non-local parity products in Eq. (1.14). This will be solved in Sec. 2.1. There we shall also define a_p and b_v fields explicitly in terms of non-local spin operators.

We shall also generalize our results to a periodic spin lattice. Here the situation is more complex. As is clear from the discussions in Secs. 1.1 and 1.2, the quasiparticle Hilbert space must incorporate the constraints (1.4) and the topological \mathbb{Z}_2 degrees of freedom corresponding to $W_{x,y}^{\text{TC}}$ and $T_{x,y}^{\text{TC}}$. Given that $W_{x,y}^{\text{TC}}$ and $T_{x,y}^{\text{TC}}$ correspond to motions of m and e traversing the entire lattice, their eigenvalues must be related to the boundary conditions of m and e . In Sec. 2.1, we show that the inclusion of these degrees of freedom results in a modification of Eq. (1.14): the operators that traverse the lattice boundaries are multiplied by additional external \mathbb{Z}_2 operators which correspond to $W_{x,y}^{\text{TC}}$ and $T_{x,y}^{\text{TC}}$. Here diagonalizing $W_{x,y}^{\text{TC}} = \pm 1$ means that the m -bosons have periodic or anti-periodic boundary conditions along x -, y -directions. As a result, the total Hilbert space consists of four quasiparticle Hilbert spaces, each with a different combination of periodic/anti-periodic boundary conditions for m -bosons along x - and y -directions, corresponding to the four super-selection sectors. The e -boson pair-creations across lattice boundaries then cause transitions between these super-selection sectors. Similarly one can diagonalize $T_{x,y}^{\text{TC}}$, then e -bosons have definite boundary conditions whereas cross-boundary motion of m changes the super-selection sectors. Moreover, each of these quasiparticle Hilbert spaces must have even total parities for e - and m -parities due to the constraints (1.4). Therefore, only even total parity states in the quasiparticle Hilbert space are physical, and odd parity states must be removed.

1.4 The ε -fermions

The discussions in Sec. 1.3 can be repeated for the case of mapping to e -bosons and ε -fermions degrees of freedom. This is also the more interesting and important case for this thesis, due to the large number of known topological phenomena in fermionic systems. In this thesis, we will use the mapping to construct a series of \mathbb{Z}_2 lattice models with free and superconducting ε -fermions. The connection between \mathbb{Z}_2 topological order and topology in fermionic systems will then become clear. Before discussing the mapping, let us recall some definitions for ε -fermion operators on an infinite spin lattice.

Since the ‘elementary’ particles are ε -fermions and e -bosons, the e -boson parity operator A_v in Eq. (1.2) is no longer adequate, as it also measures the ε -fermion parity on the North-East plaquette; see Fig. 4 and the end of Sec. 1.2. Due to the binding convention of ε -fermions, the e -parity operator must have the form:

$$A_v B_{\text{NE}(v)},$$

where $\text{NE}(v)$ is the North-East plaquette to the vertex v . However, B_p can be used as parity operators for ε -fermions. To distinguish from the (e, m) case, we write the parity operators in new notation:

$$\Gamma_v^e = A_v B_{\text{NE}(v)}, \quad \Gamma_p^\varepsilon = B_p. \quad (1.15)$$

Note that on a torus, one obtains similar constraints to Eq. (1.4) on global e - and ε -parities:

$$\prod_v \Gamma_v^e = 1, \quad \prod_p \Gamma_p^\varepsilon = 1. \quad (1.16)$$

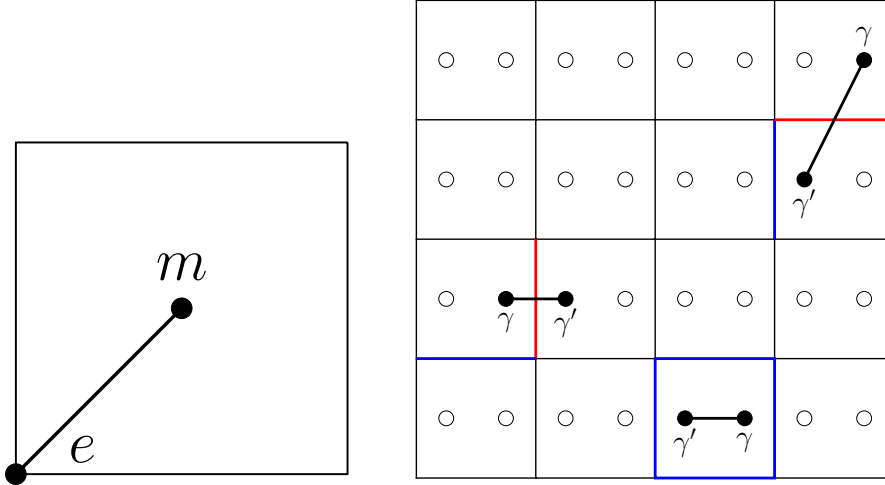


Figure 4: Left: the binding convention for an ε -fermion. Each e -bosons is binded with an m -boson to its North-East. Right: illustrations of pair-creation (1.17) and parity operators (1.15) for ε -fermions. Their mapping to Majorana couplings (1.18) are shown explicitly.

The pair-creation operator $U_{v_1 v_2}^e$ for e -bosons retains its form in Eq. (1.7). Naturally one can define the nearest neighbour ε -fermion pair-creation operators as simultaneous pair-creation of e - and m -bosons. Using Eqs. (1.7) and (1.8), and the binding convention for ε -fermions we obtain:

$$U_{p_1 p_2}^\varepsilon = X_{p_1 p_2} Z_{v_1 v_2}, \quad (1.17)$$

where v_1 and v_2 are vertices to the South-West of p_1 and p_2 respectively. $U_{p_1 p_2}^\varepsilon$ operators for vertical and horizontal pair-creation are shown in Fig. 4. Contrary to Eq. (1.8), the $U_{p_1 p_2}^\varepsilon$ operator is not symmetric with respect to p_1, p_2 . Therefore, we have the ‘directionality’ convention that for horizontal translations, p_1 is to the left of p_2 and for vertical translations, p_1 is above p_2 . Note that as a result of fermion statistics of ε -particles, not all U_{p_1, p_2}^ε operators in Eq. (1.17) commute. For example, a horizontal $U_{p_1 p_2}^\varepsilon$ anti-commutes with vertical $U_{p_3 p_2}^\varepsilon$ and $U_{p_1 p_4}^\varepsilon$, where p_3 is above p_2 and p_4 is below p_1 .

The mapping of Eqs. (1.15) and (1.17) to bilinears of Majorana operators on both infinite and open, finite lattices has been obtained in Ref. [41] in the absence of e -bosons: $\Gamma_v^e = 1$ on all vertices are imposed. The mapping reads:

$$U_{p_1 p_2}^\varepsilon \rightarrow i\gamma_{p_1} \gamma'_{p_2}, \quad \Gamma_p^e = -i\gamma_p \gamma'_p, \quad (1.18)$$

The Majorana operators are defined in terms of complex fermion annihilation operators as $c_p = (\gamma_p + i\gamma'_p)/2$, which are just the annihilation operators of ε -fermions. The mapping (1.18) satisfies the commutation relations of $U_{p_1 p_2}^\varepsilon$ and Γ_p^e on the spin lattice. From the same considerations as in Sec. 1.3, we see that the presence of e -bosons will modify Eq. (1.18) by introducing products of e -parity operators Γ_v^e in the mapping for $U_{p_1 p_2}^\varepsilon$, as a result of the mutual anyonic statistics between e -bosons and ε -fermions. Analogously to Eq. (1.14), we

then have on an infinite lattice:

$$U_{p_1 p_2}^\varepsilon \rightarrow i\gamma_{p_1} \gamma'_{p_2} \left(\prod_v e^{i\pi b_v^\dagger b_v} \right), \quad (1.19a)$$

$$U_{v_1 v_2}^e \rightarrow (b_{v_1}^\dagger + b_{v_1})(b_{v_2}^\dagger + b_{v_2}) \left(\prod_p -i\gamma_p \gamma'_p \right). \quad (1.19b)$$

It is clear that in the case of e - and ε -particles, the quasiparticle Hilbert space on a torus will also be characterized by global parity constraints (1.16) and topological \mathbb{Z}_2 operators analogous to $W_{x,y}^{\text{TC}}$ and $T_{x,y}^{\text{TC}}$ ($W_{x,y}^{\text{TC}}$ is inadequate because they correspond to loop motions of m -bosons and not ε -fermions). Consequently, as will be discussed in Sec. 2.2, the torus geometry modifies the mapping (1.19) which results in four quasiparticle Hilbert spaces with different ε -fermion boundary conditions and total quasiparticle parities even. The e -boson pair-creations across lattice boundaries cause transitions between these super-selection sectors.

In Sec. 2.2, we shall consider open and periodic spin lattices and define the new topological \mathbb{Z}_2 Wilson loop operators that correspond to ε -fermions. We then present explicit definitions of b_v and γ_p, γ'_p in terms of non-local spin operators; the fermions are given by a two-dimensional analogue of the Jordan-Wigner transformation. Inverting this definition and expressing local spin operators in terms of non-local quasiparticle fields, we obtain the desired mapping from spin to e and ε degrees of freedom, as well as the conventions for branch-cuts in Eq. (1.19) for both lattice geometries. This will also give, very naturally, the additional external \mathbb{Z}_2 indices that modify the mapping (1.19) for cross-boundary motion on a torus, which characterize the geometry of the underlying spin lattice.

1.5 Outline of the Thesis

The rest of this thesis is organized as follows.

In Sec. 2 we present in detail the construction of (e, m) - and (e, ε) -particle Hilbert spaces on open, infinite and periodic lattices respectively. The equivalence of e and ε to visons and Majorana fermions in the honeycomb model is then demonstrated by reconstructing the square lattice as a distorted honeycomb lattice. The results in that section were reported in Refs. [46, 66]. In Ref. [46], basing on previous results on infinite and open lattices in Ref. [41], the duality mapping for ε -fermions without e -bosons was first obtained on a periodic lattice. In Ref. [66] the mapping was then extended to include e -bosons, based on the present approach in this thesis. In Sec. 3, a trivially solvable spin Hamiltonian on a torus is considered that can be mapped to the ferromagnetic Ising model using the (e, m) -duality. We compare the solutions on the spin lattice and in the basis of m occupation numbers to illustrate certain general, important features of the mapping.

In Sec. 4, we study the energy spectrum and confinement properties of e -bosons as static, free π -vortices in ideal gases of m -bosons and ε -fermions respectively. This section is based on results in Ref. [67]. The numerical results are verified to be consistent with analytical calculations performed at the low-filling limit at which the fermion dispersion is parabolic.

Secs. 5 and 6 concern with a class of lattice models that can be mapped to static e -bosons and topological superconducting ε -fermions. They constitute what is called ‘ \mathbb{Z}_2 topological order enriched by translation symmetry’ [45–47].

In Sec. 5, the phase diagrams and ground state properties of the model considered are classified and investigated in detail in the absence of e -bosons. This is done primarily by the duality mapping and applying the theory of topological superconductivity, supplemented in certain phases by exact solutions on the spin lattice. In particular, it is shown that the ground state degeneracy in certain \mathbb{Z}_2 topological phases depends on lattice size. Previously, this phenomena in \mathbb{Z}_2 topological order with translation symmetry has been discovered in Refs. [17, 48, 49, 52, 68–71]. This section is based on results in Ref. [46].

In Sec. 6, the anyonic properties of e -bosons on top of the superconducting vacuum are studied. Here the e -vortices are ‘renormalized’ by the superconducting vacuum and become emergent anyons. The results fall into two categories: in phases with zero Chern number that correspond to stacks of one-dimensional Kitaev wires of ε -fermions, the e -bosons on two sublattices become mutual π -vortices. The sublattices are exchanged by a lattice translation. Hence we have found an explicit example of ‘weak symmetry breaking’ [17, 72] which was first reported in Ref. [46]. In the second category, the Berry phase of motion of e -bosons is computed in phases having non-zero Chern number. The results relate naturally to properties of visons in the honeycomb model. In particular, we consider e -motion around an empty square unit cell and mutual braiding of e -bosons. The results are shown to depend on the topology of the underlying superconducting phases. The braiding statistics of e -bosons agree with the prediction in Ref. [17], whereas the background flux of each unit cell is quantized to be 0 or π . These results were obtained in Ref. [66].

Finally in Sec. 7, we present some unpublished results on \mathbb{Z}_N generalization of \mathbb{Z}_2 lattice models considered in the previous two sections. They are obtained in collaboration with Inti Sodemann. Here the mapping from the lattice to quasiparticles is considerably more complex, and the models can only be solved in some limits on the lattice. Interestingly, despite the absence of a quasiparticle picture, certain properties of the exact solutions resemble their \mathbb{Z}_2 counterparts. It remains unclear if such a quasi-particle picture exists for models of \mathbb{Z}_N topological order.

In Refs. [46, 66, 67] listed above, P. Rao, O. Pozo and C. Chen participated in analytical calculations and discussions. Numerical calculations are carried out by O. Pozo and C. Chen. I. Sodemann participated in analytical calculations and discussions, and provided guidance.

2 Duality between spins and quasiparticles on \mathbb{Z}_2 lattices

As discussed in Sec. 1, spin-1/2 operators on edges of plaquettes in a square lattice can be mapped to field operators of two of the elementary excitations (e, m) or (e, ε) , regarding the third as bound states. In this section, we shall construct this mapping explicitly for these two cases on finite, open lattices and on a torus. This will be dealt with in Secs. 2.1 and 2.2.

However, before proceeding we shall discuss the modifications in constructing open lattices, and repeat our counting of degrees of freedom in Sec. 1.1. It is also possible to construct a cylindrical lattice with periodic boundary condition along one direction only. This case will be discussed in Appendix A.

Firstly we consider the same square lattice as in Sec. 1.1 but with open boundary conditions, and spins on boundary edges are independent. The extra edges will introduce additional $L_x + L_y$ degrees of freedom. To avoid unnecessary complications and to retain $2L_xL_y$ degrees of freedom as in the torus, we remove the edges along the upper and right boundaries of the lattice, as shown in Fig. 5. The number of vertices and plaquettes is then still L_xL_y and lattice operators on sites at the boundary will be modified. For example, A_v contains only three edges on vertices along the vertical left boundary, and only two edges at the bottom-left vertex. Similarly, B_p is a three-spin operator along the vertical right boundary and a two-spin operator at the upper-right plaquette. Secondly, the parity constraints (1.4) and (1.16) cease to apply. Therefore, parity operators are all independent; this fact will be proven rigorously below. We then have in total, $2L_xL_y$ independent A_v , B_p or Γ_v^e and Γ_p^ε operators. The sizes of spin and quasiparticle Hilbert spaces then coincide, which is crucial for a complete description of the original lattice in the quasiparticles picture.

The absence of global parity even constraints means that single-particle creation processes are allowed. We shall now construct explicit examples of operators that create a single e - or m -boson, the corresponding operators for ε -fermions then being a combination of both. As shown in Fig. 5, to create a single e -boson at a given vertex v , we can extend a string of Z operators from the right boundary which terminates at v . Analogously, an m -boson can be created at plaquette p by a string of X operators joining the left boundary and p . The operator thus defined anti-commutes with A_v or B_p on the given site, and commutes with all other A_v and B_p . A single ε -fermion can be created similarly.

Finally, we prove the claim that all parity operators are independent in an open or cylindrical lattice for the (e, m) case. The (e, ε) case is entirely analogous.

Global constraints for \mathbb{Z}_2 parity operators A_v and B_p can be written in the following form:

$$F_1(A_v, B_p) = 0, \quad F_2(A_v, B_p) = 0, \quad (2.1)$$

where F_1 and F_2 are functions of A_v and B_p on potentially any vertices and plaquettes. If there is an operator that anti-commutes with an arbitrary A_{v_1} or B_{p_1} but commutes with all other A_v and B_p , then it would necessarily contradict (2.1) and global constraints cannot exist. However, such operators are simply single-particle creation operators for e - and m -particles just introduced. This completes the proof.

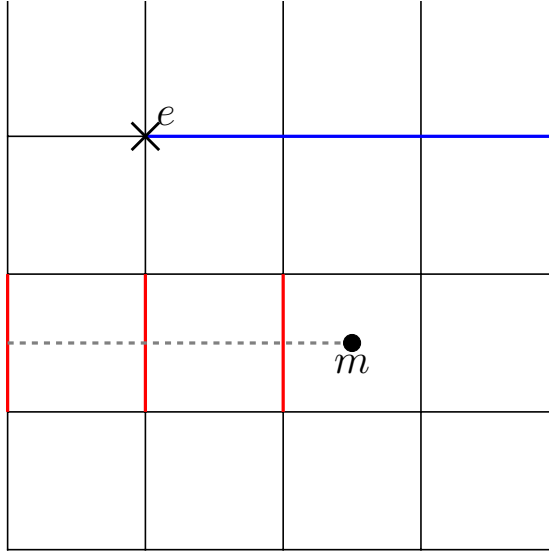


Figure 5: Open lattice configuration. The upper and right edges are removed. We also show the single-particle creation operators for e -bosons and m -bosons; c.f. (2.5). (2.6). Each particle is created by a horizontal non-local string from the lattice boundary.

2.1 Mapping between spins and e -, m -bosons

In the section, the mapping between spin and e -, m -boson fields a_p and b_v will be established. First we consider the open lattice.

2.1.1. Open Lattice

We shall describe the quasiparticle Hilbert space in more detail. As is mentioned at the beginning of this section, the spin Hilbert space has $2L_x L_y$ degrees of freedom in total. It can be alternatively described by the occupation numbers of hardcore e - and m -bosons on each vertex and plaquette:

$$|\dots n_v^e \dots, \dots n_p^m \dots\rangle; n_v^e, n_p^m = 0, 1.$$

Locally on each site, there are the equivalent of σ^x and σ^z matrices in the doublets of e - and m -particle occupation number:

$$\sigma_v^e |n_v^e\rangle = (-1)^{n_v^e} |n_v^e\rangle, \tau_v^e |0_v\rangle = |1_v\rangle, \tau_v^e |1_v\rangle = |0_v\rangle; \quad (2.2a)$$

$$\sigma_p^m |n_p^m\rangle = (-1)^{n_p^m} |n_p^m\rangle, \tau_p^m |0_p\rangle = |1_p\rangle, \tau_p^m |1_p\rangle = |0_p\rangle. \quad (2.2b)$$

Matrix τ creates or annihilates a boson on the given site whereas σ gives the local boson parity (we omit the e , m superscript when we refer to both e - and m -bosons). They satisfy $\{\tau, \sigma\} = 0$ on each site, and complete the local $SU(2)$ algebra of hardcore bosons. τ , σ are related to quasiparticle fields b_v and a_p as:

$$\tau_v^e \rightarrow b_v^\dagger + b_v, \sigma_v^e \rightarrow \exp(i\pi b_v^\dagger b_v); \tau_p^m \rightarrow a_p^\dagger + a_p, \sigma_p^m \rightarrow \exp(i\pi a_p^\dagger a_p). \quad (2.3)$$

b_v and a_p commute on different sites, and on the same site:

$$\{b_v^\dagger, b_v\} = 1, \{a_p^\dagger, a_p\} = 1, a_p^2 = b_v^2 = 0.$$

Eqs. (2.2) and (2.3) then determine b_v and a_p :

$$a_p = (\tau_p^m + \sigma_p^m \tau_p^m)/2, \quad b_v = (\tau_v^e + \sigma_v^e \tau_v^e)/2;$$

see also the footnote in Sec. 1.3.

Thus to find the mapping from spin to quasiparticle Hilbert spaces on an open lattice, it suffices to find the spin operators that map to τ , σ . The obvious identities hold for parity operators:

$$A_v \rightarrow \sigma_v^e \rightarrow \exp(i\pi b_v^\dagger b_v); \quad B_p \rightarrow \sigma_p^m \rightarrow \exp(i\pi a_p^\dagger a_p). \quad (2.4)$$

As for τ_v^e (τ_p^m) operators, they must satisfy the following commutation relations. First they must anti-commute, by definition, with A_v (B_p) but commute with other parity operators. They must also commute with the operators that map to τ_p^m (τ_v^e), as they belong to a different sector of the Hilbert space.

It is clear that τ must be single-particle creation operators with a specific convention for their contours that satisfy all requirements above. The choice of contour is not unique and here we give one such mapping. For a given τ_v^e , the corresponding spin operator is a product of Z matrices whose contour $C_e(v)$ extends from the right boundary on the same row and terminates at v :

$$\prod_{\substack{v_1, v_2 \in \\ C_e(v)}} Z_{v_1 v_2} \rightarrow \tau_v^e. \quad (2.5)$$

For τ_p^m , the contour $C_m(p)$ for X matrices begins from the left boundary on the same row and joins p :

$$\prod_{\substack{p_1, p_2 \in \\ C_m(p)}} X_{p_1 p_2} \rightarrow \tau_p^m. \quad (2.6)$$

For a visual representation of the rules just described, see Fig. 5.

The required commutation relations for spin operators are indeed satisfied. The commutation relations with parity operators automatically hold because τ_v^e and τ_p^m are single-particle creation operators. From the conventions it is also clear that the spin operators for τ_v^e and τ_p^m do not share common edges, therefore they commute.

Inverting the mapping just obtained, any spin operators can be expressed in terms of τ and σ , and in a_p and b_v after substituting (2.3). The most important ones for our purpose are the e - and m -boson nearest-neighbour pair-creation operators in Eqs. (1.7) and (1.8). For nearest-neighbours along the horizontal direction, we obtain simply:

$$Z_{v_1 v_2} \rightarrow \tau_{v_1}^e \tau_{v_2}^e \rightarrow (b_{v_1}^\dagger + b_{v_1})(b_{v_2}^\dagger + b_{v_2}), \quad (2.7a)$$

$$X_{p_1 p_2} \rightarrow \tau_{p_1}^m \tau_{p_2}^m \rightarrow (a_{p_1}^\dagger + a_{p_1})(a_{p_2}^\dagger + a_{p_2}). \quad (2.7b)$$

Along the vertical direction, $\tau_{v_1}^e \tau_{v_2}^e$ and $\tau_{p_1}^m \tau_{p_2}^m$ are highly non-local on the spin lattice. Here it is easier to write $\tau_{v_1}^e \tau_{v_2}^e$ ($\tau_{p_1}^m \tau_{p_2}^m$) explicitly on the spin lattice using Eq. (2.5) [Eq. (2.6)],

express the non-local strings of Z (X) in terms of B_p (A_v) and $Z_{v_1 v_2}$ ($X_{p_1 p_2}$) then substitute Eq. (2.3). As a result we have:

$$\begin{aligned}\tau_{v_1}^e \tau_{v_2}^e &= Z_{v_1 v_2} \left(\prod_{p \in R(v_1, v_2)} B_p \right) \rightarrow Z_{v_1 v_2} = \tau_{v_1}^e \tau_{v_2}^e \left(\prod_{p \in R(v_1, v_2)} \sigma_p^m \right), \\ \tau_{p_1}^m \tau_{p_2}^m &= X_{p_1 p_2} \left(\prod_{v \in L(p_1, p_2)} A_v \right) \rightarrow X_{p_1 p_2} = \tau_{p_1}^m \tau_{p_2}^m \left(\prod_{v \in L(p_1, p_2)} \sigma_v^e \right),\end{aligned}$$

where $R(v_1, v_2)$ means plaquettes to the right of the edge that joins v_1 and v_2 , and $L(p_1, p_2)$ are vertices to the left of the line that connects the centers of p_1 and p_2 . Substituting (2.3) gives:

$$Z_{v_1 v_2} \rightarrow (b_{v_1}^\dagger + b_{v_1})(b_{v_2}^\dagger + b_{v_2}) \left(\prod_{p \in R(v_1, v_2)} e^{i\pi a_p^\dagger a_p} \right), \quad (2.8a)$$

$$X_{p_1 p_2} \rightarrow (a_{p_1}^\dagger + a_{p_1})(a_{p_2}^\dagger + a_{p_2}) \left(\prod_{v \in L(p_1, p_2)} e^{i\pi b_v^\dagger b_v} \right). \quad (2.8b)$$

Eqs. (2.7) and (2.8) give the branch-cut conventions of e - and m -bosons: for each π -vortex attached to an e -boson at vertex v , the branch-cut extends from v towards the right boundary on the same row and terminates there. Each π -vortex attached to an m -boson at plaquette p goes left and ends at the boundary. Together, Eqs. (2.4), (2.7) and (2.8) give the mapping from the open lattice to the quasiparticle Hilbert space.

The results on an finite open lattice can be directly generalized to an infinite lattice, which can be seen as the limiting case of $L_x, L_y \rightarrow \infty$. Hence in (2.5) for τ_v^e , the contour for the product of Z matrices now extends from v to the left towards infinity. Similarly, for τ_p^m in (2.6), the contour for X matrices begins from p rightward also to infinity. Accordingly, the branch-cut for each e - and m -boson extends from the given site towards right and left to infinity.

2.1.2. Periodic Lattice

We shall repeat the above arguments for a torus, which requires certain modifications.

As is discussed in Sec. 1.3, in addition to occupation numbers of hardcore e - and m -bosons on each vertex and plaquette, the quasiparticle Hilbert space is also described by two \mathbb{Z}_2 indices $z_1, z_2 = \pm 1$ corresponding to the eigenvalues of $W_{x,y}^{\text{TC}} = \pm 1$:

$$|\dots n_v^e \dots, \dots n_p^m \dots; z_1, z_2\rangle.$$

Remember that due to the global parity even constraints (1.4), only states with even numbers of e - or m -bosons are physical. Locally on each site, the hardcore boson construction given by Eqs. (2.2) and (2.3) still holds. Thus to find the mapping from spin to quasiparticle

Hilbert spaces, it suffices to find the spin operators that map to τ , σ and z_1 , z_2 , and impose the global even parity constraints (1.4):

$$\prod_{v \in \text{lattice}} \sigma_v^e = 1, \quad \prod_{p \in \text{lattice}} \sigma_p^m = 1; \quad (2.9)$$

From the definition of z_1 , z_2 , we immediately obtain:

$$W_{x,y}^{\text{TC}} \rightarrow \hat{z}_{1,2}, \quad \hat{z}_i |n_v^e, n_p^m; z_i\rangle = z_i |n_v^e, n_p^m; z_i\rangle; \quad (2.10a)$$

$$T_{x,y}^{\text{TC}} \rightarrow \hat{x}_{2,1}, \quad \hat{x}_i |n_v^e, n_p^m; z_i\rangle = |n_v^e, n_p^m; -z_i\rangle. \quad (2.10b)$$

The operators \hat{x}_i , \hat{z}_i satisfy $\{\hat{z}_i, \hat{x}_i\} = 0$, and are the equivalent of σ^x and σ^z matrices in the global doublet sector given by $z_{1,2} = \pm 1$. Locally, the mapping for parity operators (2.4) should still hold. As for τ operators, we note that only pairs of elementary excitations can be created on a torus. So spin operators can only map to bilinears of τ . For this reason, we need to choose a ‘reference’ vertex v_0 and plaquette p_0 and find the spin operators that map to $\tau_{v_0}^e \tau_v^e$ and $\tau_{p_0}^m \tau_p^m$, where v and p are arbitrary. Here v_0 and p_0 are taken to be the bottom-left vertex and plaquette, as is shown in Fig. 6. The commutation relations that must be satisfied by the spin operators are the following: $\tau_{v_0}^e \tau_v^e$ ($\tau_{p_0}^m \tau_p^m$) must anti-commute, by definition, with A_{v_0} (B_{p_0}) and A_v (B_p) but commute with other parity operators. They must also commute with the operators that map to $\tau_{p_0}^m \tau_p^m$ ($\tau_{v_0}^e \tau_v^e$), $W_{x,y}^{\text{TC}}$ and $T_{x,y}^{\text{TC}}$, as they belong to different sectors of the Hilbert space.

One such mapping that satisfies the necessary commutation relations is the following. For a given $\tau_{v_0}^e \tau_v^e$, the corresponding spin operator is a product of Z matrices along a specific contour that joins the vertices v_0 and v :

$$\prod_{\substack{v_1, v_2 \in \\ C_e(v_0, v)}} Z_{v_1 v_2} \rightarrow \tau_{v_0}^e \tau_v^e. \quad (2.11)$$

$C_e(v_0, v)$ connects vertices v and v_0 with the following convention. if v is on the same row as v_0 , the contour is a horizontal line that joins them. Otherwise from v_0 it first goes up to the row on which v is located, then turns right and terminates at v . For a given $\tau_{p_0}^m \tau_p^m$, we have similarly:

$$\prod_{\substack{p_1, p_2 \in \\ C_m(p_0, p)}} X_{p_1 p_2} \rightarrow \tau_{p_0}^m \tau_p^m. \quad (2.12)$$

The convention for contour $C_m(p_0, p)$ is: if p is on the same row as p_0 , the contour is a horizontal line that joins the two plaquettes. For p on different rows, the contour first heads right towards the bottom-right plaquette, then goes up to the row of p and goes left and arrives at p . The conventions are shown visually in Fig. 6.

Let us check that the required commutation relations for spin operators are indeed satisfied. The commutation relations with parity operators automatically hold because $\tau_{v_0}^e \tau_v^e$ and $\tau_{p_0}^m \tau_p^m$ are products of pair-creation operators for e - and m -bosons; see Eqs. (1.7) and (1.8). From the conventions it is also clear that the spin operators for $\tau_{v_0}^e \tau_v^e$ and $\tau_{p_0}^m \tau_p^m$ do

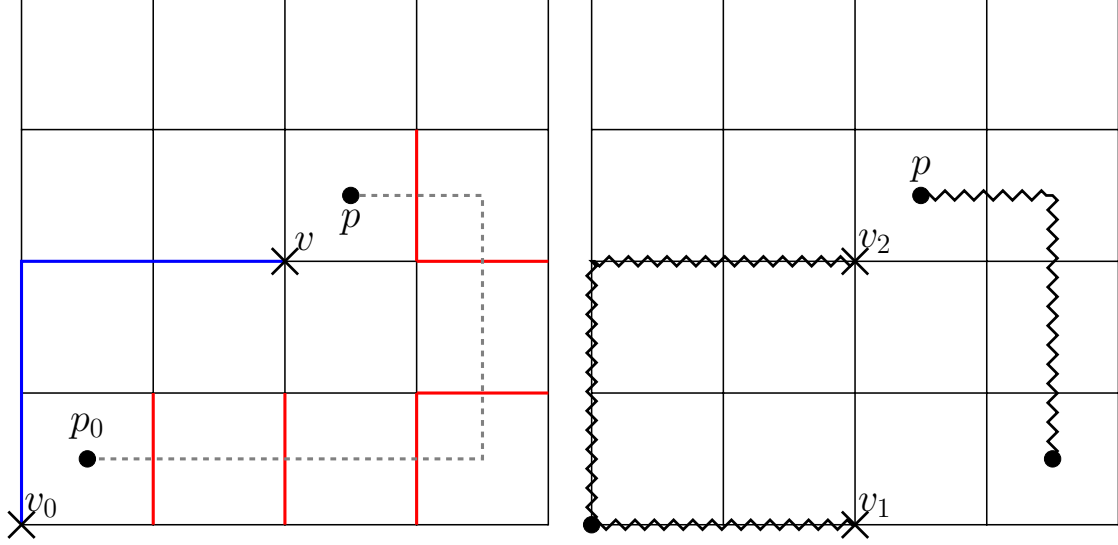


Figure 6: Left: pair-creation operators $\tau_{v_0}^e \tau_v^e$ and $\tau_{p_0}^m \tau_p^m$. The conventions of the strings are shown explicitly. Right: branch-cuts of single e - and m -particles as π -vortices. The branch-cuts from e -bosons terminate at the bottom-left vertex, and those from m -bosons at the top-left plaquette. The pair-creation operators that intersect the zigzag lines gain an additional -1 . Additionally, cross-boundary motion for e - and m -particles is multiplied by the corresponding eigenvalue of $\hat{x}_{1,2}$ or $\hat{z}_{1,2}$.

not share common edges, therefore they commute. Lastly, the contours for $\tau_{v_0}^e \tau_v^e$ and $\tau_{p_0}^m \tau_p^m$ never intersect the paths for $W_{x,y}^{\text{TC}}$ and $T_{x,y}^{\text{TC}}$ [see Eqs. (1.5) and (1.6)] which are along the upper and right rows, so they also commute.

We now express e - and m -boson nearest-neighbour pair-creation operators in Eqs. (1.7) and (1.8) in terms of τ, σ and z_1, z_2 . As in the open lattice case, we write $\tau_{v_1}^e \tau_{v_2}^e$ ($\tau_{p_1}^m \tau_{p_2}^m$) explicitly on the spin lattice, express the non-local strings of Z (X) in terms of B_p (A_v), $Z_{v_1 v_2}$ ($X_{p_1 p_2}$) and $T_{x,y}^{\text{TC}}$ ($W_{x,y}^{\text{TC}}$) then substitute Eqs. (2.3), (2.4) and (2.10)-(2.12). As a result Eq. (2.7) still holds for along the horizontal direction and away from the boundary. However, along the vertical direction the convention for non-local parity terms is different:

$$Z_{v_1 v_2} \rightarrow (b_{v_1}^\dagger + b_{v_1})(b_{v_2}^\dagger + b_{v_2}) \left(\prod_{\substack{p \in \\ L(v_1, v_2)}} e^{i\pi a_p^\dagger a_p} \right), \quad (2.13a)$$

$$X_{p_1 p_2} \rightarrow (a_{p_1}^\dagger + a_{p_1})(a_{p_2}^\dagger + a_{p_2}) \left(\prod_{\substack{v \in \\ R(p_1, p_2)}} e^{i\pi b_v^\dagger b_v} \right). \quad (2.13b)$$

$L(v_1, v_2)$ now includes plaquettes to the *left* of the edge that joins v_1 and v_2 , and $R(p_1, p_2)$ are vertices to the *right* of the line that connects the centers of p_1 and p_2 . On a torus there are also $Z_{v_1 v_2}$ and $X_{p_1 p_2}$ that traverse the lattice boundaries. Here we find that $\tau_{v_1}^e \tau_{v_2}^e$ and $\tau_{p_1}^m \tau_{p_2}^m$ (remember the non-local strings of Z and X for τ^e and τ^m do not cross lattice boundaries, so v_1, v_2 and p_1, p_2 are not ‘nearest neighbour’) are expressed not only in terms of $Z_{v_1 v_2}, X_{p_1 p_2}$ and parity operators, but also $W_{x,y}^{\text{TC}}, T_{x,y}^{\text{TC}}$; it is useful here to note that the

contours of $W_{x,y}^{\text{TC}}$, $T_{x,y}^{\text{TC}}$ can be deformed to the given row or column by products of A_v and B_p . The result is then inverted for $Z_{v_1 v_2}$ and $X_{p_1 p_2}$. This gives for horizontal pair-creation:

$$Z_{v_1 v_2} \rightarrow (b_{v_1}^\dagger + b_{v_1})(b_{v_2}^\dagger + b_{v_2}) \left(\prod_{\substack{p \in \\ \text{row above } v_1, v_2}} e^{i\pi a_p^\dagger a_p} \right) \hat{x}_2, \quad (2.14a)$$

$$X_{p_1 p_2} \rightarrow (a_{p_1}^\dagger + a_{p_1})(a_{p_2}^\dagger + a_{p_2}) \left(\prod_{\substack{v \in \\ \text{row above } p_1, p_2}} e^{i\pi b_v^\dagger b_v} \right) \hat{z}_1. \quad (2.14b)$$

And for vertical pair-creation:

$$Z_{v_1 v_2} \rightarrow (b_{v_1}^\dagger + b_{v_1})(b_{v_2}^\dagger + b_{v_2}) \left(\prod_{\substack{p \in \\ L(v_1, v_2)}} e^{i\pi a_p^\dagger a_p} \right) \hat{x}_1, \quad (2.15a)$$

$$X_{p_1 p_2} \rightarrow (a_{p_1}^\dagger + a_{p_1})(a_{p_2}^\dagger + a_{p_2}) \left(\prod_{\substack{v \in \\ R(p_1, p_2)}} e^{i\pi b_v^\dagger b_v} \right) \hat{z}_2. \quad (2.15b)$$

In deriving the first equation in (2.15), we have used the global parity constraint (2.9) for σ_p^m . The appearance of global topological operators $\hat{z}_{1,2}$ and $\hat{x}_{1,2}$ reflects the physical interpretation given in Sec. 1.2: a given super-selection sector with $z_{1,2} = \pm 1$ corresponds to periodic and anti-periodic boundary conditions for m -bosons, while e -bosons cross-boundary motion causes a transition between different super-selection sectors. Alternatively, one can choose a diagonal basis for $\hat{x}_{1,2}$, then each super-selection sector corresponds to definite boundary conditions of e -bosons. Since we consider only static e -bosons and dynamical m -bosons in this thesis, the basis in which \hat{z}_i are diagonal is more convenient.

Eqs. (2.13)- (2.15) give qualitatively different branch-cuts of e - and m -bosons on a torus from on an open lattice: for each π -vortex attached to an e -boson at vertex v , the branch-cut extends from v towards the left boundary, then goes down and terminates at v_0 . The branch-cut for each π -vortex attached to an m -boson at plaquette p goes right towards the right boundary then goes down and terminates at the bottom-right plaquette. This is shown in Fig. 6.

Eqs. (2.4), (2.7), (2.10) and (2.13)-(2.15), together with the constraints (2.9) that eliminate states with odd numbers of e - or m -bosons, give the mapping to the (e, m) quasiparticle Hilbert space.

Finally, it must be emphasized that the branch-cut convention obtained in this section is a result of the specific choices of strings for products of Z and X matrices in Eqs. (2.5), (2.6), (2.11) and (2.12). Other choices can result in different ‘gauges’. However, as mentioned in Sec. 1.3, there is no gauge invariance in our system and one cannot obtain a different branch-cut convention by a transformation of a_p and b_v . Indeed, such a transformation must have the form:

$$b_v \rightarrow b_v \left(\prod_p e^{i\pi a_p^\dagger a_p} \right), \quad a_p \rightarrow a_p \left(\prod_v e^{i\pi b_v^\dagger b_v} \right),$$

since they leave the parity operators invariant but change the parity products in pair-creation operators. But then some of the a_v and b_p operators anti-commute. However certain changes in the branch-cut conventions are permissible on a torus. For example by multiplying Eq. (2.14) with the global parity constraints (2.9), e -boson branch-cuts now go up instead of down along the left boundary and m -boson branch-cuts go up along the right boundary and terminate at the upper-right plaquette. Above also holds for the case of ε -fermions γ, γ' and b_v in Sec. 2.2.

2.2 Mapping between spins and e -boson and ε -fermions

Let us consider the mapping from the spin lattice to e, ε degrees of freedom.

2.2.1. Open Lattice

Again we start with the open lattice and consider the structure of the quasiparticle Hilbert space. As is discussed in Sec. 1.4, the spin Hilbert space can be rewritten in terms of local occupation numbers of e - and ε -fermions. The quasiparticle Hilbert space for e -bosons can then be established in the same way as in Sec. 2.1 using the hardcore boson construction, but with parity operator Γ_v^e instead of A_v :

$$\Gamma_v^e = A_v B_{\text{NE}(v)} \rightarrow \sigma_v^e, \quad \sigma_v^e \rightarrow \exp(i\pi b_v^\dagger b_v), \quad \tau_v^e \rightarrow b_v^\dagger + b_v. \quad (2.16)$$

The relation between τ_v^e and spin operators is given by Eq. (2.5).

Similarly we can define $\tau_p^\varepsilon, \sigma_p^\varepsilon$ operators in the basis of local ε -fermion occupation numbers. However, passing to the fermionic degrees of freedom is more complex than the hardcore boson case, due to the anti-commutation relation of fermions. It will be shown that Majorana operators γ_p, γ'_p describing ε -fermions can be defined in a two-dimensional analogue of Jordan-Wigner transformation using τ_p^ε and σ_p^ε . All fermion operators on different sites then anti-commute. Therefore as a first step, we establish the mapping from lattice operators to $\tau_p^\varepsilon, \sigma_p^\varepsilon$.

The mapping for σ_p^ε is:

$$\Gamma_p^\varepsilon \rightarrow \sigma_p^\varepsilon,$$

with Γ_p^ε given in (1.15). As for τ_p^ε , we write $\tau_p^m \tau_{\text{SW}(p)}^e$ defined in Sec. 2.1 that simultaneously creates an m -boson at plaquette p and an e -boson at the vertex to its South-West:

$$\left(\prod_{\substack{v_1, v_2 \in \\ C_e[\text{SW}(p)]}} Z_{v_1 v_2} \right) \times \left(\prod_{\substack{p_1, p_2 \in \\ C_m(p)}} X_{p_1 p_2} \right) \rightarrow \tau_p^\varepsilon. \quad (2.17)$$

Since $\Gamma_p^\varepsilon = B_p$, all necessary commutation relations are satisfied identically to the case of m -bosons; see the discussion below Eq. (2.4).

We now seek a two-dimensional Jordan-Wigner transformation for Majorana operators γ_p, γ'_p in the form:

$$\gamma_p = i \left(\prod_{p' \neq p} \sigma_{p'}^\varepsilon \right) \sigma_p^\varepsilon \tau_p^\varepsilon, \quad \gamma'_p = \left(\prod_{p' \neq p} \sigma_{p'}^\varepsilon \right) \tau_p^\varepsilon, \quad (2.18)$$

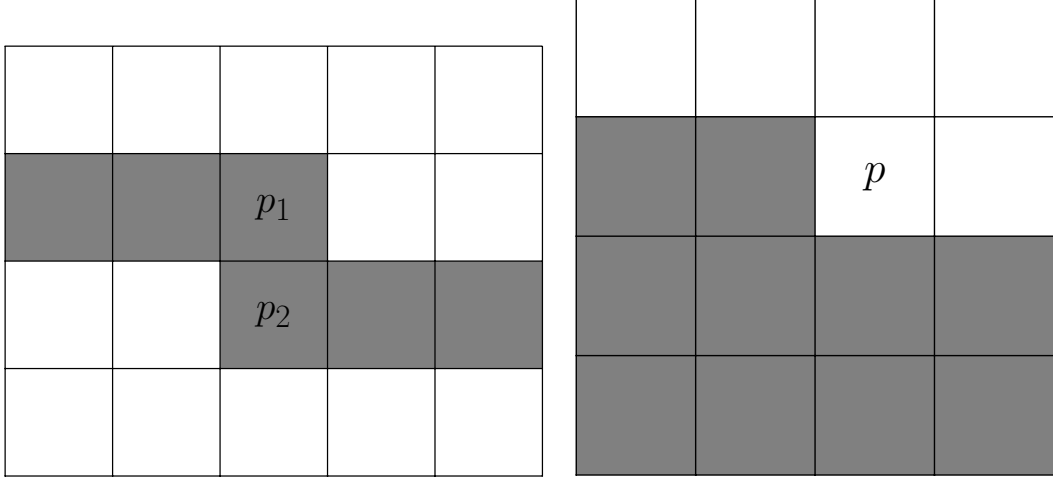


Figure 7: Left: visual illustration of mapping for vertical pair-creation operators in Eq. (2.21). The plaquettes in the non-local product of σ_p^ε is shaded in gray. Right: Convention for Jordan-Wigner transformation for γ_p and γ'_p at plaquette p in (2.18) for open lattices. The plaquettes shaded in gray are those in the non-local product of $\sigma_{p'}^\varepsilon$ in (2.18).

which are related to the complex ε -fermion annihilation operators by:

$$c_p = (\gamma_p + i\gamma'_p)/2.$$

This immediately gives for fermion parity:

$$\Gamma_p^\varepsilon \rightarrow \sigma_p^\varepsilon \rightarrow -i\gamma_p\gamma'_p = 1 - 2c_p^\dagger c_p, \quad (2.19)$$

as expected (we have used the identity $\gamma_p^2 = \gamma_p'^2 = 1$). To find the convention for the string of σ_p^ε products in (2.18), note that such a transformation should give the following mapping for the ε -fermion pair-creation operators (see Sec. 1.4):

$$U_{p_1 p_2}^\varepsilon \rightarrow i\gamma_{p_1}\gamma'_{p_2} \left(\prod_v e^{i\pi b_v^\dagger b_v} \right). \quad (2.20)$$

Since all horizontal $U_{p_1 p_2}^\varepsilon$ and $Z_{v_1 v_2}$ commute, we shall suppose that $U_{p_1 p_2}^\varepsilon \rightarrow i\gamma_{p_1}\gamma'_{p_2}$ and the e -boson branch-cuts extend also horizontally as in Sec. 2.1. It then follows from (2.17) that:

$$U_{p_1 p_2}^\varepsilon \text{ (horizontal)} \rightarrow \tau_{p_1}^\varepsilon \tau_{p_2}^\varepsilon \rightarrow i\gamma_{p_1}\gamma'_{p_2}.$$

Substituting Eq. (2.18) gives that the product of σ_p^ε for γ_p , γ'_p on the same row of plaquettes p_1 , p_2 start from the left and ends at the plaquette before p [remember that p_1 is to the left of p_2 and γ_{p_1} contains an extra $\sigma_{p_1}^\varepsilon$; see the comments below Eq. (1.17)].

We now consider vertical $U_{p_1 p_2}^\varepsilon$ with the unknown convention for e -boson branch-cuts. Expressing $U_{p_1 p_2}^\varepsilon$ in terms of spin operators for σ_v^ε , τ_p^ε and σ_p^ε :

$$U_{p_1 p_2}^\varepsilon \text{ (vertical)} \rightarrow - \left(\prod_{\substack{v \in \\ L(p_1, p_2)}} \sigma_v^\varepsilon \right) \left(\prod_{\substack{p \in \\ L(p_1), R(p_2)}} \sigma_p^\varepsilon \right) \tau_{p_1}^\varepsilon \tau_{p_2}^\varepsilon. \quad (2.21)$$

$L(p_1, p_2)$ includes all vertices to the left of the line joining p_1 and p_2 , $L(p_1)$ are all plaquettes to the left of plaquette p_1 on the same row *including* p_1 , and $R(p_2)$ are all plaquettes on the same row to the right of p_2 *including* p_2 . This is shown visually in Fig. 7. Note the additional minus sign. Comparing the τ_p^ε , σ_p^ε terms with (2.18) and (2.20), we obtain the following convention for $\sigma_{p'}^\varepsilon$ products in (2.18): for a given p , all plaquettes below the row of p are multiplied by $\sigma_{p'}^\varepsilon$; on the row of p , the $\sigma_{p'}^\varepsilon$ string contains all plaquettes to the left of p . This is shown explicitly in Fig. 7. As a result, γ_p and γ'_p on different plaquettes anti-commute. We have thus obtained for fermion pair-creation operators on an open lattice:

$$\text{Horizontal : } U_{p_1 p_2}^\varepsilon \rightarrow i\gamma_{p_1} \gamma'_{p_2} \quad (2.22a)$$

$$\text{Vertical : } U_{p_1 p_2}^\varepsilon \rightarrow i\gamma_{p_1} \gamma'_{p_2} \left(\prod_{\substack{v \in \\ L(p_1, p_2)}} e^{i\pi b_v^\dagger b_v} \right). \quad (2.22b)$$

As for e -bosons, since $B_p = \Gamma_p^\varepsilon \rightarrow -i\gamma_p \gamma'_p$, the arguments in Sec. 2.1 immediately lead to:

$$\text{Horizontal : } Z_{v_1 v_2} \rightarrow (b_{v_1}^\dagger + b_{v_1})(b_{v_2}^\dagger + b_{v_2}), \quad (2.23a)$$

$$\text{Vertical : } Z_{v_1 v_2} \rightarrow (b_{v_1}^\dagger + b_{v_1})(b_{v_2}^\dagger + b_{v_2}) \left(\prod_{\substack{p \in \\ R(v_1, v_2)}} -i\gamma_p \gamma'_p \right), \quad (2.23b)$$

where $R(v_1, v_2)$ are all plaquettes to the right of the edge joining vertices v_1 , v_2 .

In summary, Eqs. (2.16), (2.19), (2.22) and (2.23) solve the problem of mapping from an open spin lattice to the Hilbert space of quasiparticles e and ε . The gauge for e and ε quasiparticles are the following: for each π -vortex attached to an e -boson at vertex v , the branch-cut extends from v towards the right boundary on the same row and terminates there. Each π -vortex attached to an ε -fermion at plaquette p goes left towards the left boundary. The coincidence of branch-cut conventions with the (e, m) case is not accidental, because ε -fermions are composite particles of e - and m -bosons and their mutual statistics with another e -boson are determined by the m -boson.

2.2.2. Periodic Lattice

Let us now turn to the torus.

Similarly to the mapping to e -, m -bosons, the global parity constraints (1.16) for e -bosons and ε -fermions necessitate four global topological operators $T_{x,y}$ and $W_{x,y}$. These operators characterize the global topological sector of the quasiparticle Hilbert space and must be independent from local quasiparticle occupation. Therefore, they must commute with local parity operators Γ_v^e and Γ_p^ε . We can take $T_{x,y}$ to be still given by (1.6). As for the Wilson loop operators $W_{x,y}$, it must also commute with $U_{p_1 p_2}^\varepsilon$ since the global topological sector cannot be changed by fermion motion (this does not hold for the motion of e -bosons due to their non-local mutual statistics with ε -fermions). We have:

$$W_{x,y} = \prod \Gamma_{p_2}^\varepsilon U_{p_1 p_2}^\varepsilon = - \prod_{i \in \gamma_{x,y}} XZ, \quad [W_x, W_y] = 0, \quad \{W_{x,y}, T_{y,x}\} = 0; \quad (2.24)$$

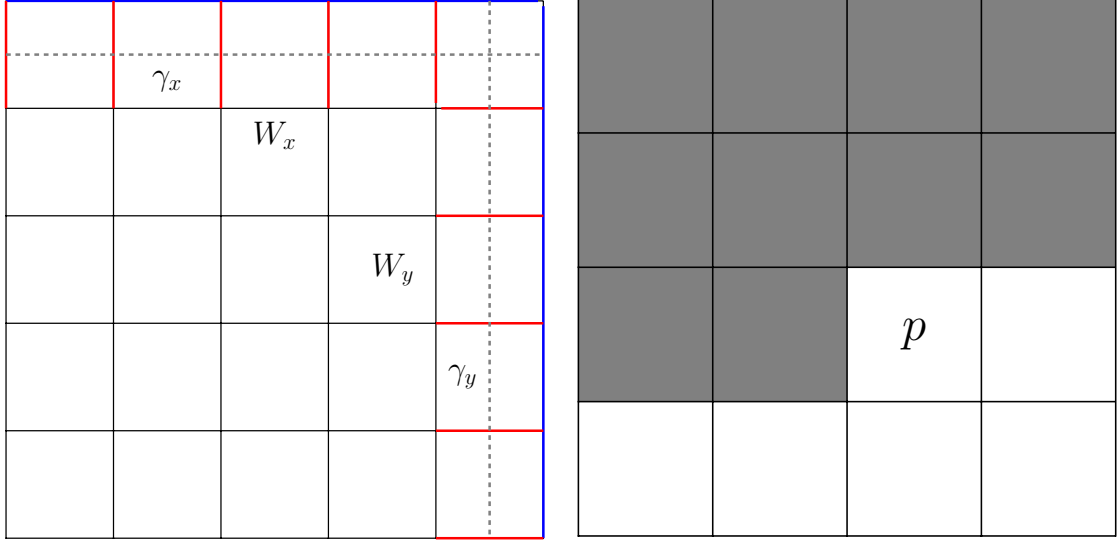


Figure 8: Left: global Wilson operators (2.24) for ε -fermions. Right: convention for Jordan-Wigner transformation for γ_p and γ'_p at plaquette p in (2.18) for periodic lattices. The plaquettes shaded in gray are those in the non-local product of $\sigma_{p'}^\varepsilon$ in (2.18).

see Fig. 8. Note the additional -1 . Eq. (2.24) can be seen as transporting an ε -fermion Majorana mode across the torus, as the parity operator transports a Majorana mode ‘within the plaquette’: $\gamma'_p \rightarrow \gamma_p$. The contours $\gamma_{x,y}$ are chosen here for later convenience, as they can be distorted by multiplication by Γ_v^e ; c.f. the (e, m) case at the end of Sec. 1.1.

We shall now discuss the mapping to the quasiparticle Hilbert space. It is clear from the previous discussions that the quasiparticle Hilbert space will contain the respective even-parity e -boson and ε -fermion sectors, as well as two \mathbb{Z}_2 indices $z_{1,2} = \pm 1$ corresponding to the eigenvalues of $W_{x,y}$:

$$W_{x,y} \rightarrow \hat{z}_{1,2}, \quad \hat{z}_i |\dots; z_i\rangle = z_i |\dots; z_i\rangle, \quad (2.25a)$$

$$T_{x,y} \rightarrow \hat{x}_{2,1}, \quad \hat{x}_i |\dots; z_i\rangle = |\dots; -z_i\rangle, \quad (2.25b)$$

and $\{x_i, z_i\} = 0$; c.f. with the (e, m) case (2.10).

Parity operators Γ_v^e and Γ_p^ε are mapped to σ_v^e and σ_p^ε respectively. As for τ operators, due to the parity even constraints (1.16), only $\tau_{p_0}^\varepsilon \tau_p^\varepsilon$ and $\tau_{v_0}^e \tau_v^e$ operators can be defined. The reference plaquette p_0 and vertex v_0 are the same as in Fig. 6. The $\tau_{v_0}^e \tau_v^e$ operators retain the same form as in Sec. 2.1. For $\tau_{p_0}^\varepsilon \tau_p^\varepsilon$, they create simultaneously a pair of m - and e -bosons at plaquettes p, p_0 and vertices v_0, v respectively as described in Sec. 2.1, where v is to the South-West of p due to the binding convention of ε -fermions. From here, the mapping to b_v and γ_p, γ'_p can be found in the same way as in the open lattice. Hence we shall simply state the results.

The Jordan-Wigner transformation that defines γ_p, γ'_p in Eq. (2.18) now has the following convention: for the given plaquette p , all rows above are multiplied by $\sigma_{p'}^\varepsilon$. On the given row, the product of all $\sigma_{p'}^\varepsilon$ includes all plaquettes to the left of p . See Fig. 8.

As a result, the mapping (2.19) for parity operators still holds. The global parity constraint (1.16) is then imposed so that only parity even states are allowed. We then have, for bulk ε -fermion pair-creation operators:

$$\text{Horizontal : } U_{p_1 p_2}^\varepsilon \rightarrow i\gamma_{p_1} \gamma'_{p_2} \quad (2.26a)$$

$$\text{Vertical : } U_{p_1 p_2}^\varepsilon \rightarrow i\gamma_{p_1} \gamma'_{p_2} \left(\prod_{\substack{v \in \\ R(p_1, p_2)}} e^{i\pi b_v^\dagger b_v} \right). \quad (2.26b)$$

$R(p_1, p_2)$ denotes all vertices to the right of the line joining p_1, p_2 . For motion across the boundary, note the additional non-local operators $W_{x,y}$, and that in the Jordan-Wigner transformation (2.18), p_1, p_2 are on two sides of the lattice in $i\gamma_{p_1} \gamma'_{p_2}$. Here as in the (e, m) case, one can first write out the products of X and Z operators for $W_{x,y}$ in (2.24) but with the paths along the row or column in question, then deform the paths to $\gamma_{x,y}$ by multiplying Γ_v^e . We obtain:

$$\text{Horizontal : } U_{p_1 p_2}^\varepsilon \rightarrow i\gamma_{p_1} \gamma'_{p_2} \left(\prod_{\substack{v \in \\ \text{row above} \\ p_1, p_2}} e^{i\pi b_v^\dagger b_v} \right) \hat{z}_1 \quad (2.27a)$$

$$\text{Vertical : } U_{p_1 p_2}^\varepsilon \rightarrow i\gamma_{p_1} \gamma'_{p_2} \left(\prod_{\substack{v \in \\ R(p_1, p_2)}} e^{i\pi b_v^\dagger b_v} \right) \hat{z}_2. \quad (2.27b)$$

The presence of $\hat{z}_{1,2}$ suggests that $W_{x,y} = \pm 1$ corresponds to periodic and anti-periodic boundary conditions for ε -fermions along the x - and y -directions. The quasiparticle Hilbert space then splits into four super-selection sectors given by $\{W_x, W_y\}$, with four combinations of the ε -fermion boundary conditions.

The mapping for e -boson spin operators has the same branch-cut convention as in the (e, m) case on a periodic lattice in Sec. 2.1, with fermion parity $-i\gamma_p \gamma'_p$ in place of $\exp(i\pi a_p^\dagger a_p)$. Inside the bulk we have:

$$\text{Horizontal : } Z_{v_1 v_2} \rightarrow (b_{v_1}^\dagger + b_{v_1})(b_{v_2}^\dagger + b_{v_2}), \quad (2.28a)$$

$$\text{Vertical : } Z_{v_1 v_2} \rightarrow (b_{v_1}^\dagger + b_{v_1})(b_{v_2}^\dagger + b_{v_2}) \left(\prod_{\substack{p \in \\ L(v_1, v_2)}} -i\gamma_p \gamma'_p \right). \quad (2.28b)$$

Across lattice boundaries:

$$\text{Horizontal : } Z_{v_1 v_2} \rightarrow (b_{v_1}^\dagger + b_{v_1})(b_{v_2}^\dagger + b_{v_2}) \left(\prod_{\substack{p \in \\ \text{row above } v_1, v_2}} -i\gamma_p \gamma'_p \right) \hat{x}_2, \quad (2.29a)$$

$$\text{Vertical : } Z_{v_1 v_2} \rightarrow (b_{v_1}^\dagger + b_{v_1})(b_{v_2}^\dagger + b_{v_2}) \left(\prod_{\substack{p \in \\ L(v_1, v_2)}} -i\gamma_p \gamma'_p \right) \hat{x}_1. \quad (2.29b)$$

As in the case of e, m quasiparticles, the motion of e -bosons across lattice boundaries cause transitions between the four super-selection sectors of the Hilbert space.

Eqs. (2.16), (2.19) and (2.25)-(2.29) solve the problem of mapping from a periodic spin lattice to the Hilbert space of quasiparticles e and ε .

2.2.3. Equivalence to the Honeycomb lattice

The construction in this subsection transfers the ‘elementary’ degrees of freedom from $1/2$ -spins on edges of square unit cells, to ε -fermions on plaquettes and e -bosons on vertices which are mutual ‘ π -vortices’ (here our discussion is confined to the infinite lattice). Equivalently, one can do away with the complex fermions c_p , and regard γ_p and γ'_p on the same plaquette on equal footing as Majorana modes on different sites. As is shown in Fig. 9, by suitably connecting the Majorana modes, the lattice can be seen as a distorted honeycomb lattice with a Majorana fermion on each site. Here we call attention to the fact that C_4 symmetry of the square lattice is broken due to the binding convention for ε -fermions. The choice for constructing the new honeycomb lattice is not unique; see Sec. 5.3 for another example.

The analogy to the honeycomb lattice carries even further. In fact on the new distorted honeycomb, the ε -fermions and e -bosons become naturally the Majorana modes and the bosonic π -vortices (the ‘visons’) of the Kitaev honeycomb model (1.3).

Let us show this equivalence. As is known, the honeycomb model (1.3) can be mapped to a model of Majorana bilinears [17]:

$$H = \frac{i}{4} \sum_{jk} J_{jk}^\alpha \hat{u}_{jk} c_j c_k, \quad (2.30)$$

where, slightly abusing the notation, we use c_i to denote Majorana modes on each site. J_{jk}^α are the couplings J_x, J_y, J_z depending on the links $\langle jk \rangle$ inside the honeycomb; see Fig. 1. The additional \hat{u}_{jk} are products of fictitious Majorana modes in the vortex sector and satisfy:

$$\prod_{j,k \in \text{honeycomb}} \hat{u}_{jk} = w_p, \quad (2.31)$$

where the product is taken over the edges of the the p -th honeycomb and $w_p = \pm 1$ corresponds to the absence or presence of a π -vortex at the center of the honeycomb.

By choosing the lattice conventions in Fig. 9, the nearest-neighbour Majorana couplings in (2.30) on the distorted honeycomb correspond to two-spin operators on the square lattice which is also reconstructed as a distorted honeycomb. They are [e -parity products are defined below Eq. (2.22)]:

$$U_{p_1 p_2}^\varepsilon = X_2 Z_1 \rightarrow i \gamma_{p_1} \gamma'_{p_2}, \quad U_{p_3 p_2}^\varepsilon = X_3 Z_2 \rightarrow i \gamma_{p_3} \gamma'_{p_2} \left(\prod_{\substack{v \in \\ L(p_3, p_2)}} e^{i\pi b_v^\dagger b_v} \right), \quad (2.32a)$$

$$U_{p_3 p_2}^\varepsilon \Gamma_{p_2}^\varepsilon U_{p_2 p_4}^\varepsilon = Y_3 Y_4 \rightarrow -i \gamma_{p_3} \gamma'_{p_4} \left(\prod_{\substack{v \in \\ L(p_3, p_2)}} e^{i\pi b_v^\dagger b_v} \right). \quad (2.32b)$$

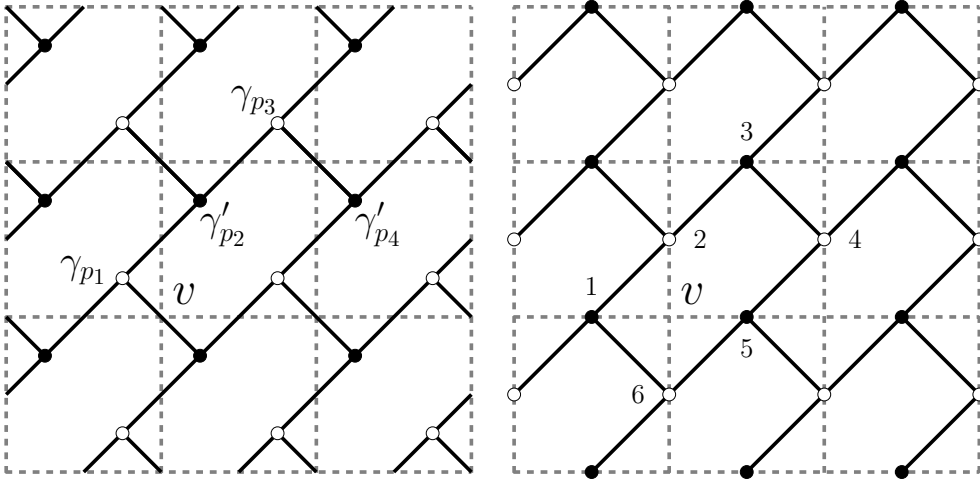


Figure 9: Left: reorganization of Majorana modes on the square lattice into the honeycomb lattice. The Majorana modes in Eq. (2.32) are shown explicitly. Right: spin lattice as distorted honeycomb lattice. White and black disks represent A, B sublattices. The spins and vertices in Eqs. (2.32) and (2.35) are shown explicitly.

Thus the following Hamiltonian on a square lattice reproduces the Majorana coupling in (2.30):

$$H = -J_x \sum_{x\text{-links}} Z_i X_j + J_y \sum_{y\text{-links}} Y_i Y_j - J_z \sum_{z\text{-links}} X_i Z_j, \quad (2.33)$$

where the x -, y -, z -links are the same as in Fig. 1 but defined on the distorted honeycomb in Fig. 9. Note the additional -1 in front of J_y . By making the following unitary transformation on spin operators at the A sublattice (indicated by the white disks in Fig. 9):

$$X_j \rightarrow Z_j, \quad Y_j \rightarrow -Y_j, \quad Z_j \rightarrow X_j, \quad (2.34)$$

the model (2.33) reduces to the original honeycomb model (1.3).

Finally, we verify that the e -bosons are indeed equivalent to the π -vortices. To check this, let us transport a Majorana mode along a honeycomb around vertex v using Eq. (2.32) without making the unitary transformation (2.34), as shown in Fig. 9:

$$(Y_1 Y_6)(X_5 Z_6)(X_4 Z_5)(Y_4 Y_3)(X_3 Z_2)(X_2 Z_1) = \Gamma_v^e. \quad (2.35)$$

This agrees with Eq. (2.31). Thus the e -boson at v is indeed the vortex at the center of the honeycomb. This proves the consistency of our construction.

Therefore, even though our mapping in this subsection is found for a square lattice, it can also be used to investigate \mathbb{Z}_2 topological order on the honeycomb lattice, as well as phenomena related to the honeycomb model. Here the mutual statistics between ‘vortices’ (e -bosons) and Majorana modes are taken into account *exactly* by the non-local e -parity terms in the couplings (2.32), without having to introduce an additional fictitious Majorana modes on each site.

3 Example: Bosonic \mathbb{Z}_2 Lattice Theory as two-dimensional Ising Model and Confinement of e -bosons

The mappings between spin and quasiparticles operators in Sec. 2 on a periodic lattice closely relate the torus geometry and properties of the quasiparticles. This in turn gives rise to non-trivial topological phases in a series of bosonic and fermionic models, which will be constructed and analyzed in Secs. 4-6. Therefore, before proceeding, it is useful to consider a simple model which nonetheless illustrates all the essential points of this interrelation. For simplicity, the elementary excitations are taken to be e and m and we use the mapping to the (e, m) Hilbert space.

The Hamiltonian that we consider in this section has \mathbb{Z}_2 symmetry due to global parity conservation (2.9):

$$\prod_{v \in \text{lattice}} \sigma_v^e = 1, \quad \prod_{p \in \text{lattice}} \sigma_p^m = 1,$$

and is chosen to be:

$$H = \Delta_e \sum_{\text{all } v} \left(\frac{1 - A_v}{2} \right) - t \sum_{\text{all } l} X_l, \quad (3.1)$$

where the summation is over all vertices in the first term and all edges of the squares in the second. Parameters $t, \Delta_e > 0$ are constant. The e -bosons are static and has a gap $2\Delta_e$ due to the first term in (3.1), while the second term is simply pair-creation operators of m -bosons in Eq. (1.8).

To solve (3.1), it is sufficient to map the Hamiltonian to τ, σ operators in the basis of local boson occupation number. The spin lattice is mapped to four Hilbert space sectors given by $z_1, z_2 = \pm 1$; see Sec. 2.1. In each of these sectors, we obtain an effective m -boson Hamiltonian corresponding to a given configuration of static e -bosons. For ground state properties (no e -bosons), we first consider the sector $z_1 = z_2 = 1$ with periodic B.C.s for m -bosons. Substituting Eqs. (2.7), (2.13)-(2.15) into (3.1) gives:

$$H = -t \sum_{\langle p, p' \rangle} \tau_p^m \tau_{p'}^m. \quad (3.2)$$

Recall that $b_v + b_v^\dagger = \tau_v^e$. We have mapped the problem to a 2D Ising model with ferromagnetic coupling. The ground state spontaneously breaks \mathbb{Z}_2 symmetry and is doubly-degenerate with average spontaneous moments $\langle \tau_p^m \rangle = \pm 1$. However, each of these ground states does not conserve total m -parity: $\prod_p \sigma_p^m$ causes a transition between them. The global parity constraint (2.9) then makes the physical ground state unique as a symmetric combination of the two states. In mapping to other sectors with anti-periodic boundary conditions for m -bosons, it is clear that the corresponding ground state energy increases by a term proportional to the lattice size, due to the anti-ferromagnetic coupling in the Hamiltonian along the boundaries. Therefore, the physical ground state for (3.1) is unique. This can be also seen directly by noting that the ground state is simply given by $A_v = X_l = 1$ on the spin lattice.

We now study the properties of e -bosons at low energies. Let us create two e -bosons connected by a horizontal path γ whose length L is small compared with lattice dimensions. The Hamiltonian in the sector $z_1 = z_2 = 1$ is:

$$H = -t \sum_{\langle p,p' \rangle \notin \gamma} \tau_p^m \tau_{p'}^m + t \sum_{\langle p,p' \rangle \in \gamma} \tau_p^m \tau_{p'}^m + 2\Delta_e. \quad (3.3)$$

The second term sums over all pairs of plaquettes intersected by γ , and the additional minus sign is a result of the branch-cut of e -bosons given in Eq. (2.13). The pair of e -bosons then have a large energy cost $\Delta E = 2tL$ linear in their distance: the e -bosons are *confined*. This result is of course ‘gauge-invariant’: it does not depend on the convention of the branch-cut, i.e. the e -bosons can be on different rows. For given two e -bosons on any two points of the lattice and an arbitrary branch-cut connecting them, we can connect them in the shortest path with length L on the lattice. The lowest energy state clearly corresponds to having a domain wall inside the region bounded by the branch-cut and the path, with energy cost $\Delta E = 2tL$ as before.

4 \mathbb{Z}_2 vortices in an ideal gas of anyons with $U(1)$ global symmetry

In Sec. 3, it is shown that in a specific model with \mathbb{Z}_2 symmetry, e -bosons are strongly confined with a interaction potential linear in their distance. In this section, we shall study the properties of static e -bosons placed in ideal gases of m -bosons and ε -fermions on an open lattice at zero and finite temperatures. In each case, the particle number, not just parity, is conserved and the system has global $U(1)$ symmetry. Due to the hardcore-boson constraint, the m -bosons form a finite density Bose-Einstein condensate even at zero temperature. The pair-interaction energy of e -bosons depends logarithmically on their mutual distance at asymptotically large separations. The e -bosons are thus *marginally deconfined*. In an ideal fermi-gas of ε -fermions, the e -bosons are *deconfined*: they are completely screened by the fermions and their interaction energies tend to a finite limit at large separations.

4.1 Static e -vortices in an ideal m -boson gas

Global $U(1)$ symmetry for the m -bosons implies the conservation of m particle number. What are the operators that have such a symmetry? The local parity operator $B_p \rightarrow 1 - 2a_p^\dagger a_p$ conserves particle number by definition. The pair-creation operator $X_{p_1 p_2}$ conserves global m -boson parity but not its number. The operator that conserves m -boson number and transports an m -boson from p_1 to p_2 is:

$$X_{p_1 p_2} \left(\frac{1 - B_{p_1}}{2} \right) \left(\frac{1 + B_{p_2}}{2} \right). \quad (4.1)$$

Here $(1 \pm B_p)/2$ projects the corresponding plaquette to m -boson occupation number $n_p^m = 1, 0$ respectively. Therefore, Eq. (4.1) is non-zero only if p_1 is occupied and p_2 is empty in the initial state. The pair-creation operator $X_{p_1 p_2}$ then transports the m -boson from p_1 to p_2 .

Then the local Hamiltonian for free m -bosons which conserves particle number is:

$$H = -t \sum_{p_1, p_2} X_{p_1 p_2} \left(\frac{1 - B_{p_1}}{2} \right) \left(\frac{1 + B_{p_2}}{2} \right) + \Delta_e \sum_{\text{all } v} \left(\frac{1 - A_v}{2} \right) + \Delta_m \sum_{\text{all } p} \left(\frac{1 - B_p}{2} \right). \quad (4.2)$$

Since we are interested in the confinement properties of e -bosons, we consider an open lattice for simplicity. According to Sec. 2.1, after ‘bosonization’ we obtain a non-local Hamiltonian in terms of quasiparticle fields. However, in this section we are only concerned with the energy levels of the system in the presence of static e -bosons. It is therefore permissible to choose a different ‘gauge’, by regarding each e -boson as a point magnetic vortex which in turn generates a vector potential \mathbf{A} coupled minimally to m -bosons. The local vector potential then replaces the non-local e -parity terms in the hopping amplitude. With this in mind, we substitute Eqs. (2.13)-(2.15) into (4.2) and obtain the following Hamiltonian for m -bosons:

$$H = -t \sum_{\langle p, p' \rangle} \left(e^{iA_{pp'}} a_p^\dagger a_{p'} + e^{-iA_{pp'}} a_{p'}^\dagger a_p \right) + \Delta_m \sum_{\text{all } p} a_p^\dagger a_p + \Delta_e \sum_{\text{all } v} b_v^\dagger b_v. \quad (4.3)$$

$A_{pp'}$ is the vector potential along the edge given by p, p' and satisfies:

$$\prod_{\langle p, p' \rangle \in \partial M} e^{iA_{pp'}} = \exp \left(i\pi \sum_{v \in M} n_v^e \right), \quad (4.4)$$

where M is a given bounded region and the product is taken over plaquettes along its boundary ∂M .

We shall calculate the interaction energies of static e -bosons with small densities for (4.3). At sufficiently low-temperatures, the m -bosons at zero momentum form a Bose-Einstein condensate. The m -boson field-operators thus acquire a non-zero vacuum expectation value on each plaquette:

$$\langle a_p \rangle = \frac{1}{2} (\langle \tau_p^m \rangle + \langle \sigma_p^m \tau_p^m \rangle) = \sqrt{\rho} e^{i\phi},$$

Due to the macroscopic occupation number of the condensate bosons, the ‘condensate wave-function’ $\Psi_m \sim \langle a_p \rangle$ is quasi-classical and the condensate density ρ and phase ϕ are well-defined functions of coordinates. At low energies, the gapless Goldstone modes correspond to the breaking of $U(1)$ symmetry by the condensate phase ϕ . We can then assume ρ to be constant (ρ of course depends on the temperature) and write down the Ginzburg-Landau free energy for the model (4.3):⁶

$$F[\phi] = \int \frac{\rho}{2} |(\nabla - i\mathbf{A}) \Psi_m|^2 d^2x = \int \frac{\rho}{2} (\nabla\phi - \mathbf{A})^2 d^2x.$$

We choose the Coulomb gauge $\nabla \cdot \mathbf{A} = 0$. This gives for the free energy, after integration by parts:

$$F[\phi] = \int \frac{\rho}{2} \left[(\nabla\phi)^2 + \mathbf{A}^2 \right] d^2x. \quad (4.5)$$

The second term in Eq. (4.5) includes the interaction energies of e -bosons and determines their confinement properties.

We now calculate the free energy (4.5) for static e -bosons with small densities. The continuum limit of Eq. (4.4) for the vector potential \mathbf{A} is:

$$\oint \mathbf{A} \cdot d\mathbf{r} = \sum_i \Phi_i \rightarrow \nabla \times \mathbf{A} = \sum_i \Phi_i \delta(\mathbf{r} - \mathbf{r}_i) \mathbf{n}_z, \quad (4.6)$$

where the sum is over all e -bosons with vortices $\Phi_i = \pi$ enclosed by the loop and \mathbf{r}_i is their respective position. \mathbf{n}_z is the directional vector along the z -axis. Eq. (4.6) formally corresponds to the limit of small Ginzburg-Landau parameter $\kappa = \delta/\xi \ll 1$ in a conventional superconductor under external magnetic field, where δ is the penetration length of the magnetic field and ξ is the correlation length of the condensate. Note that in an actual

⁶In fact, the condensate density ρ vanishes near a single vortex with size ξ and only tends to a constant at distance $r \gg \xi$. In taking ρ constant, we have assumed that the vortex size is negligible; see below Eq. (4.8).

superconductor, the vortices are metastable in the limit $\kappa \ll 1$ due to the surface tension between the normal and superconducting phases [73].

In what follows it is more convenient to rewrite \mathbf{A} as:

$$A_x = -\frac{\partial\psi}{\partial y}, \quad A_y = \frac{\partial\psi}{\partial x}.$$

The gauge condition $\nabla \cdot \mathbf{A} = 0$ is then satisfied identically and Eq. (4.6) becomes:

$$\Delta\psi = \sum_i \Phi_i \delta(\mathbf{r} - \mathbf{r}_i).$$

The real solution for ψ is, up to a constant:

$$\psi = \sum_i \frac{\Phi_i}{2\pi} \log \frac{|\mathbf{r} - \mathbf{r}_i|}{\xi}. \quad (4.7)$$

Substituting Eq. (4.7) into the second term of Eq. (4.5) and integrating by parts gives:

$$-\frac{\rho}{2} \int \psi \Delta\psi \, d^2x = \sum_{\text{all } i} \left(E_c(\Phi_i) - \frac{\rho}{2\pi} \sum_{i \neq j} \Phi_i \Phi_j \log \frac{|\mathbf{r}_i - \mathbf{r}_j|}{\xi} \right), \quad (4.8)$$

where E_c corresponds to the self-interaction energy of a vortex and formally diverges logarithmically. We impose an upper cut-off at the system size R and a lower cut-off at the size of a single vortex ξ . Then $E_c \sim \log(R/\xi)$. Eq. (4.8) is derived by assuming that the vortex size ξ is negligible. Including effects due to finite ξ leads to subsequent terms in powers of the ratio ξ/d , where d is the average distance between e -bosons. The requirement $\xi \ll d \sim n^{-1/2}$ determines the condition on the average density n of e -bosons.

Eq. (4.8) shows that the mutual potential for e -bosons is logarithmic at large distances: they are *marginally deconfined* in a Bose-Einstein condensate of m -bosons. This is in sharp contrast to both their strong linear confinement in the confined phase of \mathbb{Z}_2 lattice gauge theory considered in Sec. 3, and full deconfinement in the Toric Code. Moreover, in this case the Coulomb phase remains separated by a BKT transition [74–76] from the Toric Code phase even at finite temperature. This contrast with the confined phase of \mathbb{Z}_2 lattice gauge theory, which is smoothly connected to the Toric Code at finite temperature [3]. In this sense, one could say that the m -boson superfluid is more robust at finite temperature.

Finally, we discuss the situation on a torus and consider its geometric effects on the ground state of (4.2). After mapping to m -bosons (there are no e -bosons) we obtain the same Hamiltonian (4.5), but the vector potential \mathbf{A} must incorporate the B.C.s of m -bosons. For example, for $(z_1, z_2) = (1, -1)$:

$$\int_0^{L_x} A_x dx = 0, \quad \int_0^{L_y} A_y dy = \pi.$$

We choose a constant solution $A_x = 0$, $A_y = \pi/L_y$ which satisfies the Coulomb gauge. The second term in (4.5) then gives an additional energy costs $\pi^2 \rho L_x / (2L_y)$. In summary, we have for different (z_1, z_2) :

$$\Delta F|_{(z_1, z_2)=(1,1)} = 0, \quad (4.9)$$

$$\Delta F|_{(z_1, z_2)=(-1,1)} = \frac{\pi^2 \rho L_y}{2 L_x}, \quad (4.10)$$

$$\Delta F|_{(z_1, z_2)=(1,-1)} = \frac{\pi^2 \rho L_x}{2 L_y}, \quad (4.11)$$

$$\Delta F|_{(z_1, z_2)=(-1,-1)} = \frac{\pi^2 \rho L_x^2 + L_y^2}{2 L_x L_y}. \quad (4.12)$$

We conclude that on a torus, the ground state of (4.2) is unique, characterized by:

$$(W_x^{\text{TC}}, W_y^{\text{TC}}) \rightarrow (z_1, z_2) = (1, 1),$$

corresponding to the ground state of the m -boson Hilbert space with periodic B.C.s. The energy differences to ground states of other sectors depend on the aspect ratio of the lattice.

4.2 Static e -vortices in an ideal ε -fermion gas

We now turn to the confinement properties of e -bosons in an ideal gas of ε -fermions with global $U(1)$ symmetry. Similarly to Eq. (4.1), the conservation of ε -fermion number gives the following fermion transport operator from p_1 to p_2 :

$$U_{p_1 p_2}^\varepsilon \left(\frac{1 - \Gamma_{p_1}^\varepsilon}{2} \right) \left(\frac{1 + \Gamma_{p_2}^\varepsilon}{2} \right). \quad (4.13)$$

and we obtain the free fermi-gas Hamiltonian on an open lattice:

$$H = -t \sum_{p_1, p_2} U_{p_1 p_2}^\varepsilon \left(\frac{1 - \Gamma_{p_1}^\varepsilon}{2} \right) \left(\frac{1 + \Gamma_{p_2}^\varepsilon}{2} \right) + \Delta_e \sum_{\text{all } v} \left(\frac{1 - \Gamma_v^\varepsilon}{2} \right) + \Delta_\varepsilon \sum_{\text{all } p} \left(\frac{1 - \Gamma_p^\varepsilon}{2} \right). \quad (4.14)$$

The arguments leading to the m quasiparticle Hamiltonian (4.3) now give for (4.14):

$$H = -t \sum_{\langle p, p' \rangle} \left(e^{iA_{pp'}} c_p^\dagger c_{p'} + e^{-iA_{pp'}} c_{p'}^\dagger c_p \right) + \Delta_\varepsilon \sum_{\text{all } p} c_p^\dagger c_p + \Delta_e \sum_{\text{all } v} b_v^\dagger b_v, \quad (4.15)$$

where $A_{pp'}$ satisfies Eq. (4.4). For a given fermionic system, the presence of $A_{pp'}$ changes the energy levels which incorporate the energy from e -bosons. The confinement properties of e -bosons are then determined by the difference between total energies of $N \rightarrow \infty$ number of ε -fermions with and without a single vortex:

$$\Delta E = \lim_{N \rightarrow \infty} [E(N, \Phi = \pi) - E(N, \Phi = 0)]. \quad (4.16)$$

If the e -boson is confined, ΔE should tend to infinity with lattice size. For a deconfined e -boson, ΔE tends to a constant as the e -boson is completely screened by fermions.

It will be shown below that the vortex is completely screened by the fermions with a finite correlation length for arbitrary ε -fermion filling fraction. Given that on a square lattice, the ε -fermion dispersion is approximately parabolic in the limit of small filling fractions, we expect that our results in this section at small filling will be reproduced for a free fermion Hamiltonian with parabolic dispersion, as long as the system dimension is much larger than the correlation length. This will be verified in Appendix B, which confirms the correctness of the approach in this section.

Returning to the square lattice, we numerically compute Eq. (4.16) for the model (4.15) on an open lattice. The periodic lattice case is not considered here. In order to study the properties of e -bosons in the thermodynamic limit, we introduce a chemical potential μ and a finite temperature T . This leads to the Fermi-Dirac occupation $n_F(E, \mu, T)$ for single particle states of energy E , and the following expressions for the total energy and particle number:

$$n_F(E, \mu, T) = \frac{1}{\exp[(E - \mu)/T] + 1}, \quad (4.17a)$$

$$N(\Phi, \mu, T) = \sum_{i=1}^{\infty} n_F(E_i, \mu, T), \quad (4.17b)$$

$$E(\Phi, \mu, T) = \sum_{i=1}^{\infty} n_F(E_i, \mu, T) E_i(\Phi), \quad (4.17c)$$

where i is a label for all the single particle states and the Boltzmann constant k_B is taken unity. The difference in total energies is then due to the shift of single-particle energy levels E_i in the field produced by an e -boson as a point vortex.

We take lattices with an odd number of plaquettes so that the vortex can be placed in a unique central plaquette. To characterize the differences between ground states with and without the vortex in the thermodynamic limit, we must first take the limit $T \rightarrow 0$ then $N \rightarrow \infty$ in Eq. (4.16). Fig. 10 illustrates the energy cost to insert the vortex in the thermodynamic limit at $T \rightarrow 0$, which we find to remain finite regardless of the lattice filling of the ε -fermions. This energy cost can be equivalently determined by computing the energy difference between the states with and without the vortex with fixed ε particle number, as shown in Fig. 10a), or by computing the difference in the thermodynamic potential, $\Delta F = \Delta E - \mu \Delta N$, at fixed chemical potential, as shown in Fig. 10b). We have verified numerically that both ways of computing provide the same energy value for the insertion of the vortex in the thermodynamic limit, as shown in Fig. 10c). Interestingly, this value approaches zero as $T \rightarrow 0$. Thus the e -boson remains fully deconfined in an ideal gas of ε -fermions with global $U(1)$ symmetry. Finally, to find correspondence with the free parabolic dispersions in Appendix B, Fig. 10d) shows the energy difference at fixed N and low filling fraction in units of fermi energy ϵ_F :

$$\lim_{N \rightarrow \infty} \{E(N, \Phi = \pi) - E(N, \Phi = 0)\}_{T=0} = \frac{\epsilon_F}{8}; \quad \epsilon_F = \mu + 4t, \quad (4.18)$$

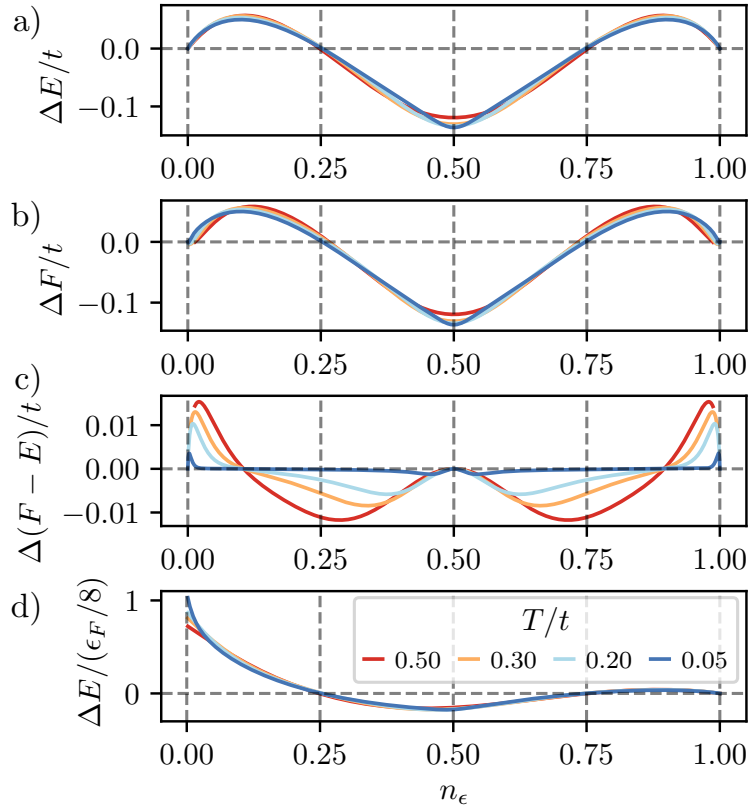


Figure 10: a) Energy difference between the π -vortex and empty configurations at fixed particle density n_ϵ . b) Difference in the thermodynamic potential ΔF between the π -vortex and empty configurations at fixed chemical potential μ . c) Difference $\Delta(F - E)$ between the energy values of a) and b). d) At fixed particle number N , the energy difference in units of fermi energy. Here $\epsilon_F = \mu - E_0$, with $E_0 = -4t$ is the energy of the bottom of the band. Results are obtained with the lattice model (4.15) and 120×120 plaquettes.

where $-4t$ is the energy of the bottom of the band.

We now turn to the change in ϵ -fermion number due to the vortex. The deconfinement of e -bosons implies that they are completely screened by ϵ -fermions. The density of the screening fermion cloud depends on the filling fraction. We check this explicitly. Fig. 11a) shows the total particle number difference between the state with and without the vortex as a function of ϵ filling-fractions. Generally, a single e -vortex can increase or decrease fermion density near itself, as can be seen in Fig. 11a). The precise value of this fraction depends on the filling fraction. Note that $\Delta N = 0$ at the three special fillings, marked by dots in Fig. 11a). At small fillings, it approaches the value $\Delta N = -1/8$. This is consistent with (4.18), as can be understood by considering adiabatically inserting the vortex into the system. The change in total energy is:

$$\Delta E = \Delta E|_N + \frac{\partial E}{\partial N} \Delta N.$$

The first term is the change due to a shift of the single-particle levels at constant N , and the second term corresponds to the change due to the change in particle number N at constant

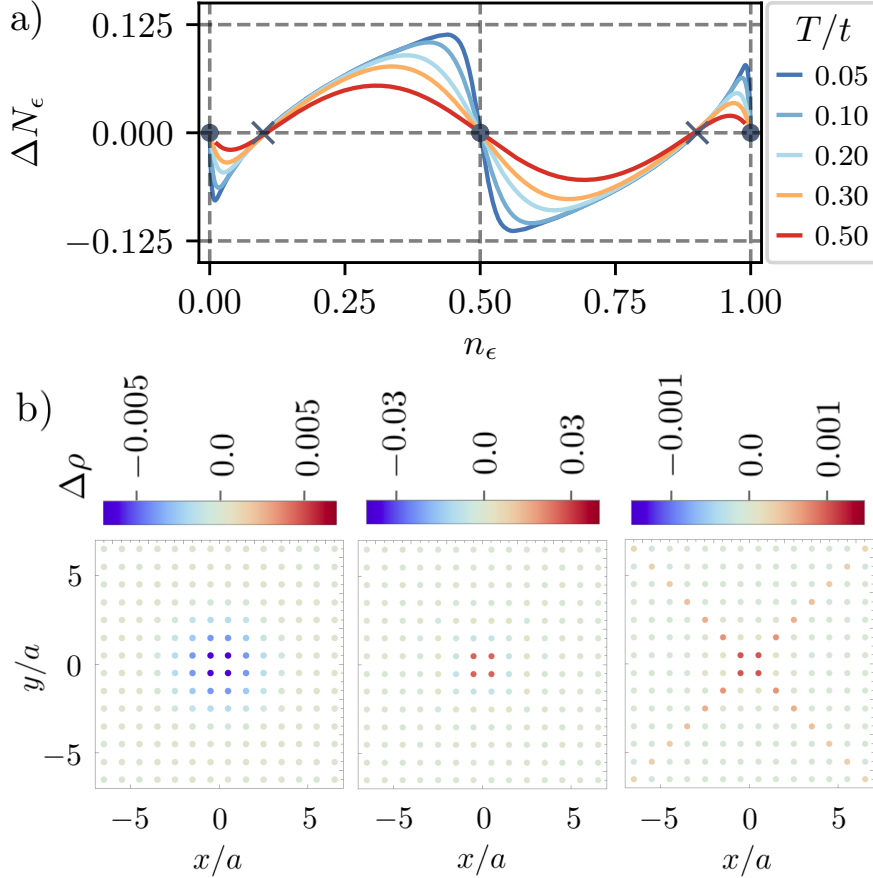


Figure 11: a) Particle number difference between the π and zero flux configurations at fixed chemical potential μ . The dots (crosses) indicate the fillings that are stable (unstable) to dilute insertions of e -bosons. b) From left to right, local density difference between having a π -vortex and no vortices near the fillings $n_\epsilon = 0, 1/4$ and $1/2$, respectively. Results are obtained with the lattice model (4.15) on 120×120 plaquettes and temperature $T/t = 0.05$.

μ , as single-particle levels are shifted. By definition $\Delta E = 0$ since no work is done on the system and $\Delta E|_N$ is just Eq. (4.18). This gives:

$$\Delta E \Big|_N = -\epsilon_F \Delta N.$$

It follows that by comparing with (4.18) $\Delta N = -1/8$ at low filling, as is indeed the case.

From Fig. 11a), one can see that the difference in the thermodynamic density of states with and without the vortex:

$$\Delta\nu_F = \left. \frac{\partial N(\mu, T)}{\partial \mu} \right|_{\Phi=\pi} - \left. \frac{\partial N(\mu, T)}{\partial \mu} \right|_{\Phi=0} \quad (4.19)$$

is sharply peaked at fillings $0, 1/2, 1$. This reflects the states in the energy resolved spectrum from which the screening cloud of ϵ particles is primarily made out of. Thus (4.18) can also be

understood by noting that when inserting the vortex, a fraction of particles is removed deep below the Fermi level due to the change of density of states. The fraction is redistributed to states near half filling when the vortex is inserted at fixed particle number.

Lastly, we also investigate the spatial structure of the fermion cloud excited by the vortex. As shown in Fig. 11b), the additional ε -fermions are localized near the vortex at various fillings, although its precise shape changes with the behavior near $1/2$ filling being sharply anisotropic resembling the underlying C_4 symmetry of the lattice. The apparently long-range nature of the fermion cloud at $1/2$ filling might be related to the van-Hove singularities present in the density of states in the tight-binding approximation on the square lattice.

5 \mathbb{Z}_2 Topological Order of Superconducting ε -fermions Enriched by Lattice Translation Symmetry

So far we have considered static e -bosons on a background of ideal gas of m or ε quasiparticles. The results depend on the global symmetry of the system and illustrate the effects of global invariants (Wilson loop operators) due to lattice periodicity. However the mappings in Sec. 2 can also be used to construct m - or ε -Hamiltonians that are in themselves ‘topological’ regardless of periodicity of the spin lattice. In this section and Sec. 6 we only consider \mathbb{Z}_2 spin Hamiltonians that map to ‘topological superconductors’: the ε -fermions form a condensate of Cooper pairs and the superconducting ground state admits classification by certain global invariants; see Appendix C. The e -bosons are stationary. The models constitute what is called \mathbb{Z}_2 topological order ‘enriched by lattice translation symmetry’ [45, 47] due to the presence of the lattice.

We will discuss the general interrelation between \mathbb{Z}_2 topological order and topological superconductivity. This makes possible explaining ground state properties of the \mathbb{Z}_2 spin models that we consider, which contain no e -bosons. This constitutes the primary focus of this section and we defer to Sec. 6 the study of emergent properties of e -bosons on top of the superconducting vacuum. Lastly, we shall show that the Kitaev Honeycomb model [17] is equivalent to the model considered in this section.

5.1 Relation between \mathbb{Z}_2 Topological Order and Topological Superconductivity

Let us consider spin Hamiltonians that can be mapped to Majorana bilinears and free, static e -bosons. For classification purposes we assume that there are no e -bosons. Generally, such a quasiparticle Hamiltonian has inversion symmetry, and can be written in quasimomentum and particle-hole space as:

$$H = \frac{1}{2} \sum_{\mathbf{k}} \Psi^\dagger(\mathbf{k}) \begin{pmatrix} \varepsilon(\mathbf{k}) & \Delta(\mathbf{k}) \\ \Delta^*(\mathbf{k}) & -\varepsilon(\mathbf{k}) \end{pmatrix} \Psi(\mathbf{k}); \quad \Psi(\mathbf{k}) = \begin{pmatrix} c_{\mathbf{k}} \\ c_{-\mathbf{k}}^\dagger \end{pmatrix}. \quad (5.1)$$

where $\varepsilon(\mathbf{k})$ is the fermion dispersion and $\Delta(\mathbf{k}) = \langle c_{\mathbf{k}} c_{-\mathbf{k}} \rangle$ is the gap function.

The classification of topological superconductors is reviewed in detail in Appendix C. Here we only summarize the results. On an infinite lattice, each Hamiltonian of the form (5.1) can be classified by the integer Chern number C and four global \mathbb{Z}_2 invariants $\{\zeta_1, \dots, \zeta_4\}$ corresponding to the ground state fermion number at the four high-symmetry quasimomenta \mathbf{k}_{0i} in the Brillouin zone:

$$\mathbf{k}_{0i} = \{(0, 0), (0, \pi), (\pi, 0), (\pi, \pi)\}, \quad \zeta_i = 1 - \Theta[\varepsilon(\mathbf{k}_{0i})], \quad (5.2)$$

where $\Theta(x)$ is the step function. The ground state contains a fermion at quasimomenta \mathbf{k}_{0i} if $\zeta_i = 1$ and $\zeta_i = 0$ otherwise. The four \mathbb{Z}_2 invariants are related to the Chern number by the following identity [51]:

$$(-1)^C = \prod_i^4 (-1)^{\zeta_i}. \quad (5.3)$$

Therefore each superconducting phase can be characterized by the integer Chern number C and three of the four \mathbb{Z}_2 invariants in a $\mathbb{Z} \times (\mathbb{Z}_2)^3$ scheme.

So far the classification scheme refers to superconducting Hamiltonians on an infinite lattice. On a finite torus the classification scheme remains valid and, as we shall see, is closely related to properties of the \mathbb{Z}_2 topological order of the original spin Hamiltonian.

In going over to a finite, periodic lattice, quasimomentum becomes discrete depending on the boundary conditions and lattice size:

$$k_{x,y} = \frac{2\pi n}{L_{x,y}} \text{ (periodic B.C.s)}, \quad k_{x,y} = \frac{(2n+1)\pi}{L_{x,y}} \text{ (anti-periodic B.C.s)}; \quad n \in \mathbb{Z}. \quad (5.4)$$

The relation of the classification scheme to \mathbb{Z}_2 topological order on a finite torus is then the following. From the torus a given spin Hamiltonian is mapped to four quasiparticle Hamiltonians corresponding to the four super-selection sectors $\{z_1, z_2\}$ with the corresponding ε -fermion boundary conditions; remember that $z_{1,2} = \pm 1$ corresponds to periodic or anti-periodic boundary conditions for ε -fermions along x -, y -directions. The ground states from all sectors are degenerate (however the degeneracy might be removed by dynamics of e -bosons). In each sector, the ground state parity is determined by fermion occupation numbers on the four \mathbf{k}_{0i} points, namely by the four \mathbb{Z} invariants $\{\zeta_i\}$ which are the same across all sectors. For a given $\zeta_i = 1$, the ground state only contains the fermion at \mathbf{k}_{0i} if \mathbf{k}_{0i} is allowed by quasimomentum quantization (5.4). Thus in a given super-selection sector the fermion parity for an eigenstate in phases with non-zero $\{\zeta_i\}$ can depend on the lattice size. However, due to the global parity constraint (1.16), only even fermion-parity states across super-selection sectors remain as the actual, physical states of the original spin Hamiltonian. It is then clear that the fermion parity of each state changes with the lattice size if the fermion Hamiltonian is in a phase with non-zero $\{\zeta_i\}$.

As an immediate result of the discussions above, the ground state degeneracy of the spin Hamiltonian can depend on lattice size for a phase with non-zero $\{\zeta_i\}$. To make this statement more precise, one considers a given set of $\{\zeta_i\}$ and the four sectors given by $\{z_1, z_2\}$. In each sector and for each $\zeta_i = 1$, one then determines from (5.4) if the corresponding \mathbf{k}_{0i} is allowed under different lattice sizes. This will determine the ground state parity in each sector and, accordingly, the number of physical parity-even ground states. It turns out that for given $\{\zeta_i\}$, the ground state degeneracy depends only on if $L_{x,y}$ is even or odd. The result is then summarized in table 1 [49]; see Sec. 5.2.3 below for a detailed example. We mention here in passing a series of works [17, 48, 49, 52, 68–71], in which lattice-size-dependent ground state degeneracy in \mathbb{Z}_2 topological order with translation symmetry has also been discovered.

Finally, the $\mathbb{Z} \times (\mathbb{Z}_2)^3$ classification scheme is based on single-particle superconducting models with lattice translation symmetry. The question naturally arises of its stability against interactions and disorder. In fact, it is known that certain symmetry protected topological superconducting phases, such as 1D superconductors with $T^2 = +1$ time-reversal (1D BDI class), are not stable against interactions. There interaction effects break the single-particle \mathbb{Z} classification down to \mathbb{Z}_8 [77–80]. Other examples include Refs. [55–58, 81–83].

	(e-e)	(o-e)	(e-o)	(o-o)		(e-e)	(o-e)	(e-o)	(o-o)
(0000)	4	4	4	4	(0110)	4	2	2	2
(1000)	3	3	3	3	(0101)	4	2	4	2
(0100)	3	3	3	3	(0011)	4	4	2	2
(0010)	3	3	3	3	(1110)	3	3	3	1
(0001)	3	3	3	3	(1101)	3	3	3	1
(1100)	4	4	2	2	(1011)	3	3	3	1
(1010)	4	2	4	2	(0111)	3	3	3	1
(1001)	4	2	2	2	(1111)	4	4	4	-

Table 1: Ground state degeneracy for all combinations of $\{\zeta_i\}$ and system size. (e-o) corresponds to L_x even and L_y odd for example. In the entry (1111), $-$ means the degeneracy is macroscopic, i.e. proportional to system size; see the discussions in 5.2.2 below. The table is taken from Ref. [49].

However, we provide some simple arguments that the bulk topological properties should be stable against disorder and interaction effects.

First, the Chern number C is expected to be stable against interactions. Second, we can provide an alternative definition of the \mathbb{Z}_2 parity indices $\{\zeta_i\}$ in terms of many-body properties without reference to the single particle BdG spectrum. This can be done by noting that when the system is placed on a torus with L_x and L_y both odd, $\{\zeta_i\}$ can be defined as the parity of the many-body fermion ground state, $N_f \bmod 2$, under periodic and anti-periodic fermion boundary conditions as follows:

$$\{\zeta_1, \zeta_2, \zeta_3, \zeta_4\} = \{N_f(1, 1), N_f(1, -1), N_f(-1, 1), N_f(-1, -1)\} \bmod 2, \quad L_{x,y} \text{ odd.} \quad (5.5)$$

Here $N_f(z_1, z_2)$ is the ground state fermion number in the super-selection sector $\{z_1, z_2\}$. Since fermion parity of the many-body ground state will not change by adding interactions, unless a bulk-gap closing phase transition is induced, the \mathbb{Z}_2 parity indices will remain quantized to be $\zeta_i = 0, 1$ and the $\mathbb{Z} \times (\mathbb{Z}_2)^3$ classification of translationally invariant superconductors is expected to remain stable upon adding fermion interactions. One can argue for the stability of $\mathbb{Z} \times (\mathbb{Z}_2)^3$ topological phases against disorder along similar lines, because disorder is not expected to change the fermion parity of a many-body gapped state unless a bulk phase transition occurs. Previously the robustness of ‘weak’ topological systems⁷ against disorder has been emphasized in the case of time-reversal-invariant weak topological insulators [84, 85] and topological superconductors with other symmetries [86].

⁷‘Weak’ topological systems, i.e. the KW phases in Sec. 5.2.3 and Appendix D which are stacks of one-dimensional Kitaev wires, are stackings of lower-dimensional topological systems. Sometimes in the literature, an alternative definition is used: the eigenstates of ‘weak topological systems’ defined on the Brillouin zone cannot be classified by homotopy groups, whereas those of ‘strong’ topological systems can be; see Appendix C for a detailed formulation of the conditions for topological classification.

5.2 Model

We now illustrate the points made so far in this section with a concrete model in tori. The Hamiltonian is taken to be:

$$H = -h_x \sum_{p \in \text{horizontal}} U_{p_1 p_2}^\varepsilon - h_y \sum_{p \in \text{vertical}} U_{p_1 p_2}^\varepsilon - h_z \sum_p \Gamma_p^\varepsilon - \Delta_e \sum_v \Gamma_v^e, \quad (5.6)$$

where h_x, h_y and h_z are real parameters and $\Delta_e > 0$ is a constant energy gap for the e -bosons. The first summation in (5.6) includes all horizontal nearest-neighbour $U_{p_1 p_2}^\varepsilon$ and the second is for all vertical $U_{p_1 p_2}^\varepsilon$. For convenience we shall take Δ_e to be much larger than the energy scale of fermions and restrict to the low energy sector without e -bosons. Substituting the mapping (2.26) and (2.27) into Eq. (5.6) gives:

$$H = -h_x \sum_{p \in \text{horizontal}} i\gamma_{p_1} \gamma'_{p_2} - h_y \sum_{p \in \text{vertical}} i\gamma_{p_1} \gamma'_{p_2} + h_z \sum_p i\gamma_p \gamma'_p. \quad (5.7)$$

Here i, j are row and column indices of a given plaquette. The Majorana modes can be expressed in terms of fermion creation and annihilation operators as:

$$c = \frac{1}{2}(\gamma + i\gamma'), \quad c^\dagger = \frac{1}{2}(\gamma - i\gamma').$$

As a result, Eq. (5.7) acquires the following form with pairing terms:

$$H = - \sum_{i,j} \left(h_x c_{i,j}^\dagger c_{i,j+1} + h_y c_{i,j}^\dagger c_{i+1,j} - h_z c_{i,j}^\dagger c_{i,j} + h_x c_{i,j} c_{i,j+1} + h_y c_{i,j} c_{i+1,j} \right) + \text{h.c.} \quad (5.8)$$

The system described by Eq. (5.8) is a spinless $p + ip$ superconductor. It will be shown later in this section that certain phases of Eq. (5.7) are gapless, which makes the Chern number C ill-defined. Therefore, in these gapless phases we add to (5.7) and by extension (5.8), a perturbation which creates a gap:

$$V = \frac{i\delta}{2} \sum_p \left[U_{y,p}^\varepsilon \left(\Gamma_p^\varepsilon + \Gamma_{N(p)}^\varepsilon \right) \right] \rightarrow V = -i\delta \sum_{i,j} c_{i,j} c_{i+1,j} + \text{h.c.}, \quad \delta > 0. \quad (5.9)$$

$N(p)$ is the plaquette to the north of p . The perturbation V does not otherwise affect bulk properties and the phase diagram of the system.

Passing to quasimomentum, the Hamiltonian $H + V$ can be rewritten in BdG form (5.1) with:

$$\varepsilon(\mathbf{k}) = -2(h_x \cos k_x + h_y \cos k_y - h_z), \quad \Delta(\mathbf{k}) = 2\delta \sin k_y - 2i(h_x \sin k_x - h_y \sin k_y), \quad (5.10)$$

and the quasiparticle spectrum:

$$E(\mathbf{k}) = \pm [\varepsilon(\mathbf{k})^2 + |\Delta(\mathbf{k})|^2]^{1/2} \quad (5.11)$$

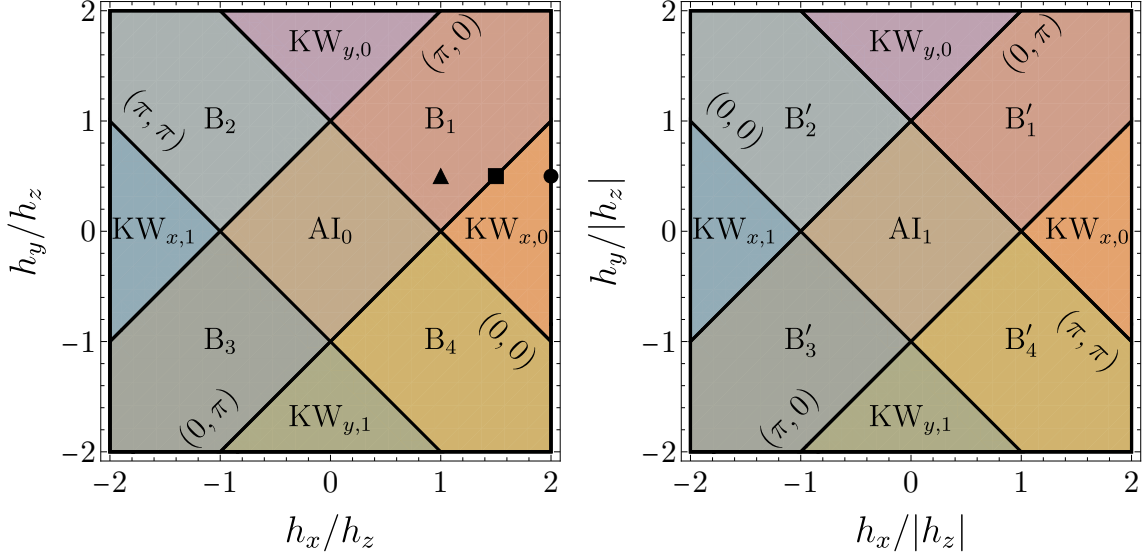


Figure 12: Phase diagram for the Hamiltonian (5.8). Left: $h_z > 0$. The three disks corresponds to the points at which edge modes are calculated on an cylindrical lattice; see Sec. 5.2.5. Right: $h_z < 0$.

5.2.1. Phase Diagram

We now discuss the phases of the Hamiltonian (5.6) by applying the classification scheme outlined in Sec. 5.1 to its dual quasiparticle Hamiltonian (5.7). To find the critical lines, note that the system has gap closings at phase transitions. The phase boundaries are then obtained by solving for $E(\mathbf{k}) = 0$ which only corresponds to gap closing at the high-symmetry quasimomenta points. The gap closings there are also necessary for change of ζ_i indices. As a result, with $\varepsilon(\mathbf{k})$ given in (5.10), the phase diagram in the parameter space of (h_x, h_y, h_z) is given in Fig. 12. The phase boundaries are given by: $|h_x| = |h_y| = |h_z|$. The Hamiltonian (5.8) contains fourteen out of all sixteen possible phases. In the $\{C; \zeta_1, \zeta_2, \zeta_3, \zeta_4\}$ classification scheme, they correspond to:

$$\begin{aligned}
C = 0 &: \text{AI}_0 \{0000\}, \text{AI}_1 \{1111\}, \text{KW}_{x,0} \{1100\}, \\
&\quad \text{KW}_{x,1} \{0011\}, \text{KW}_{y,0} \{1010\}, \text{KW}_{y,1} \{0101\}; \\
C = 1 &: \text{B}_1 \{0010\}, \text{B}_2 \{1000\}, \text{B}'_3 \{1101\}, \text{B}'_4 \{0111\}; \\
C = -1 &: \text{B}_3 \{0100\}, \text{B}_4 \{0001\}, \text{B}'_1 \{1011\}, \text{B}'_2 \{1110\}.
\end{aligned} \tag{5.12}$$

The topological numbers in (5.12) are calculated using Eqs. (C.7) and (C.12). Note that under charge conjugation, $h_x \rightarrow -h_x, h_y \rightarrow -h_y, h_z \rightarrow -h_z$ and $\zeta_i \rightarrow 1 - \zeta_i$ since the occupied quasimomenta point becomes empty and vice versa.

The phases in (5.12) can be summarized as follows. The B, B' phases have $C = \pm 1$ and are gapless without the perturbation. The AI phases contain static fermions with a definite average density on each site, and are the so-called ‘atomic insulators’. They are equivalent to the Toric Code. $\text{KW}_{x,y}$ phases are ‘weak topological phases’ (see the first footnote of this section) and correspond to stacks of one-dimensional Majorana wires along x - and y -directions.

Finally, the two phases that are not included in the phase diagram correspond to the stacking of one-dimensional Majorana wires along the two diagonal directions. They also have $C = 0$ and:

$$\text{KW}_{x+y,0} : \{1001\}; \text{KW}_{x+y,1} : \{0110\}.$$

Their properties are studied in detail in Appendix D.

In the following let us analyse each phase in (5.12) in more detail.

5.2.2. Atomic Insulator phases (AI)

First we discuss the $\text{AI}_{0,1}$ ('atomic insulator') phases in (5.12). Their properties are most easily studied at $h_x = h_y = 0$, $h_z = \pm 1$. The spin Hamiltonian is:

$$H = -h_z \sum_p \Gamma_p^\varepsilon - \Delta_e \sum_v \Gamma_v^e. \quad (5.13)$$

Γ_p^ε and Γ_v^e commute. For $h_z = 1$, the ground states have $\Gamma_v^e = \Gamma_p^\varepsilon = 1$ and (5.13) is equivalent to the Toric Code with the global parity constraint (1.15):

$$\prod_v \Gamma_v^e = 1, \quad \prod_p \Gamma_p^\varepsilon = 1,$$

where $\Gamma_v^e, \Gamma_p^\varepsilon$ take the place of A_v, B_p in Eq. (1.4). Therefore we attribute to AI_0 the same ground state degeneracy and mutual anyon statistics as the Toric Code (remember that ε -particles are fermions with respect to themselves); see Sec. 1.1. For $h_z = -1$, the lowest energy states have $\Gamma_v^e = 1$, $\Gamma_p^\varepsilon = -1$. This corresponds to each plaquette being occupied by ε -fermions. However, on a periodic lattice with L_x, L_y odd, this contradicts the global fermion parity constraints:

$$\prod_p \Gamma_p^\varepsilon = (-1)^{L_x L_y} = -1.$$

The physical ground state should have $\Gamma_p^\varepsilon = 1$ on a single plaquette, and the degeneracy is macroscopic, i.e. proportional to lattice size. The ground state degeneracy agrees naturally with Table 1.

5.2.3. Weak Topological Superconductor phases (KW)

The other four phases in (5.12) with $C = 0$ are $\text{KW}_{x,0}$, $\text{KW}_{x,1}$, $\text{KW}_{y,0}$ and $\text{KW}_{y,1}$. They correspond to stacking of one-dimensional superconducting Kitaev wires along the x -, y -directions. They are 'weak topological superconductors' (see the first footnote of this section). As will be demonstrated explicitly, these phases have non-trivial topological properties even though the Chern number $C = 0$. In what follows we discuss only the KW_x phases since KW_y phases are entirely analogous. In Fig. 13, Majorana coupling between KW_x phases are shown explicitly in the limit of $h_y = h_z = 0$.

On an infinite lattice, the system contains a superconducting gap. As has been shown in Table 1, the ground state degeneracy for $\text{KW}_{x,0}$ on a torus is 2 or 4 depending on the number of Kitaev Wires, i.e. on the lattice size L_y odd or even. This can be proven by the

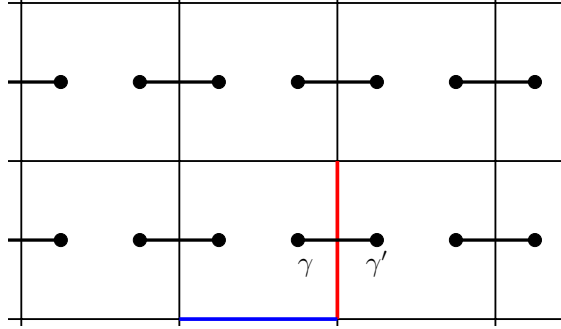


Figure 13: KW_x phases in the limit of $h_y = h_z = 0$ as horizontal stacks of one-dimensional Majorana wires. The coupling between Majorana wires is shown in solid bonds. The spin operator $U_{p_1 p_2}^\varepsilon \rightarrow i\gamma_{p_1} \gamma'_{p_2}$ is also shown for one such coupling.

general arguments in Sec. 5.1 and we shall repeat the discussion for this specific case as an example. Consider $KW_{x,0}$ for example. From (5.12) its ζ_i indices are $\{1100\}$, so the high-symmetry quasimomenta points $(0, 0), (0, \pi)$ are of concern. Now consider quasimomentum quantization (5.4) for these points across the four super-selection sectors $\{z_1, z_2\}$ with the associated ε -B.C.s ($z_{1,2} = \pm 1$ corresponds to periodic or anti-periodic boundary conditions along x -, y -directions) and varying system sizes. We investigate the resulting ground state fermion parity (it is convenient to consider the limit $h_y = h_z = 0$). Denoting by a tick if the corresponding quasimomenta point is allowed and a cross otherwise, the results depend only on L_y and can be expressed as:

L_y even:				L_y odd:			
$\{z_1, z_2\}$	$(0, 0)$	$(0, \pi)$	GS Parity	$\{z_1, z_2\}$	$(0, 0)$	$(0, \pi)$	GS Parity
$\{1, 1\}$	✓	✓	1	$\{1, 1\}$	✓	×	-1
$\{1, -1\}$	×	×	1	$\{1, -1\}$	×	✓	-1
$\{-1, 1\}$	×	×	1	$\{-1, 1\}$	×	×	1
$\{-1, -1\}$	×	×	1	$\{-1, -1\}$	×	×	1

As can be seen, ground state parity for all super-selection sectors is even for L_y even. The physical ground states are therefore four-fold degenerate. For L_y odd, the super-selection sectors $\{1, 1\}$ and $\{1, -1\}$ have odd ground state parity. These ground states are removed from the physical Hilbert space and the ground state degeneracy for the original spin Hamiltonian is two.

Similarly, for $KW_{x,1}$ phases the corresponding quasimomenta are $(\pi, 0), (\pi, \pi)$. quasimomentum quantization depends on both L_y and L_x . The results are summarized below:

L_y even, L_x odd:				L_y even, L_x even:			
$\{z_1, z_2\}$	$(\pi, 0)$	(π, π)	GS Parity	$\{z_1, z_2\}$	$(\pi, 0)$	(π, π)	GS Parity
$\{1, 1\}$	✓	✓	1	$\{1, 1\}$	×	×	1
$\{1, -1\}$	×	×	1	$\{1, -1\}$	×	×	1
$\{-1, 1\}$	×	×	1	$\{-1, 1\}$	×	×	1
$\{-1, -1\}$	×	×	1	$\{-1, -1\}$	×	×	1

L_y odd, L_x odd:				L_y odd, L_x even:			
$\{z_1, z_2\}$	$(\pi, 0)$	(π, π)	GS Parity	$\{z_1, z_2\}$	$(\pi, 0)$	(π, π)	GS Parity
$\{1, 1\}$	\times	\times	1	$\{1, 1\}$	\checkmark	\times	-1
$\{1, -1\}$	\times	\times	1	$\{1, -1\}$	\times	\checkmark	-1
$\{-1, 1\}$	\checkmark	\times	-1	$\{-1, 1\}$	\times	\times	1
$\{-1, -1\}$	\times	\checkmark	-1	$\{-1, -1\}$	\times	\times	1

In this case, the ground state degeneracy is also four for L_y even and two for L_y odd. For both L_x, L_y odd, physical ground states with even parity have only periodic horizontal boundary conditions for ε -fermions. For L_y odd but L_x even, they allow only anti-periodic horizontal boundary conditions. But the ground state degeneracy is always two.

The conclusion just obtained might appear contradictory: in the limit of $|h_x| \rightarrow \infty$, the KW_x phases are equivalent to horizontal stacks of seemingly decoupled one-dimensional Majorana wires under the duality mapping, yet the ground state degeneracy depends on the number of stacks. This is because the ground state satisfies the local constraint $\Gamma_v^e = 1$, which couples spin operators on each row. After the duality mapping, this is reflected in the following identity for the topological operator $W_x \rightarrow \hat{z}_1$, whose contour can be distorted to be along any rows by multiplying the constraint $\Gamma_v^e = 1$:

$$W_x = - \prod_{\text{row } n} U_{p_1 p_2}^\varepsilon \prod_{\text{row } n} \Gamma_p^e. \quad (5.14)$$

The row-independence of W_x then imposes certain constraints between different Majorana wires. It is therefore instrumental to give another derivation of the ground state degeneracy which directly makes use of this fact.

Consider the points $h_y = h_z = 0$, $h_x = \pm 1$ in the phase diagram for KW_x phases. The spin Hamiltonian on a periodic lattice is:

$$H = -h_x \sum_{\substack{p_1, p_2 \in \\ \text{horizontal}}} U_{p_1 p_2}^\varepsilon - \Delta_e \sum_v \Gamma_v^e. \quad (5.15)$$

The spin operators $U_{p_1 p_2}^\varepsilon$ are shown in Fig. 13. We apply the duality mapping in Sec. 2.2 for a periodic lattice, and write (5.15) in terms of τ and σ matrices (the superscript ε is neglected in what follows). This gives:

$$H = -h_x \sum_{n,m} \tau_{n,m} \tau_{n,m+1} - h_x \sum_n \theta_n \tau_{n,L_x} \tau_{n,1}, \quad \theta_n = - \left(\prod_{p \in \text{row } n} \sigma_p \right) \hat{z}_1. \quad (5.16)$$

Here n, m are row and column indices respectively, and we have separated out the horizontal pair-creation terms that cross the lattice boundary. The θ_n term arises from lattice periodicity, and the last identity in (5.16) is obtained by substituting the relation $\theta_n = \prod_{\text{row } n} U_{p_1 p_2}^\varepsilon$ into Eq. (5.14).

Consider first the $\text{KW}_{x,0}$ phase with $h_x > 0$. It is clear from (5.16) that the ground state has $\theta_n = 1$ and $\tau = \pm 1$ (ferromagnetic) on each row. However, the total parity of each

chain:

$$\Pi_n = \prod_{p \in \text{row } n} \sigma_p,$$

commutes with $\tau_{n,m}\tau_{n,m+1}$ and their eigenvalues must also be specified. Π_n reverses the eigenvalues of all τ on the n -th row, and $\Pi_n = \pm 1$ corresponds to symmetric and anti-symmetric combinations of the two ferromagnetic ground states $\tau_{n,m} = \pm 1$. We shall see that there are certain constraints on eigenvalues of Π_n precisely due to the last identity in (5.16). For inverting this identity gives:

$$- \hat{z}_1 = \Pi_n \theta_n = \Pi_m \theta_m, \quad (5.17)$$

which relates θ_n and parity Π_n on different rows. Setting $\theta_n = 1$ then gives:

$$\Pi_n = \Pi_m.$$

This in combination of the global ε -parity constraint (1.16):

$$\prod_n \Pi_n = 1,$$

gives that $\Pi_n = \pm 1$ for L_y even, and $\Pi_n = 1$ for L_y odd. This in turn gives:

$$\begin{aligned} L_y \text{ even} : z_1 &= \pm 1; \\ L_y \text{ odd} : z_1 &= -1. \end{aligned}$$

For the $\text{KW}_{x,1}$ phase, each chain is anti-ferromagnetic and the ground state on each row is also two-fold degenerate with spins of the two magnetic sublattices reversed. θ_n now depends on L_x : for L_x even, the spins on two sides of the boundary are opposite hence $\theta_n = 1$. For L_x odd the boundary spins are parallel and $\theta_n = -1$ to minimize the energy. Π_n exchanges the two magnetic sublattices and its eigenvalue selects the unique ground state for each chain. This difference to the $\text{KW}_{x,0}$ phase only affects the determination of z_1 in Eq. (5.17). We then still have $\Pi_n = \pm 1$ for L_y even, and $\Pi_n = 1$ for L_y odd. This in turn gives for z_1 :

$$\begin{aligned} L_y \text{ even} : z_1 &= \pm 1; \\ L_y \text{ odd} : z_1 &= -1, L_x \text{ even}; z_1 = 1, L_x \text{ odd}. \end{aligned}$$

Thus we have re-derived the ground state degeneracy for KW_x phases (remember z_2 is a separate degenerate degree of freedom).

The two derivations that are presented so far make use of the duality. To verify the correctness of the duality, we shall provide yet another derivation of the lattice-dependence of ground state degeneracy, by solving directly the spin Hamiltonian. The solution is similar to that given for the Toric Code in Sec. 1.1, by counting the number of independent operators. Consider again the Hamiltonian (5.15) at $h_y = h_z = 0$, $h_x = \pm 1$ in the phase diagram. Its constituent operators in (5.15) are $L_x L_y$ number of horizontal ε -fermion pair-creation

operators $U_{p_1 p_2}^\varepsilon$ and Γ_v^e . They commute with each other and with Wilson loop operators $W_{x,y}$ given by Eq. (2.24). Therefore, the ground states can be characterized by the eigenvalues of these operators [accordingly the quasiparticle spectrum (5.11) at $h_y = h_z = 0$, $h_x = \pm 1$ is flat]. As is in the case of the Toric Code, for the total Hilbert space of dimension $2^{2L_x L_y}$, these operators are not all independent. The first constraint is given by (1.16) for total e -boson parity:

$$\prod_v \Gamma_v^e = 1. \quad (5.18)$$

We have also found a second global constraint related to $U_{p_1 p_2}^\varepsilon$. Interestingly, the form of this constraint depends on whether L_y is even or odd. For L_y even:

$$\left(\prod_{\text{odd rows}} \Gamma_v^e \right) \left(\prod_{p \in \text{horizontal}} U_{p_1 p_2}^\varepsilon \right) = 1, \quad (5.19)$$

where the first product is taken over the lower vertices of squares on odd rows. Note that although $U_{p_1 p_2}^\varepsilon = -1$ for the $\text{KW}_{x,1}$ ground state ($h_x = -1$), it is still consistent with (5.19) since L_y is even. Eqs. (5.18) and (5.19) give two constraints relating operators in the Hamiltonian (5.15), and the ground states are four-fold degenerate specified by eigenvalues of $W_{x,y}$.

For L_y odd we find:

$$\left(\prod_{\text{odd rows}}^{\text{row } L_y - 2} \Gamma_v^e \right) \left(\prod_{p \in \text{horizontal}} U_{p_1 p_2}^\varepsilon \right) = -W_x, \quad (5.20)$$

where the first product is taken over all vertices on odd rows up to and including the $(L_y - 2)$ -th row, and the second product includes all horizontal pair-creation operators. In contrast to the L_y even case, the constraint relates W_x to Γ_v^e and $U_{p_1 p_2}^\varepsilon$ operators in the Hamiltonian. Therefore, W_x eigenvalue cannot be assigned arbitrarily, and the ground state degeneracy is two characterized by W_y only; the transitions within the ground state sector is given by T_x . For example, for $h_x = 1$ (phase $\text{KW}_{x,0}$) $U_{p_1 p_2}^\varepsilon = \Gamma_v^e = 1$ in the ground state and Eq. (5.20) gives $W_x = -1$: periodic boundary condition along the x -direction is forbidden. For $h_x = -1$ (phase $\text{KW}_{x,1}$), $U_{p_1 p_2}^\varepsilon = -1, \Gamma_v^e = 1$ in the ground state, and Eq. (5.20) leads to:

$$W_x = (-1)^{L_x L_y + 1}.$$

Thus, for L_y odd, the x -direction boundary condition is anti-periodic for L_x even and periodic for L_x odd. The discussions given here agree, naturally, with the previous two approaches in this subsection: the forbidden W_x eigenvalues for given L_x, L_y are precisely those of the corresponding super-selection sectors with unphysical odd ground state fermion parity.

The degrees of freedom counting for KW_x phases can be summarized as:

operators	degrees of freedom
Γ_v^e	$L_x L_y - 1$
$U_{p_1 p_2}^\varepsilon$ (horizontal)	$L_x L_y - z$
W_x	z
W_y	1

$$z = \begin{cases} 1, & L_y \text{ even} \\ 0, & L_y \text{ odd} \end{cases}$$

The ground state degeneracy is then 2^{1+z} , where $1+z$ is the number of independent $W_{x,y}$ operators.

Note that both Eqs. (5.19) and (5.20) are not invariant under lattice translation along the y -direction by unity, and Γ_v^e on even and odd rows become in a sense distinct. Anticipating Sec. 6, this is a manifestation of ‘weak breaking’ of translation symmetry in KW phases. As will be shown in Sec. 6.1, here e -bosons on even and odd rows under the superconducting vacuum acquire emergent mutual anyonic statistics.

5.2.4. Phases with non-zero Chern number

The remaining eight phases B, B' in (5.12) have Chern number $C = \pm 1$.

On an infinite lattice, the Hamiltonian (5.8) in these phases is gapless with two cones in the Brillouin zone. Solving for $E(\mathbf{k}) = 0$ in Eq. (5.11) with $\delta = 0$ gives positions of the cones:

$$k_x = \arccos \left[\frac{1}{2h_x h_z} (h_y^2 - h_x^2 - h_z^2) \right], \quad k_y = \arccos \left[\frac{1}{2h_y h_z} (h_x^2 - h_y^2 - h_z^2) \right], \quad \text{mod } 2\pi.$$

In fact a solution exists only if the following inequalities are satisfied:

$$(h_x + h_z)^2 \geq h_y^2 \geq (h_x - h_z)^2; \quad (h_y + h_z)^2 \geq h_x^2 \geq (h_y - h_z)^2. \quad (5.21)$$

which corresponds to exactly the region in the phase diagram for the B, B' phases. The spectrum near each zero-energy point has the form:

$$\varepsilon = \pm \left[h_x^2 k_x^2 + h_y^2 k_y^2 - (h_x^2 + h_y^2 - h_z^2) k_x k_y \right]^{1/2}.$$

The positive definite requirement for the polynomial gives again the inequalities (5.21).

The cones create singularities for the quasiparticle dispersion, and make the Chern number C ill-defined. Adding the perturbation V in (5.9) creates a gap of the order δ at these points. In a way the exact value of C is conventional and thus unphysical, because C depends on the choice of V and changes sign as $\delta \rightarrow -\delta$. But the $\{\zeta_i\}$ indices which characterize bulk topology are well-defined.

On a torus, the dependence of GSD of the B, B' phases on lattice size is given by Table 1. However, in this case the system cannot be solved directly on the spin lattice as in Sec. 5.2.3. This follows from a general theorem that Hamiltonians with non-zero C necessarily contain non-commuting operators [87].

In Sec. 6, we shall also study the emergent anyon statistics of e -bosons in phases with non-zero Chern number.

5.2.5. Bulk-Edge Correspondence

So far we have discussed the phase diagram of the Hamiltonian (5.6) on infinite or finite, periodic lattices. We shall now discuss briefly the open lattice case in which topologically non-trivial phases contain edge modes.

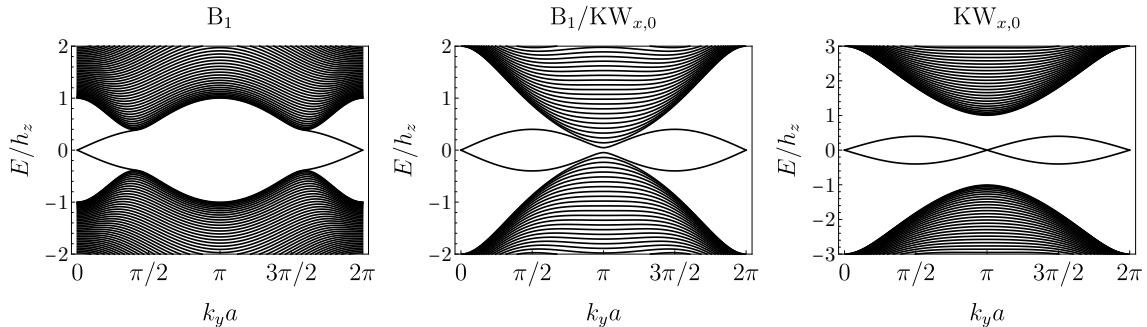


Figure 14: Edge mode dispersions for the Hamiltonian (5.8) on a cylindrical lattice. The vertical direction is taken infinite and $L_x = 100$. The parameters are $h_y = h_z/2 = 1/2$, $\delta = 0.2$ and $h_z > 0$. From left to right, $h_x = 1, 1.5, 2$ respectively. $h_x = h_z$ (left) and $h_x = 2h_z$ (right) belong to phases B_1 and $KW_{x,0}$. $h_x = 1.5h_z$ (center) is at the critical line between phases B_1 and $KW_{x,0}$. Their locations on the phase diagram are marked with triangle, square and circle respectively in Fig. 12.

The existence of zero modes along open boundaries for gapped topologically non-trivial phases is proven for free, non-interacting fermionic systems (the so-called *bulk-edge correspondence*). In topological superconductors with lattice translation symmetry, the zero edge modes are naturally the ground state fermions at high-symmetry quasimomenta classified by the $\mathbb{Z} \times (\mathbb{Z}_2)^3$ scheme; see Sec. 5.1 and Appendix C.

Let us show the existence of edge modes for KW_x phases. We again take the limit $h_y = h_z = 0$ or $|h_x| \rightarrow \infty$, and the Hamiltonian (5.7) becomes a series of decoupled one-dimensional Kitaev wires:

$$H = -h_x \sum_{p \in \text{horizontal}} i\gamma_{p_1} \gamma'_{p_2}. \quad (5.22)$$

On an open lattice, γ' on the first column and γ on the last do not enter into the Hamiltonian (5.22). Thus they have zero energy and constitute the edge modes. At non-zero h_x and h_z , the edge modes acquire dispersion. However, they remain gapless at the corresponding high-symmetry quasimomentum points.

To demonstrate these zero edge modes at arbitrary points of the phase diagram, we numerically diagonalize the Hamiltonian (5.8) with the perturbation V (5.9) on a cylindrical lattice which is infinite along the y -direction and finite along the x -direction. The energy levels are functions of k_y and their number is $2L_x$ (due to the presence of both particles and holes).

In Fig. 14, we show the energy levels in phase B_1 , at the critical point between B_1 and $KW_{x,0}$, and in phase $KW_{x,0}$ respectively. As can be seen, in each phase the edge mode energy becomes zero at the corresponding high-symmetry quasimomenta \mathbf{k}_{0i} of the phase (the edge mode is gapped at other quasimomenta but is protected at \mathbf{k}_{0i}). At the critical point, the bulk gap closes at the corresponding \mathbf{k}_{0i} whose ζ_i changes and, after crossing into the new phase, either the original edge mode disappears or a new edge mode remains there.

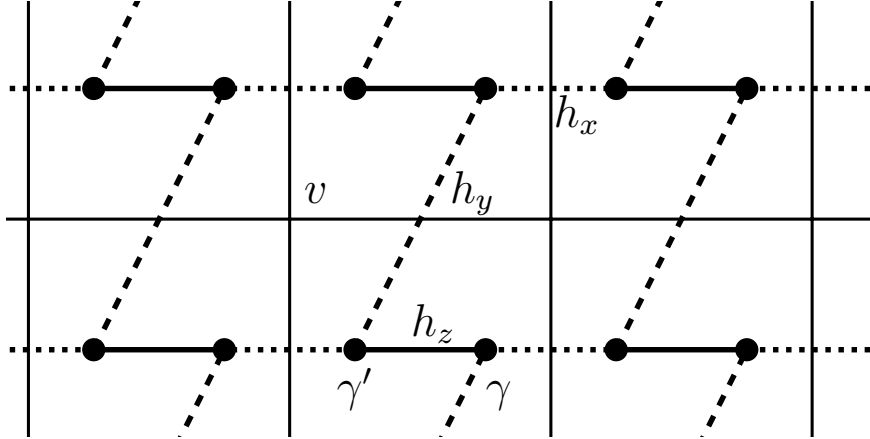


Figure 15: Majorana modes γ, γ' on square lattices as on a ‘distorted’ honeycomb. The Majorana coupling terms in (5.7) are represented visually by connecting the corresponding two modes with coefficients h_x, h_y or h_z . Each honeycomb contains one vertex. Moving a Majorana mode around, for example, the honeycomb that contains v gives the parity of e -bosons on v .

5.3 Equivalence to the Kitaev Honeycomb Model

The phase diagram Fig. 12 for the Hamiltonian (5.6) and its topological properties resemble that of the Kitaev Honeycomb model. This is not accidental and is related to that \mathbb{Z}_2 spin models on a square lattice can be seen as defined on a distorted honeycomb lattice; see Sec. 2.2.3. In this subsection, we use a lattice reconstruction different from Sec. 2.2.3, and explicitly demonstrate the equivalence between the Hamiltonian (5.6) and the Kitaev Honeycomb model (1.3) [17]:

$$H = -J_x \sum_{x\text{-links}} X_i X_j - J_y \sum_{y\text{-links}} Y_i Y_j - J_z \sum_{z\text{-links}} Z_i Z_j. \quad (5.23)$$

The situation is different from (2.33) in Sec. 2.2.3, as Γ_p^ε is a four-spin operator.

Let us consider instead of (5.6) the corresponding fermion Hamiltonian (5.7). We regard each γ and γ' as Majorana modes defined on different sites, and connect those that are coupled via operators $U_{p_1 p_2}^\varepsilon$ and Γ_p^ε ; see Fig. 15. We obtain as a result a new honeycomb, and the Hamiltonian (5.7) couples nearest-neighbour Majorana modes. This resembles the fermion representation of Eq. (5.23) given by (2.30):

$$H = \frac{i}{4} \sum_{jk} J_{jk}^\alpha \hat{u}_{jk} c_j c_k,$$

where, as in Sec. 2.2.3, we use c to denote Majorana modes on each site. Here J_{jk}^α are the couplings h_x, h_y, h_z depending on the links $\langle jk \rangle$ inside the honeycomb; see Fig. 15. The additional \hat{u}_{jk} operators contain fictitious Majorana modes for the vortex (e -bosons) sector and satisfy:

$$\prod_{j,k \in \text{honeycomb}} \hat{u}_{jk} = w_p, \quad (5.24)$$

where $w_p = \pm 1$ corresponds to the absence or presence of a π -vortex at the center of the p -th honeycomb. It can be shown that by multiplying $U_{p_1 p_2}^\varepsilon$ and Γ_p^ε operators (the parity operator $\Gamma_p^\varepsilon \rightarrow -i\gamma_p \gamma'_p$ transports the Majorana mode ‘within the plaquette’) along the smallest ‘honeycomb’ in Fig. 15, the result is Γ_v^e inside the honeycomb. Thus we have derived the relation (5.24) from our model (5.6) without introducing fictitious Majorana degrees of freedom, and showed that (5.7) is identical to the fermionic representation of the honeycomb model (2.30).

6 Berry phase and Emergent Anyon Statistics from Motion of e -bosons

In Sec. 5, we have studied the superconducting ε -fermion Hamiltonian (5.6) without e -bosons, which are taken static and have a gap $2\Delta_e$. In the limit $\Delta_e \ll \Delta_0$ where Δ_0 is the gap for fermion quasiparticles, the low-energy levels correspond to a given configuration of static e -bosons placed on top of the superconducting vacuum. In this section, we investigate the ensuing associated *emergent anyon statistics* between e -bosons. In this case, the e -particles might possess different anyonic statistics due to their ‘renormalization’ by the superconducting vacuum: each ‘bare’ e -boson (a point π -vortex) excites a fermion cloud around itself, which in turn induces the non-trivial mutual statistics. The results depend on the bulk topological properties of the underlying superconducting phases as described in Sec. 5.1 and Appendix C. Namely the mutual anyon statistics are determined by the $\{C; \zeta_i\}$ indices.⁸

Our results in this section fall into two categories, the first being the KW phases in Sec. 5.2.3 with Chern number $C = 0$. The low-energy e -bosons split into two groups of quasiparticles, bosonic within each group, with non-trivial mutual statistics. The lattices for two groups are exchanged by a lattice translation (‘*weak symmetry breaking*’ [17, 46, 68, 72]). In the second category, the phases have non-zero C . The mutual braiding rules of e -bosons in this case depend on C and are predicted in Ref. [17]. Using the spin-particle duality construction, we calculate this braiding explicitly. In addition, we also calculate the background flux for e -bosons from the superconducting vacuum, which is quantized to be 0 or π depending on bulk topology. This is related to properties of the vison band in α -RuCl₃ [23, 27].

Let us first outline the method used in this section.

What are the quantities that characterize anyon statistics? As is discussed in Sec. 1, anyons can be regarded as mutual point magnetic vortices, and the non-local parity terms in the quasiparticle motion operators U^e, U^ε are essentially the vector potentials for fluxes pinned to e - and ε -particles in a specific gauge; see also Sec. 2. By transporting one anyon around another in a closed loop, the *Berry phase* acquired by the wave-function is simply the magnetic flux of the other anyon, which then gives the mutual anyon statistics.

More concretely on the spin lattice, define an initial state $|i\rangle$ and a contour γ which has, at its one end, a static e -boson. The result for transporting the e -boson along the trajectory γ using $U_{v_1 v_2}^e = Z_{v_1 v_2}$ is given by the matrix elements:

$$\langle f | \prod_{v \in \gamma} Z_{v_j v_k} | i \rangle, \quad (6.1)$$

where the final state has the e -boson at the other end of γ . For our present purpose, γ is taken to be a closed loop that encircles another e -boson. For the Toric Code, Eq. (6.1) is just (1.9)

⁸Here it is important that the superconducting vacuum is stable against addition of e -bosons. In our case, the stability is guaranteed since e -particles are static and non-interacting.

which is a trivial case. Generally, the motion of e -bosons excites fermion quasiparticles, since adiabatic transport is impossible on a lattice due to the minimal step size being the lattice constant. As a result, the matrix elements (6.1) contain transitions between many eigenstates under given e -configurations. However as is discussed, for emergent anyon statistics only transitions between ground states are relevant. Hence, in place of Eq. (6.1) we can write:

$$\prod_{v \in \gamma} \langle 0_{jm} | Z_{v_j v_k} | 0_{kn} \rangle, \quad (6.2)$$

where m, n are indices for the ground state multiplets. $|0_{jm}\rangle$ is a ground state whose e -configuration differs from that of $|0_{kn}\rangle$ only by having one of the e -bosons at v_j instead of v_k . If the ground state is unique, there is only one type of emergent ‘abelian’ anyons and Eq. (6.2) gives a scalar whose phase is naturally the Berry phase ϕ . For degenerate ground states, each state corresponds to a given type of emergent anyons. To see this, consider, for example, two (‘bare’) π -vortices σ in a spinless p -wave superconductor. The superconducting gap Δ vanishes near each vortex which can contain a zero-energy Majorana mode as an Andreev bound state. The ground states are consequently two-fold degenerate: one state contains no fermions and the other contains one complex fermion Ψ which is distributed as two Majorana modes inside the vortices. Here the vortices with and without the zero modes are taken to be two types of anyons. Processes involving two σ -vortices allow emission or absorption of a complex fermion, and exchanging two vortices can change the anyon types: the statistics is therefore ‘non-abelian’. Here it means that transition elements in (6.2) are non-zero between the two degenerate ground states. In general, non-abelian anyon statistics are reflected in the ‘fusion rules’ of the form $a \times b = \sum_i c_i$. This has the meaning that processes involving particles a and b can emit particles c_i . For example, the fusion rule for the present case is $\sigma \times \sigma = 1 + \Psi$, where 1 is the vacuum. Braiding phases of a, b can be written as $R_{c_i}^{a,b}$, namely in the channel which involves an anyon of type c_i .

Generally Eq. (6.2) is a product of matrices and the results give both the self- and mutual-statistics of all emergent anyons. In this section, we will consider the periodic spin lattice because, as it turns out, computing the matrix (6.2) for all phases considered in this section reduces to calculating the scalar Berry phase. In an open lattice there are in general zero-energy edge modes, which greatly expand the size of the ground state multiplets; see Sec. 5.2.5.

6.1 Weak Symmetry Breaking in KW phases

Let us again start from KW_x phases. To study the emergent statistics of e -bosons, it is convenient to start from the Hamiltonian (5.15) on the spin lattice:

$$H = -h_x \sum_{p \in \text{horizontal}} U_{p_1 p_2}^\varepsilon - \Delta_e \sum_v \Gamma_v^e, \quad (6.3)$$

whose solution is particularly simple; see Sec. 5.2.3. Since we are only concerned with e -bosons within the superconducting ground state, all horizontal ε -fermion pair-creation

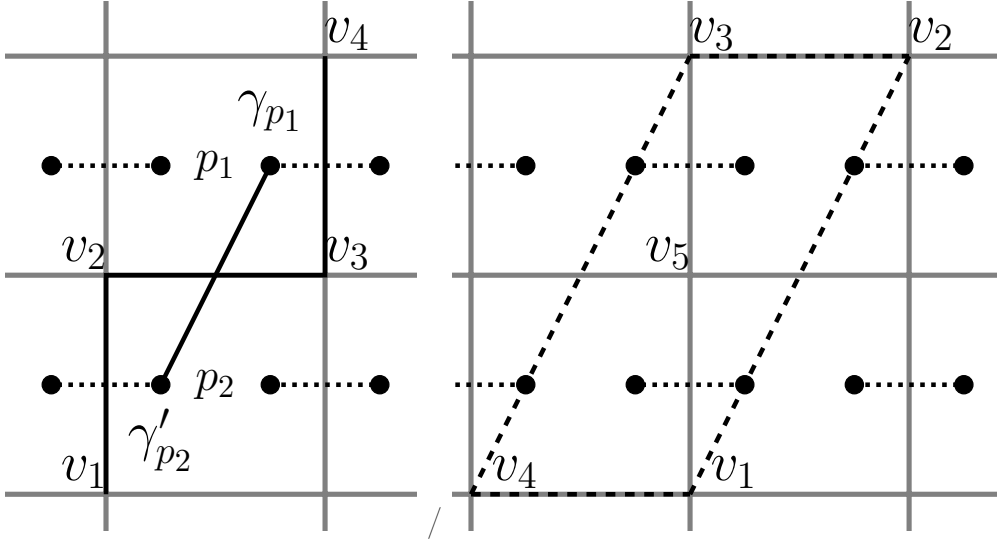


Figure 16: Left: transport of an e -boson from v_1 through v_2 and v_3 to v_4 ; see Eq. (6.4). The path of the boson shown in black intersects Majorana bonds shown by dotted lines. The Majorana coupling term in (6.4) is also shown explicitly. Right: transport of e -bosons along a closed loop, shown as dashed lines, in one sublattice given by Eq. (6.5). The contour encircles v_5 and the loop motion measures its e -parity.

operators $U_{p_1 p_2}^\varepsilon = \pm 1$ for $\text{KW}_{x,0}$ and $\text{KW}_{x,1}$. Vertical pair-creation operators $U_{v_1 v_2}^e$ for e -bosons (1.7) anti-commute with $U_{p_1 p_2}^\varepsilon$ for v_1 and v_2 along the edge between plaquettes p_1 and p_2 . Such a process excites the superconducting vacuum. It turns out that, in the KW_x phases, *local* e -transport within the superconducting vacuum is only possible between even or odd rows, and e -bosons on even and odd rows are mutual emergent π -vortices.

We now set out to prove the above statement. It is simpler, for this purpose, to find, instead of the projected matrix elements in (6.2), the ‘renormalized’ transport operators \tilde{U}^e for the emergent anyons which commute with $U_{p_1 p_2}^\varepsilon$. As is already noted, $U_{v_1 v_2}^e = Z_{v_1 v_2}$ is no longer suitable for transporting e -bosons between adjacent rows (it can still be used for transport within one row as horizontal $Z_{v_1 v_2}$ commute with $U_{p_1 p_2}^\varepsilon$). This process is generally impossible by local operators without exciting the superconducting vacuum, as can be seen in Fig. 16 by regarding $U_{p_1 p_2}^\varepsilon = \pm 1$ as a bond between the Majorana modes $\gamma_{p_1}, \gamma'_{p_2}$. A vertical e -translation necessarily breaks this bond with energy cost $2h_x$. However, it is possible to transport e -bosons across two rows with the trajectory shown in Fig. 16. In this case, the two broken bonds are restored by vertically creating an additional pair of ε -fermions. The ‘renormalized’ e -boson pair-creation operator across two rows is therefore a composite operator:

$$\tilde{U}_{v_1 v_4}^e = \left(\prod_v Z_{v_i v_j} \right) U_{p_1 p_2}^\varepsilon, \quad (6.4)$$

which is demonstrated in Fig. 16. \tilde{U}^e thus defined commutes with all horizontal $U_{p_1 p_2}^\varepsilon$. In a sense, one may regroup $\gamma_{p_1}, \gamma'_{p_2}$ across two plaquettes as belonging to an ‘effective’ complex fermion Ψ' . $U_{p_1 p_2}^\varepsilon \rightarrow i\gamma_{p_1} \gamma'_{p_2} = \pm 1$ then correspond to a definite parity of Ψ' . $U_{v_1 v_2}^e$ across a

single row changes the fermion parity, hence it is only possible to maintain $U_{p_1 p_2}^\varepsilon = \pm 1$ for crossing two rows, which would leave the parity invariant.

Consequently the KW_x vacua distinguish e -bosons on adjacent rows. It is now simple to calculate their mutual statistics. It is clear that, by using the ‘renormalized’ e -transport operators (6.4) for emergent anyons in (6.1) instead of $Z_{v_i v_j}$ (remember that e -motion within one row is still given by $\tilde{U}_{v_i v_j}^e = Z_{v_i v_j}$), there is no need for explicit projection to the ground state multiplets. With this in mind, we transport an e -boson on say an odd row along the smallest allowed contour that contain a single vertex v_5 on an even row; see Fig. 16. This gives:

$$\prod_{v_i, v_j \in \gamma} \tilde{U}_{v_i v_j}^e |0\rangle = \Gamma_{v_5}^e |0\rangle, \quad (6.5)$$

where we have used the ground state identity: $U_{\text{horizontal}}^\varepsilon |0\rangle = \mp |0\rangle$, $h_x \leq 0$. Eq. (6.5) shows that low-energy e -bosons on adjacent rows are mutual π -vortices.

Before proceeding, let us comment on some consequences of the results obtained so far in this subsection.

First, Eqs. (6.5) and (6.4) are examples of a general phenomena of ‘*weak symmetry breaking*’ [17, 46, 68, 72]: translation symmetry is broken since the structure of the Hilbert space, having two sublattices of inequivalent e -bosons, is no longer invariant under lattice translations, which exchange the two sublattices. This is unrelated to the usual spontaneous symmetry breaking in a second order phase transition, due to the absence of a local order parameter. Generally, we find ‘weak breaking of translation symmetry’ to be present in other models that are stacks of one-dimensional Kitaev wires [this is completely natural from the considerations below Eq. (6.4)]. For KW_y phases, by arguments almost identically to the ones given here, the e -bosons on adjacent columns are emergent mutual π -vortices. For diagonal stackings of Kitaev wires, which are the two phases not contained in the model (5.6) considered in Sec. 5:

$$\text{KW}_{x+y,0} : \{1001\}; \text{KW}_{x+y,1} : \{0110\},$$

the two inequivalent e -sublattices are found in Appendix D.

Secondly, so far we have only shown that e -bosons cannot be transported *locally* between the two sublattices. Such a process is, however, in principle possible with a non-local operator on the torus. Consider, for example, again the KW_x phases. Let us transport an e -boson on the first row upwards. Repeating this operation vertically across the entire lattice, we see that for L_y even the quasiparticle is brought back to its original position after traversing the lattice boundary. For L_y odd however, the e -boson now arrives at the second row and we have transported the quasiparticle between adjacent rows.

Closely related to this observation is the following alternative derivation of KW_x ground state degeneracy and emergent e -anyon statistics. The derivation shows that e -bosons on even and odd rows become emergent e' - and m' -bosons of an ‘effective Toric Code’ under the superconducting vacuum (we use the prime to denote that these are ‘effective’ anyons). Such a re-designation of e -bosons can only be consistent if L_y is even or infinite and low-energy transitions between them are not possible.

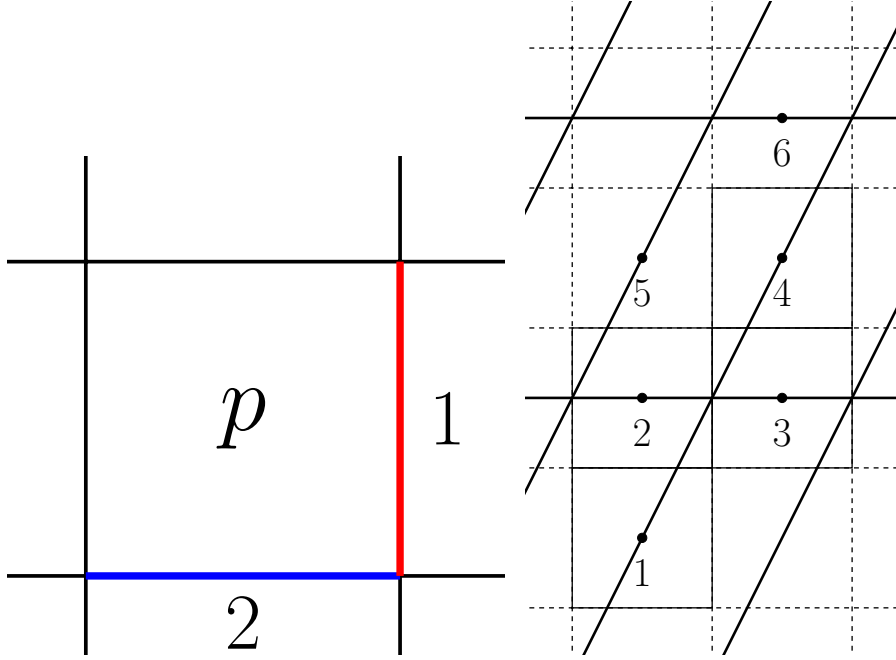


Figure 17: Left: the reduction of two degrees of freedom on links 1, 2 to one at plaquette p under the constraint (6.6). Right: the new lattice under which Γ_v^e becomes effective A'_v and B'_p operators in the Toric Code.

For this purpose, we consider the Hamiltonian (6.3) for KW_x phases, and project it into the following subspace:

$$U_{p_1 p_2}^\varepsilon = \mp 1, \quad h_x \leq 0, \quad (6.6)$$

which is satisfied by the ground states. To prove our statement, it suffices to show that, for L_y even, Γ_v^e operators projected to the subspace of Eq. (6.6) becomes A'_v and B'_p (1.2) of the Toric Code on even and odd rows. They correspond to the two groups of effective e' - and m' -anyons described above. This is the main idea behind the proof which we shall lay out below.

In the subspace given by Eq. (6.6), we can choose a new basis such that the horizontal and vertical links in horizontal $U_{p_1 p_2}^\varepsilon$ are simultaneously diagonal with respect to Z and X . For $h_x = \pm 1$, Z and X have opposite (the same) eigenvalues, and can be treated as one degree of freedom defined on the plaquette p . Thus, in the notation of Fig. 17, we have the mapping:

$$Z_2 \rightarrow \sigma_p^z, \quad X_1 \rightarrow \mp \sigma_p^z, \quad h_x \leq 0. \quad (6.7)$$

σ_p^z is the third Pauli matrix acting on the plaquette p with the eigenvalue of Z_2 . A simultaneous operation of X_2 and Z_1 on horizontal and vertical links of p anticommutes with Z_2 or X_1 yet still satisfies Eq. (6.6), so we have another mapping within the subspace:

$$X_2 Z_1 \rightarrow \sigma_p^x. \quad (6.8)$$

Γ_v^e then becomes a four-plaquette operator $\tilde{\Gamma}_p^e$ with p being the plaquette to the north-east of v . For $h_x = \pm 1$ (both $\text{KW}_{x,0}$ and $\text{KW}_{x,1}$ phases), $\tilde{\Gamma}_p^e$ has the same form. For example, in

Fig. 17:

$$\tilde{\Gamma}_3^e \rightarrow \sigma_1^z \sigma_2^y \sigma_3^y \sigma_4^z. \quad (6.9)$$

It is more convenient to define a new lattice in which $\tilde{\Gamma}_p^e$ operators such as in Eq. (6.9) have the explicit form of A'_v and B'_p operators in TC. We join, for all $\tilde{\Gamma}_p^e$ on odd rows, the centers of plaquettes and treating them as the mid-points of links of the new lattice. For example, in Fig. 17 this is done for $\tilde{\Gamma}_3^e$ by joining plaquettes 2, 3 and 1, 4. Then $\tilde{\Gamma}_p^e$ becomes the A'_v and B'_p operators in the Toric Code on odd and even rows ($\tilde{\Gamma}_3^e$ and $\tilde{\Gamma}_4^e$ in Fig. 17). As is already pointed out, for this mapping to be self-consistent, the lattice must be infinite or L_y is even, otherwise the construction breaks down along the two rows across the horizontal boundary.

Thus in the subspace of KW_x ground states given by Eq. (6.6), the Hamiltonian (6.3) is equivalent to the Toric Code at low energies for an infinite lattice or L_y is even. This means that, for a finite lattice with L_y even, the usual Toric Code constraints apply:

$$\prod_{p \in \text{odd rows}} \tilde{\Gamma}_p^e = 1, \quad \prod_{p \in \text{even rows}} \tilde{\Gamma}_p^e = 1, \quad (6.10)$$

and the corresponding ground state is four-fold degenerate. Since for odd L_y , only the total e -parity constraint $\prod_v \Gamma_v^e = 1$ in Eq. (1.16) applies as discussed above, the ground state is two-fold degenerate for L_y odd. This agrees with the results in Sec. 5.2.3. Note that by substituting Eq. (6.6) into (5.19) and using (5.18), we obtain (6.10) as it should. In this new construction, a translation along the y -direction by unity in the original lattice exchanges e' - and m' -bosons in the new lattice. This is another manifestation of the ‘weak symmetry breaking’ discussed in this subsection.

Finally, let us mention the numerical results relating to ‘weak symmetry breaking’ away from the exactly solvable limit (6.3). For the KW_x phases with two e -bosons, the fermion parity of the quasiparticle ground state in each super-selection sector depends on L_y and relative positions of e -bosons; for details about the ground state wave-function in the quasiparticle picture, see the next subsection and Appendix E. For L_y even, if both e -bosons are on the same e' - or m' -sublattice, the four ground states in each sector have parity even and the physical ground state degeneracy is four (this also confirms the conclusions in Sec. 5.2.3). When one e -boson is transported to a different sublattices, all ground states have negative parity and become unphysical. This illustrates the impossibility of transporting e -bosons between e' - and m' -sublattices while remaining in the physical ground state. For L_y odd, only two of the ground states have parity even for the two e -bosons on the same sublattice (remember under L_y odd and without e -bosons, the ground state degeneracy is two-fold). After transporting one of the e -boson to another sublattice, the four ground states have their parities exchanged while the physical ground state is still two-fold degenerate. This is because, as is discussed above, under L_y odd, transporting an e -boson between sublattices within the ground state is possible, by moving it across the lattice boundary. However, as is shown in Eq. (2.29), cross-boundary motion of e -bosons also causes a transition between super-selection sectors.

6.2 Berry phase and Emergent Anyon Statistics in phases with non-zero Chern number

To study the emergent e -boson statistics in \mathbb{Z}_2 topological phases with $C \neq 0$, it is not convenient to solve the spin lattice Hamiltonian as in Sec. 6.1, since the constituent operators do not generally commute [87]. The problem is considerably simplified however, for certain such spin models which map to quadratic Hamiltonians of ε -fermions and static e -bosons; in fact, we have only considered such models in this thesis. A complete solution can then be obtained using the quasiparticle picture because the elementary excitations are free, which gives exactly the wave-functions and associated matrix elements. Here it is important that e -bosons are static, otherwise they interact with fermions due to anyonic effects in quasiparticle motion.

To calculate the matrix elements (6.2) in the quasiparticle picture, we first note that the local e -transport operators $Z_{v_1 v_2}$ inside the bulk cannot cause transitions between different super-selection sectors. Therefore, emergent anyon statistics in these sectors can be studied independently. Secondly, the physical ground states must have even fermion parity. With this understanding, we only consider in Eq. (6.2) matrix elements between parity-even superconducting ground states in the same super-selection sector. Under these constraints, the ground state is unique in each sector for our models in this section, and the matrix (6.2) is diagonal. These states are obtained by exact diagonalization of the quasiparticle Hamiltonian under the corresponding fermion boundary conditions. This can be done only numerically since, although the wave-functions have the standard BCS form, the system is no longer translationally invariant due to the presence of e -bosons as vortices. The construction of the BCS ansatz in this case is elucidated in Appendix E.

Accordingly we go over to the quasiparticle picture by substituting Eq. (2.28) for $Z_{v_1 v_2}$ inside the bulk on a torus into (6.2), which then becomes a product of matrix elements of the form:

$$\langle \Omega_i | \Omega_j \rangle, \quad \langle \Omega_i | \prod_p (-i\gamma_p \gamma'_p) | \Omega_j \rangle,$$

where $|\Omega_j\rangle$ are the parity-even BCS ground states with respect to given e -configurations and boundary conditions [they are the fermionic parts of $|0_{jm}\rangle$ in (6.2) written in terms of quasiparticle fields]. Analytical expressions for these matrix elements are derived in Appendix F.⁹ However their exact values can only be evaluated numerically.

In the rest of this subsection, we will consider phases with Chern number $C = \pm 1, -2$. In calculating (6.2), we shall apply the formalism just outlined to two cases, the first being γ is along an empty square unit cell. Here the Berry phase is due to the effective ‘magnetic flux’ of the background superconducting vacuum. The background flux turns out to be non-zero

⁹In physical systems, i.e. candidate ‘Kitaev materials’ such as α -RuCl₃, e -vortex (‘vison’) transport is generally not provided by $Z_{v_1 v_2}$ itself, but arises from additional terms in the Hamiltonian. These operators can be expressed as products of e -, ε -motion operators. In the Berry phase, they correspond to additional matrix elements of the form: $\langle \Omega_i | (-i\gamma_{p_1} \gamma'_{p_2}) | \Omega_j \rangle$. For completeness we also show their analytical expressions in Appendix F. These matrix elements give rise to a dispersive vison band, which is considered using the parton construction in Ref. [23] and the present duality in Ref. [27].

in certain phases and quantized. Therefore, in the second case, to study the mutual emergent anyon statistics of e -boson, instead of taking the trajectory γ to encircle another e -boson, we use a different approach that automatically subtracts this background contribution.

6.2.1. $C = \pm 1$ phases

Although in Sec. 5 the Hamiltonian (5.6) contains B, B' phases with $C = \pm 1$, we shall start from a different model (2.33) that is equivalent to the Kitaev honeycomb model [17]:

$$H_K = -J_x \sum_{x\text{-links}} Z_i X_j + J_y \sum_{y\text{-links}} Y_i Y_j - J_z \sum_{z\text{-links}} X_i Z_j; \quad (6.11)$$

see Sec. 2.2.3 and Fig. 9 for the relevant derivations. This is more convenient for checking the predictions made for that model and because of its relevance in materials such as α -RuCl₃; the latter point is discussed at the end of this section.

Let us recall some properties of the effective Kitaev honeycomb model (6.11). As follows from Eq. (2.32), its constituent operators correspond to Majorana bilinears with non-local e -boson parity terms. The e -bosons remain of course static and non-interacting. Omitting the e -parity and boundary-crossing terms, (6.11) is written as:

$$H_K = -J_x \sum_p i\gamma_p \gamma'_{p-\hat{y}} - J_y \sum_p i\gamma_p \gamma'_{p+\hat{x}-\hat{y}} - J_z \sum_p i\gamma_p \gamma'_{p+\hat{x}}. \quad (6.12)$$

\hat{x}, \hat{y} are unit lattice vectors. Passing to momentum representation, the Hamiltonian (6.12) has the BdG form (5.1) with:

$$\begin{aligned} \varepsilon(\mathbf{k}) &= -2 [J_x \cos k_y + J_y \cos(k_x - k_y) + J_z \cos k_x]; \\ \Delta(\mathbf{k}) &= -2i [-J_x \sin k_y + J_y \sin(k_x - k_y) + J_z \sin k_x]. \end{aligned} \quad (6.13)$$

Substituting $\varepsilon(\mathbf{k})$ from (6.13) into (C.12), the $\{\zeta_1, \zeta_2, \zeta_3, \zeta_4\}$ classification scheme gives:

(J_x, J_y, J_z)	$(0, 0)$	$(0, \pi)$	$(\pi, 0)$	(π, π)
$(1, 1, 1)$	1	0	0	0
$(-1, 1, 1)$	1	1	0	1
$(1, -1, 1)$	1	1	1	0
$(1, 1, -1)$	1	0	1	1
$(1, 0, 0)$	1	0	1	0
$(0, 1, 0)$	1	0	0	1
$(0, 0, 1)$	1	1	0	0

Other values of (J_x, J_y, J_z) that differ by an overall minus sign can be obtained by $\zeta \rightarrow 1 - \zeta$.

The phase diagram is also given by Fig. 12 with $h_i \rightarrow J_i$, and the B, B' phases are gapless. Again it is necessary to induce a gap in these phases. It is customary to use the so-called ‘Haldane mass’ term: in the presence of an external magnetic field, it can be shown that the low energy effective Hamiltonian will include three-spin couplings [17]:

$$V = -\kappa \sum_{j,k,l} X_j Y_k Z_l, \quad (6.14)$$

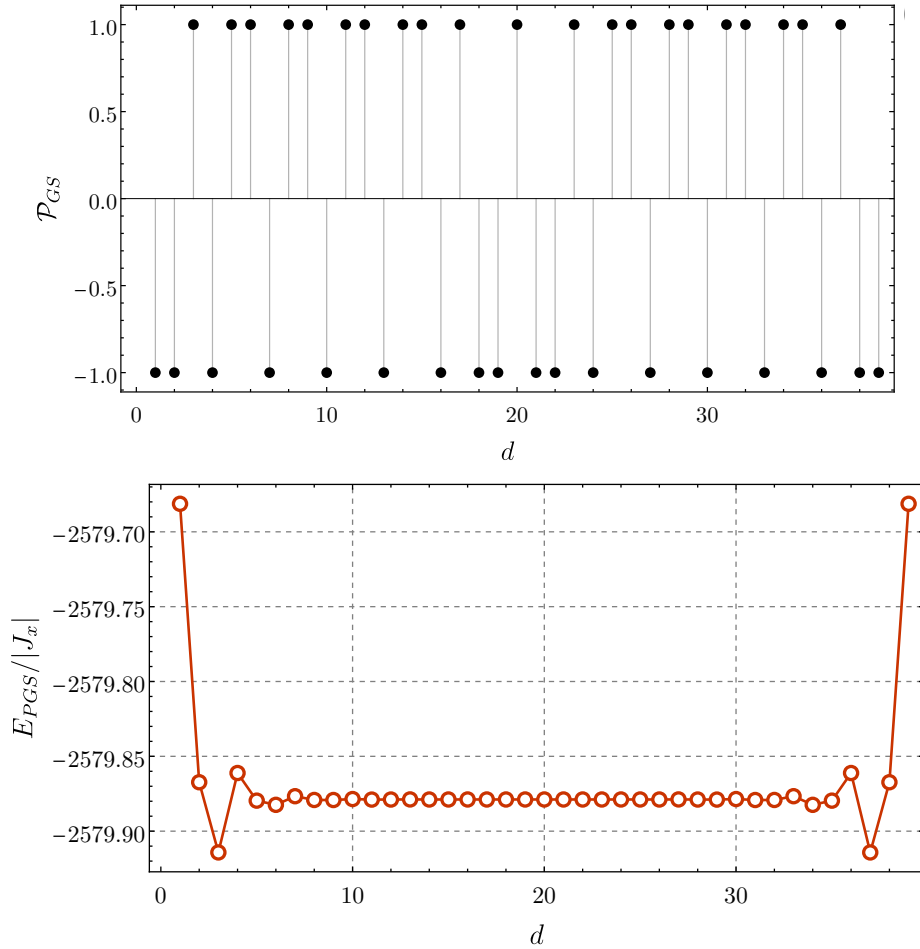


Figure 18: Ground state parity (top) and energy (bottom) of the effective Kitaev honeycomb model (6.12) as a function of e -vortices distance d on a periodic lattice. The two e -vortices are horizontally apart. Lattice size $L_x = L_y = 50$. The symmetry of the features in the bottom figure is due to lattice periodicity. The energy value stabilizes quickly as e -vortices move apart, suggesting that they are deconfined. Ground state parity is calculated using matrix elements of the Hamiltonian written in Majorana bilinears [17].

where the three spins belong to a common hexagon. The perturbation (6.14) can be also mapped to Majorana bilinears of the form $\gamma\gamma, \gamma'\gamma'$; c.f. (5.9). We shall not write them down explicitly, but merely note that the B, B' phases acquire a gap as a result. The Chern number C is then well-defined for these phases depending on the sign of κ . For the rest of this subsection, unless stated otherwise, we consider the phase with $(J_x, J_y, J_z) = (1, \pm 1, 1)$ and $\kappa = 0.1$, which gives $C = \pm 1$. Moreover, $L_x = L_y = L$ is always even.

As a preliminary step, we check the confinement properties of e -bosons. For this purpose we calculate the physical ground state energy for two e -bosons using exact diagonalization; see Appendix E for details. We choose $\{z_1, z_2\} = \{-1, -1\}$ and $J_y = 1$, since then the ground state fermion at $\mathbf{k}_0 = (0, 0)$ is always forbidden by quasimomenta quantization (5.4) under anti-periodic boundary conditions. Here there are two e -bosons at distance d apart and the ground state is approximately two-fold degenerate. This is due to the Majorana zero

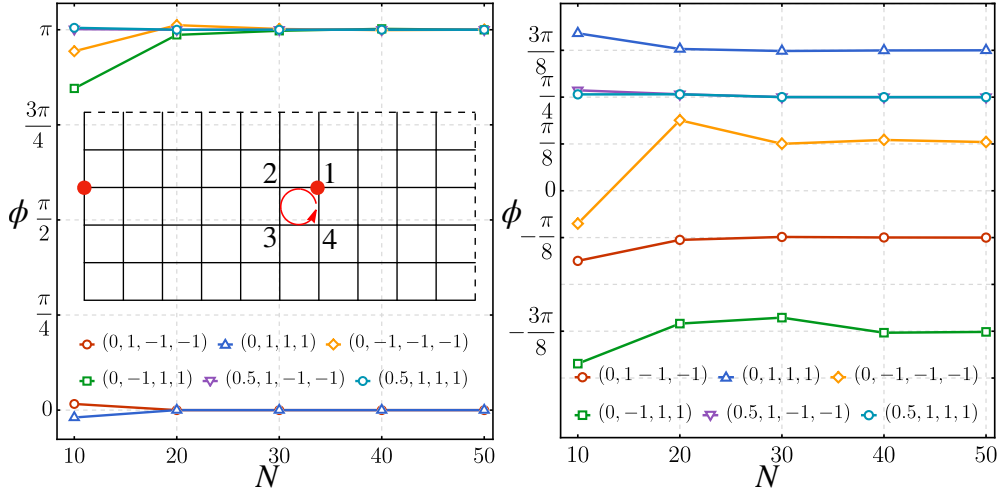


Figure 19: Left: Berry phase from motion of an e -boson around the square unit cell (shown schematically in the inset). The parameter sets in the legend are (t, J_y, z_1, z_2) . In this case $t = 0.5$ corresponds to phases with Chern number $C = -2$. Right: Berry phase from mutual braiding of e -bosons using the Levin-Wen protocol in Fig. 20.

modes inside e -vortices as is the case in p -wave superconductors discussed at the beginning of this section. In fact, the energy of Majorana bound states in vortices has been known to depend on the Chern number in a spinless superconductor, and is zero for C odd [17, 88]; see also Ref. [89] and references therein for quantum vortices in Helium-3. Therefore, one of the two states without the Majorana bound states has ε -parity even while the other has parity odd. In fact the two energy levels cross and oscillate with d , alternately becoming the ground state; see Fig. 18. Thus, at each d one must choose the BCS wave-function with even parity; see Appendix E.1. The physical (parity-even) ground state energy E_0 is then computed numerically with two e -bosons at distance d apart. In Fig. 18, E_0 is plotted as a function of d for $J_x = J_y = J_z = 1$. There it is shown that E_0 converges quickly to a constant limit, and the e -bosons are deconfined.

Having established this fact, we now study the emergent anyon properties of e -bosons by computing the Berry phase (6.2) with BCS ground state wave-functions as discussed at the beginning of this subsection. We first choose the path γ to be along the smallest empty square unit cell, shown schematically in Fig. 19. The Berry phase is:

$$\phi = -i \arg \left[\langle \Omega_1 | \prod_{p \in L(4,1)} (-i \gamma_p \gamma'_p) | \Omega_4 \rangle \langle \Omega_4 | \Omega_3 \rangle \langle \Omega_3 | \prod_{p \in L(3,2)} (-i \gamma_p \gamma'_p) | \Omega_2 \rangle \langle \Omega_2 | \Omega_1 \rangle \right], \quad (6.15)$$

which gives the ‘magnetic flux’ for emergent anyons from the superconducting background. We found that for $J_y = 1$, ϕ converges to 0 as system size L increases; for $J_y = -1$, ϕ converges to π . This value is independent from fermion boundary conditions given by $\{z_1, z_2\}$. The results are presented in Fig. 19.

One can now compute the Berry phase corresponding to mutual braiding of two emergent anyons. However since there are background flux from the superconducting vacuum, instead

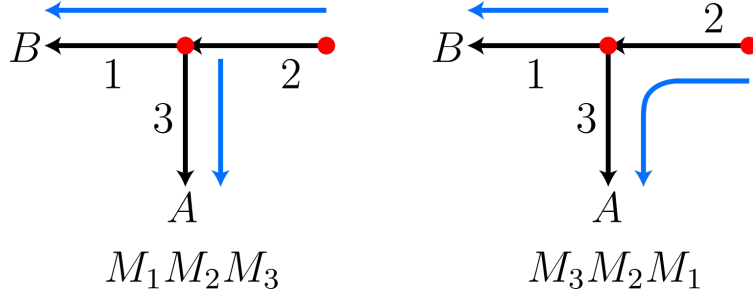


Figure 20: The Levin-Wen protocol [90] for braiding of two e -bosons. Two processes involving two identical abelian anyons moving along three paths 1, 2, 3. Left: the first process ($M_1M_2M_3$) in which the anyon on the left travels to point A and the anyon on the right travels to point B . Right: the second process ($M_3M_2M_1$) in which the anyon on the left travels to B followed by the anyon on the right travelling to A . The final states of the two processes differ by the exchange statistics of the anyons. Figure taken from Ref. [90].

of taking γ in (6.2) to encircle another e -boson, it is more convenient to use a different approach [17, 37, 90]. Here the two e -bosons are adjacent and are moved in sequence in two ways as is shown in Fig. 20. After the movement, the e -boson positions are exchanged with the paths in the opposite orientation. The difference in Berry phases from the two processes then gives the braiding statistics, subtracting the background flux contribution. We will consider only $\{z_1, z_2\} = \pm\{1, 1\}$ at even system size L , because at $\{z_1, z_2\} = \{1, 1\}$ the ground state for $J_y = \pm 1$ without the zero mode has parity odd. The physical ground state thus contains the Majorana bound state. Analogously at $\{z_1, z_2\} = \{-1, -1\}$, the physical ground state does not contain the Majorana mode. Thus by suitably choosing the fermion boundary conditions, we can separate out the desired emergent anyons in question. The results for mutual anyon Berry phase are presented in Fig. 19 for $J_y = \pm 1$. To summarise:

$$\begin{aligned}
 J_y = 1, C = 1: \quad \phi &= \begin{cases} 3\pi/8, \{z_1, z_2\} = \{1, 1\} \text{ (periodic B.C.s)} \\ -\pi/8, \{z_1, z_2\} = \{-1, -1\} \text{ (anti-periodic B.C.s)} \end{cases} \\
 J_y = -1, C = -1: \quad \phi &= \begin{cases} -3\pi/8, \{z_1, z_2\} = \{1, 1\} \text{ (periodic B.C.s)} \\ \pi/8, \{z_1, z_2\} = \{-1, -1\} \text{ (anti-periodic B.C.s)} \end{cases}
 \end{aligned} \tag{6.16}$$

The results in (6.16) accord with the braiding rules in Ref. [17]. As is stated above, for $\{z_1, z_2\} = \{1, 1\}$, the braiding of two e -vortices occurs in the presence of the Majorana bound state, whereas for $\{z_1, z_2\} = \{-1, -1\}$, the braiding is between two e -vortices only. Therefore, adapting the notation in Ref. [17] to our case, the anyon braiding phases are:

$$R_\varepsilon^{e,e} = \exp[i(3\pi/8)C], \quad R_1^{e,e} = \exp[-i(\pi/8)C].$$

For $C = \pm 1$, this is exactly Eq. (6.16).

For reference, we list the ‘fusion rules’ between non-abelian anyons for the $C = \pm 1$ case [17]:

$$\varepsilon \times \varepsilon = 1, \quad \varepsilon \times e = e, \quad e \times e = 1 + \varepsilon,$$

6.2.2. $C = -2$ phase

For generality, we shall also study the emergent anyon properties in another Hamiltonian which has $C = -2$.

Such a Hamiltonian can be constructed by adding four-spin coupling terms to Eqs. (6.11) and (6.14). Regarding the square lattice as a honeycomb shown in Fig. 21, they are operators of the form:

$$X_1 Z_2 X_3 Z_4, Y_2 X_3 Y_4 X_5, Z_3 Y_4 Z_5 Y_6, X_4 Z_5 X_6 Z_1, Y_5 X_6 Y_1 X_2, Z_6 Y_1 Z_2 Y_3. \quad (6.17)$$

In Fig. 21 we also show them explicitly on a square lattice:

$$Z_{6,2} Z_{2,3} Z_{7,3} Z_{6,7} \leftrightarrow -i\gamma_6 \gamma'_6, \quad (6.18a)$$

$$Y_{6,7} Z_{11,7} Y_{10,11} Z_{14,10} \leftrightarrow (-1)^{n_7^e + n_8^e + n_{11}^e + n_{12}^e} (-i\gamma_6 \gamma'_{14}), \quad (6.18b)$$

$$X_{7,3} Y_{6,7} X_{10,6} Y_{5,6} \leftrightarrow (-1)^{n_6^e} (-i\gamma_5 \gamma'_7), \quad (6.18c)$$

$$X_{6,7} X_{10,6} X_{5,6} X_{6,2} \leftrightarrow (-1)^{n_6^e} (-i\gamma_6 \gamma'_6), \quad (6.18d)$$

$$Y_{10,6} X_{5,6} Y_{6,2} X_{2,3} \leftrightarrow (-1)^{n_3^e + n_4^e + n_6^e + n_7^e + n_8^e} (-i\gamma_2 \gamma'_{10}), \quad (6.18e)$$

$$Z_{5,6} Y_{6,2} Z_{2,3} Y_{7,3} \leftrightarrow -i\gamma_5 \gamma'_7; \quad (6.18f)$$

In terms of the Majorana representation defined in Ref. [17], these terms corresponds to third-nearest-neighbor Majorana couplings. The full Hamiltonian is:

$$H = H_K + V + \tilde{H}_t, \quad (6.19)$$

$$\tilde{H}_t = \frac{t}{2} \sum_p (-i\gamma_p \gamma'_p - i\gamma_p \gamma'_{p+2\hat{x}} - i\gamma_p \gamma'_{p-2\hat{y}}).$$

V is given by Eq. (6.14) and t is a constant. We have neglected the e -parity terms in \tilde{H}_t . The gapless dispersion at $\kappa = 0$ is of the form $(p + ip)^2$ and therefore, as can be also shown directly using (C.7), under the parameterization: $J_x = J_y = J_z = 1$, $\kappa = 0.1$ and $t = 0.5$, the $\mathbb{Z} \times (\mathbb{Z}_2)^3$ classification scheme gives $C = -2$ and $\{1111\}$.

We now present numerical results of Berry phase (6.2) for the Hamiltonian (6.19) in super-selection sectors $\{z_1, z_2\} = \pm\{1, 1\}$. In each or the two sectors, the boundary conditions for ε -fermions along x - and y -directions are both periodic or anti-periodic, and the corresponding unique ground state has parity even. This is due to that vortices with C even do not contain Majorana zero modes. As in Sec. 6.2.1, we consider the Berry phase ϕ due to background flux and emergent anyon braiding.

The background flux by moving one e -vortex along the smallest empty plaquette gives $\phi = \pi$; the dependence of ϕ on system size and its convergence to π are shown for $\{z_1, z_2\} = \pm\{1, 1\}$ in Fig. 19.

For anyon braiding, even though the ground state in each super-selection sector is unique, the result somehow depends on the positions of the two anyons inside the lattice. This problem can be circumvented by adding opposite constant potentials to the four plaquettes around each e -vortex. The results are shown numerically in Fig. 19. We found that the

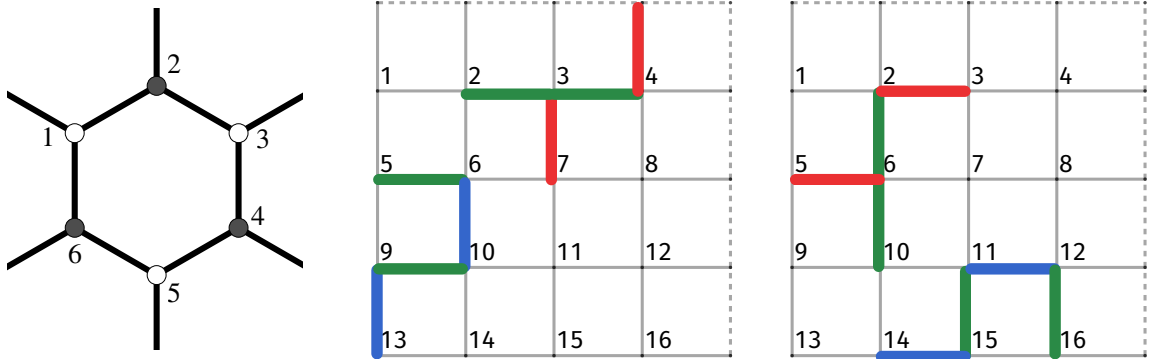


Figure 21: Left: the numbering of spin degrees of freedom on the honeycomb lattice. Center and right: some of the four-spin coupling terms shown explicitly on the square lattice. Each number represents both a vertex and the plaquette to its North-East. The green lines mean Y operators on the corresponding edge.

Berry phase then converges to $\phi = \pi/4$, which accords with the following anyon braiding rule in Ref. [17]:

$$R_1^{a,\bar{a}} = \exp[i(\pi/8)C].$$

Here a and \bar{a} are two types of anyons that fuse into a fermion.

The fusion rules between quasiparticles for the $C = -2$ case are [17]:

$$a \times \varepsilon = \bar{a}, \quad \bar{a} \times e = a, \quad \varepsilon \times \varepsilon = 1, \quad a \times a = \bar{a} \times \bar{a} = \varepsilon, \quad a \times \bar{a} = 1.$$

6.3 Discussion of Results and Experimental Relevance

We have found, using explicit numerical computations, the mutual statistics of low-energy e -bosons on a superconducting background with non-trivial topology. For $C = \pm 1, -2$, the results agree with the predictions made in Ref. [17]. Here even though the braiding is non-abelian (it depends on the presence or absence of an ε -fermion), the cases with and without fermions are effectively separated in our system. This is because braiding can occur only in a given super-selection sector with the corresponding fermion boundary conditions. In all cases under consideration, the physical ground state which has fermion parity even, is unique and calculating the matrix elements (6.2) reduces to calculating a scalar. They correspond to braiding with or without fermions depending on quasimomentum quantization of the ground state fermions at high-symmetry quasimomenta.

Similarly, the calculation of (6.2) for e -motion around the smallest empty plaquette also reduces to calculating the scalar Berry phase. We found that the Berry phase ϕ is quantized to be 0 or π , depending on the underlying topology of the superconducting phase of ε -fermions. We emphasize that although the value of ϕ depends on $\{\zeta_i\}$, it might be unrelated to the actual ground state fermions that $\{\zeta_i\}$ correspond to. This is because the value of ϕ is independent from the choice of fermion boundary conditions in all cases we considered, while the ground state fermions might be absent due to quasimomentum quantization. In this sense, the background magnetic flux in each plaquette seems to be an invariant characteristic of the underlying bulk topology of the superconducting vacuum,

which is classified by the $\{\zeta_i\}$ indices. The problem remains of determining analytically their relation to ϕ for a given superconducting phase.

However, our numerical results support the following conjecture: $\phi = 0$ for topological phases with less than two of the four ζ_i indices being unity, and $\phi = \pi$ for phases with more than two of the four ζ_i indices being unity. Remember that phases with two ζ_i indices non-zero exhibit weak symmetry breaking, which forbids e -bosons from travelling to certain adjacent sites at low energy. This conjecture is further supported by the Atomic Insulator phases in (5.13). In this case, the Berry phase is simply given by the parity of each plaquette, and is 0 for $h_z > 0$ with $\{0000\}$, and π for $h_z < 0$ with $\{1111\}$.

7 \mathbb{Z}_N Topological Order

In this section, we shall discuss topological order in certain models which are generalizations of \mathbb{Z}_2 theories to \mathbb{Z}_N with $N \geq 3$. As we shall see, the situation becomes considerably more complex than the \mathbb{Z}_2 case. To avoid confusion, the notations in this section are independent from those in the rest of the thesis.

As will be shown in Sec. 7.1, the number of types of elementary excitations in a \mathbb{Z}_N lattice theory is $N^2 - 1$. They generally have ‘para-statistics’ with respect to themselves (‘*parafermions*’). It turns out that, contrary to the \mathbb{Z}_2 case, constructing explicit particle operators for parafermions is not generally possible in a \mathbb{Z}_N theory for $N > 2$. This point will be discussed in Secs. 7.2 and 7.3. But as will be shown, certain \mathbb{Z}_N Hamiltonians that are generalizations of the models considered in Sec. 5 can be solved exactly on the spin lattice, and exhibit similar properties to the corresponding \mathbb{Z}_2 topological order. The results are presented in Sec. 7.4.

7.1 Definitions and Elementary Excitations

In a \mathbb{Z}_2 theory on a square lattice, the local spin-1/2 degrees of freedom are on each edge with $s_z = \pm 1/2$ being two internal states of a given edge. In a \mathbb{Z}_N theory, each edge has N internal states: $|n\rangle, n = 0, 1, \dots, N-1$. We now have, instead of Pauli matrices σ_x, σ_z which satisfy $\sigma_x^2 = \sigma_z^2 = 1$, their \mathbb{Z}_N analogues X, Z :

$$\begin{aligned} Z|n\rangle &= \omega^n |n\rangle, \quad X|n\rangle = |n+1\rangle \pmod{N}, \quad \omega = \exp\left(\frac{2\pi i}{N}\right), \\ ZX &= \omega XZ, \quad X^N = Z^N = 1; \quad \sum_{n=0}^{N-1} \omega^n = 0. \end{aligned} \tag{7.1}$$

From (7.1) we define generalized electric and magnetic charge operators on vertices and plaquettes:

$$Q_v = X_1 X_2 X_3^\dagger X_4^\dagger, \quad \Omega_p = Z_5 Z_6 Z_7^\dagger Z_8^\dagger. \tag{7.2}$$

These operators are shown graphically in Fig. 22. The new operators mutually commute with eigenvalues $\omega^k, k = 0, 1, \dots, N-1$; compare with operators in the Toric Code in (1.2). We then define the ‘ \mathbb{Z}_N Toric Code’ Hamiltonian:

$$H = - \sum_v Q_v - \sum_p \Omega_p + \text{h.c.} \tag{7.3}$$

The summation is taken over all vertices and plaquettes on the lattice. Repeating the same arguments as given in Sec. 1.2, we can regard Q_v and Ω_p as local \mathbb{Z}_N charge operators of certain elementary excitations. $Q_v = \Omega_p = 1$ still designates the vacuum. For $Q_v = \omega$ at a given vertex, the vertex is occupied by a quasiparticle e with \mathbb{Z}_N electric charge ω . Similarly, quasiparticle m with \mathbb{Z}_N magnetic charge ω occupies a plaquette p if $\Omega_p = \omega$. Other internal states on each vertex and plaquettes corresponding to other eigenvalues of Q_v and Ω_p , can be seen as composite particles of multiple e - or m -particles. In fact, generally

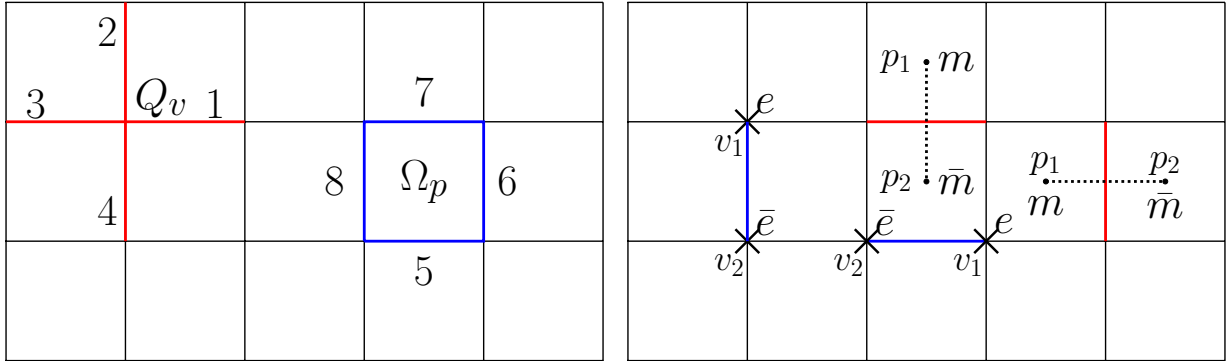


Figure 22: Left: electric and magnetic charge operators in Eq. (7.2). Right: pair-creation operators (7.5) of (e, \bar{e}) and (m, \bar{m}) are also shown. Note the directionality of v_1, v_2 and p_1, p_2 . Edges multiplied by X or X^\dagger (Z or Z^\dagger) are shown in red (blue).

in \mathbb{Z}_N lattice theories, there are $N^2 - 1$ types of particles, constructed from the ‘elementary’ e - and m -particles. We write for each particle type:

$$(\alpha, \beta) : e^\alpha \times m^\beta, \quad \alpha, \beta = 0, 1, \dots, N-1. \quad (7.4)$$

The $\alpha = \beta = 0$ case is the vacuum. For a particle η given by (α, β) , its anti-particle is given by $\bar{\eta}$ and has charges $(N - \alpha, N - \beta)$. In particular, the anti-particles of e and m are not themselves, which have different \mathbb{Z}_N charges. They are denoted by \bar{e} and \bar{m} .

We can define analogous nearest-neighbour pair-creation operators for e and m :

$$U_{v_1 v_2}^{e, \bar{e}} = Z_{v_1 v_2}, \quad U_{p_1 p_2}^{m, \bar{m}} = X_{p_1 p_2}, \quad (7.5)$$

which creates an e -, \bar{e} -particle pair on vertices v_1, v_2 , and an m -, \bar{m} -particle pair on plaquettes p_1, p_2 respectively. Here the convention is as follows: for horizontal pair-creation, v_1 is to the right of v_2 while p_1 is to the left of p_2 ; for vertical pair-creation, both v_1 and p_1 are above v_2 and p_2 . The pair-creation operators for any composite particles given by (α, β) are defined similarly as products of operators in (7.5). As in the \mathbb{Z}_2 case, the local pair-creation operators conserve electric and magnetic charges. On a periodic spin lattice, this corresponds to the following global constraint for \mathbb{Z}_N charges:

$$\prod_{p \in \text{lattice}} \Omega_p = 1, \quad \prod_{v \in \text{lattice}} Q_v = 1. \quad (7.6)$$

It follows from (7.6) that the ‘ \mathbb{Z}_N Toric Code’ (7.3) has ground state degeneracy N^2 . On an open lattice, charges can be created with non-local operators; see the analogous \mathbb{Z}_2 case in Sec. 2.

From Eq. (7.5) and analogous arguments to those in Sec. 1.2, e - and m -particles are bosonic with respect to themselves, but have mutual statistical angle π/N . Bound states of both e - and m -particles have ‘para-statistics’ with respect to themselves: after encircling one such composite particle by another, the wave-function acquires a phase of $(\alpha + \beta)\pi/N$. These

are therefore parafermions. As will be discussed in Sec. 7.3, parafermions are considerably more complex than the ε -fermions in \mathbb{Z}_2 theories.

As in the \mathbb{Z}_2 case, the choice of ‘elementary particles’ is not unique. The problem therefore arises of whether all types of particles can be formed by a given set of ‘elementary particles’. In fact, the composite-particle configurations in (7.4) can be seen as a $\mathbb{Z}_N \times \mathbb{Z}_N$ group, and the e - and m -charges $(1, 0)$ and $(0, 1)$ are the corresponding generators. If $\mathbb{Z}_N \times \mathbb{Z}_N$ has subgroups, then it is possible to choose for a given theory a reduced set of ‘elementary particles’. For instance, by choosing them to be $(2, 0)$ and $(0, 2)$ in a \mathbb{Z}_4 theory, we obtain the $\mathbb{Z}_2 \times \mathbb{Z}_2$ subgroup. A theory containing only these two particles and their bound-states is equivalent to the \mathbb{Z}_2 theories considered in the rest of this thesis. We shall neglect such cases and always assume an ‘irreducible’ set of ‘elementary particles’. This can be done, for example, by taking N to be prime. Note that for such an ‘irreducible’ set, other types of ‘elementary particles’ than e and m are possible. Geometrically, the problem is equivalent to finding two independent lattice vectors in a unit cell with side-length N and sites at integer coordinates given by (α, β) . Due to the aforementioned complexity associated with parafermions, we shall choose the ‘elementary particles’ to be e and m .

7.2 Duality Mapping

Let us construct the Hilbert space of e - and m -particles for the \mathbb{Z}_N case.

We start from the open lattice. The construction of the open boundaries is explained at the beginning of Sec. 2. Similarly to the \mathbb{Z}_2 case in Sec. 2.1, we pass from the \mathbb{Z}_N basis to the basis of local occupation numbers of e - and m -particles on each vertex and plaquette:

$$|\dots n_v^e \dots, n_p^m \dots\rangle; n_v^e, n_p^m = 0, 1, \dots, N - 1.$$

Under the new basis, we define the τ and σ operators:

$$\tau|n\rangle = |n + 1\rangle, \sigma|n\rangle = \omega^n|n\rangle, \tau|N - 1\rangle = |0\rangle. \quad (7.7)$$

As in Sec. 2, we neglect the e , m superscript when referring to both particles. τ and σ satisfy the algebra:

$$\sigma\tau = \omega\tau\sigma, \sigma^N = \tau^N = 1.$$

It is clear that Q_v and Ω_p operators map to σ_v^e and σ_p^m . Then the non-local products of Z^\dagger and X^\dagger operators with the same paths in (2.5) and (2.12) map to τ^e and τ^m . Note the directionality of the strings which distinguishes X, Z from X^\dagger, Z^\dagger , as the τ_v^e strings go from right to left towards v and τ_p^m from left to right towards p ; see the discussions below (7.5).

We can now construct the quasiparticle operators. For concreteness we discuss the case for e -particle annihilation operator b_v and neglect the superscript e . Annihilation operators for m -particles a_p are constructed in an entirely similar way. On a given vertex, b_v satisfies the usual bosonic algebra:

$$b|n\rangle = \sqrt{n}|n - 1\rangle, b^\dagger|n\rangle = \sqrt{n + 1}|n + 1\rangle, n \neq 0; b|0\rangle = b^\dagger|N - 1\rangle = 0. \quad (7.8)$$

To find b in terms of τ and σ , it is useful to define the local projection operators P_n to a given occupation number n :

$$P_n|m\rangle = \delta_{nm}|m\rangle. \quad (7.9)$$

P_n can be expressed in terms of σ :

$$P_n = \frac{1}{N} \sum_{k=0}^{N-1} \omega^{-nk} \sigma^k. \quad (7.10)$$

To see this, consider:

$$P_n|m\rangle = \frac{1}{N} \sum_{k=0}^{N-1} \omega^{(m-n)k} |m\rangle.$$

For both $m = n$ and $(m - n)$ prime with respect to N , the result agrees with (7.9), as follows from the identity $\sum_{n=0}^{N-1} \omega^n = 0$. If N is divisible by $(m - n)$: $N = (m - n)l$, then it is clear that the sum over k decomposes into $m - n$ number of identical sums over powers of $\omega^{(m-n)}$. Each of these sums vanishes due to the identity: $\sum_{n=0}^{l-1} \omega'^n = 0$, $\omega' = \omega^{(m-n)}$, $\omega'^l = 1$.

The projectors satisfy the following relations:

$$\tau P_n = P_{n+1} \tau, \quad \tau^\dagger P_n = P_{n-1} \tau^\dagger, \quad P_n P_m = \delta_{nm} P_n, \quad \sum_{n=0}^{N-1} P_n = 1. \quad (7.11)$$

It follows from Eqs. (7.8) and (7.9) that, in terms of projectors P_n and τ , b is written as:

$$b = \tau^\dagger \left(\sum_{n=1}^{N-1} \sqrt{n} P_n \right), \quad b^\dagger = \left(\sum_{n=1}^{N-1} \sqrt{n} P_n \right) \tau. \quad (7.12)$$

The boson commutation relation on the same site is:

$$\begin{aligned} [b, b^\dagger] &= \left[\tau^\dagger \left(\sum_{n=1}^{N-1} \sqrt{n} P_n \right), \left(\sum_{m=1}^{N-1} \sqrt{m} P_m \right) \tau \right] \\ &= \tau^\dagger \left(\sum_{n,m=1}^{N-1} \sqrt{n} \sqrt{m} P_n P_m \right) \tau - \left(\sum_{n,m=1}^{N-1} \sqrt{n} \sqrt{m} P_m P_n \right) \\ &= \tau^\dagger \left(\sum_{n=1}^{N-1} n P_n \right) \tau - \sum_{n=1}^{N-1} n P_n \\ &= \sum_{n=0}^{N-2} P_n - (N-1) P_{N-1}. \end{aligned}$$

Eq. (7.12) generalizes the \mathbb{Z}_2 hardcore boson construction (2.3) to the \mathbb{Z}_N case. It is not clear if Eq. (7.12) can be inverted and if τ can be expressed in terms of b, b^\dagger for $N \geq 3$. Formally, using the last two identities in (7.11) and substituting (7.12), we have:

$$\left(\sum_{n=1}^{N-1} \frac{1}{\sqrt{n}} P_n \right) b^\dagger = \left(\sum_{n=1}^{N-1} P_n \right) \tau = (1 - P_0) \tau.$$

But $(1 - P_0)$ is not invertible. Alternatively, $P_0\tau = P_0b\tau^2$ and one can write:

$$\tau = \left(\sum_{n=1}^{N-1} \frac{1}{\sqrt{n}} P_n \right) b^\dagger + P_0 b \tau^2, \quad (7.13)$$

where we have substituted Eqs. (7.11) and (7.12). For $N = 2$:

$$P_1 = b^\dagger b, \quad P_0 = 1 - b^\dagger b, \quad b^2 = b^{\dagger 2} = 0, \quad \tau^2 = 1,$$

and we return to (2.3). However for $N > 2$, Eq. (7.13) is non-linear in τ . Therefore, it seems that τ can at most be mapped to a sum in powers of b and b^\dagger .

The mapping from pair-creation operators (7.5) to τ, σ can then be constructed along similar lines to Sec. 2.1, and we shall simply state the results. We then have, for horizontal pair-creations:

$$U_{v_1 v_2}^{e, \bar{e}} \rightarrow \tau_{v_1}^e \tau_{v_2}^{e\dagger}, \quad U_{p_1 p_2}^{m, \bar{m}} \rightarrow \tau_{p_1}^m \tau_{p_2}^{m\dagger}. \quad (7.14)$$

Along the vertical direction:

$$U_{v_1 v_2}^{e, \bar{e}} \rightarrow \tau_{v_1}^e \tau_{v_2}^{e\dagger} \left(\prod_{\substack{p \in \\ R(v_1, v_2)}} \sigma_p^{m\dagger} \right), \quad U_{p_1 p_2}^{m, \bar{m}} \rightarrow \tau_{p_1}^m \tau_{p_2}^{m\dagger} \left(\prod_{\substack{v \in \\ L(p_1, p_2)}} \sigma_v^e \right). \quad (7.15)$$

$R(v_1, v_2)$ means plaquettes to the right of the edge that joins v_1 and v_2 , and $L(p_1, p_2)$ are vertices to the left of the line that connects the centers of p_1 and p_2 . As the next step, one should substitute τ in terms of quasiparticle operators a_p, b_v . But as is shown above, it is not clear how this is done for τ . One can only obtain mappings of the form $b_{v_1}^\dagger b_{v_2}, a_{p_1}^\dagger a_{p_2}$, by multiplying $U_{v_1 v_2}^{e, \bar{e}}$ and $U_{p_1 p_2}^{m, \bar{m}}$ with appropriate powers of projectors, which follows from (7.12).

On a periodic spin lattice, due to the global constraints (7.6), the proper counting of independent degrees of freedom again necessitates Wilson and t' Hooft operators. They correspond to creating a particle-antiparticle pair which is then annihilated after the particle traversing the entire lattice. They are given by the same expression as in Eqs. (1.5) and (1.6) with eigenvalues $1, \omega, \omega^2, \dots, \omega^{N-1}$. The commutation relation is now given by:

$$T_x W_y = \omega W_y T_x, \quad T_y W_x = \omega W_x T_y.$$

The mapping between \mathbb{Z}_N operators and τ, σ can be constructed in the same way as in the \mathbb{Z}_2 case in Sec. 2.1 on the torus. Note that strings of operators that defines τ_p^m, τ_v^e now have directionality, as follows from the convention of pair-creation operators (7.5). For τ_p^m strings extending right and down, the operators become now X^\dagger whereas for strings extending left and up they remain X . For τ_v^e strings, the operators are Z^\dagger for extending left and down, and Z for up and right. We shall not repeat the derivation here but merely mention that the branch-cut conventions, and the relation between $W_{x,y}$ and m -particle boundary conditions are entirely similar.

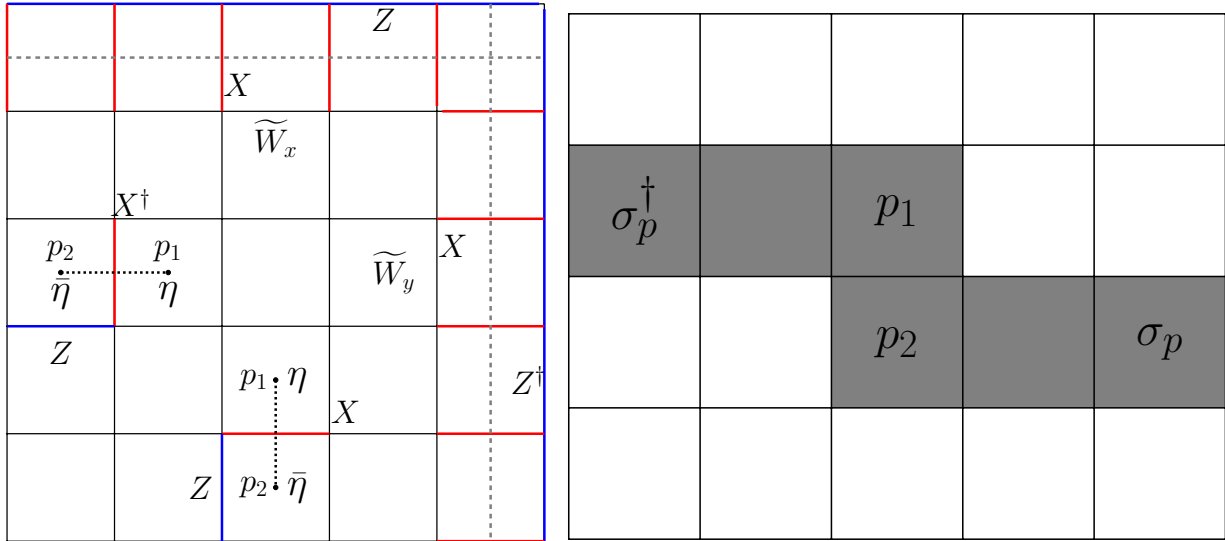


Figure 23: Left: Wilson loop operators (7.20), and horizontal and vertical pair-creation operators in (7.21) for parafermions η . Right: the duality mapping for vertical pair-creation operators (7.22). Shaded plaquettes on the upper row are multiplied by σ_p^\dagger whereas those on the lower row are multiplied by σ_p .

7.3 Parafermion Operators

As has been shown so far in this section, it is possible to construct e - and m -particle operators and their Hilbert spaces in a general \mathbb{Z}_N theory similarly to the \mathbb{Z}_2 case.

The situation is considerably more complex for bound-states of e and m . For concreteness, let us consider the bound states η of a single e - and m -particle. As is mentioned in Sec. 7.1, η are parafermions and have statistical angle $2\pi/N$ with respect to itself. Its field operators on different sites then must satisfy commutation relations of the form:

$$\eta_i \eta_j = \omega \eta_j \eta_i, \quad i > j. \quad (7.16)$$

In writing $i > j$ we have taken a certain ordering of sites. However, it immediately follows that the commutation relations for a pair of parafermion fields η_i, η_j depend on their relative positions i, j . For reading Eq. (7.16) backwards then gives:

$$\eta_i \eta_j = \omega^* \eta_j \eta_i, \quad i < j.$$

As a result, parafermions couple to each other non-uniformly in space by definition. The spatial non-uniformity is generally a result of interactions and it is not clear if ‘free parafermions’ can be defined physically, despite the similarity between certain free fermion models and their \mathbb{Z}_N generalizations.¹⁰

In what follows we shall describe some attempts towards constructing parafermion fields η based on the \mathbb{Z}_2 analogue. We again define η_p at a plaquette p as a composite particle of

¹⁰We mention in this connection a work by P. Fendley [91], in which ‘free parafermions’ are defined. But the Hamiltonians turn out to be non-Hermitian.

an m -charge at p and an e -charge to the South-West vertex. The electric charge operator is then written in terms of Q_v and Ω_p defined in (7.2):

$$\tilde{Q}_v = Q_v \times \Omega_{\text{NE}(v)}^\dagger, \quad (7.17)$$

while Ω_p is reserved for the parafermion charge operator $\tilde{\Omega}_p$. The operators that create η - $\bar{\eta}$ pairs on adjacent plaquettes are given by:

$$U_{p_1 p_2}^{\eta, \bar{\eta}} = X^\dagger Z, \text{ (horizontal); } U_{p_1 p_2}^{\eta, \bar{\eta}} = X Z, \text{ (vertical),} \quad (7.18)$$

which are illustrated in Fig. 23. On a periodic lattice, \tilde{Q}_v and $\tilde{\Omega}_p$ satisfy the global constraints:

$$\prod_{p \in \text{lattice}} \tilde{\Omega}_p = 1, \quad \prod_{v \in \text{lattice}} \tilde{Q}_v = 1. \quad (7.19)$$

We suppose that the resulting Wilson loop operators for parafermions also commute with \tilde{Q}_v in (7.17), and its contour can be deformed by multiplication of \tilde{Q}_v . This determines $\tilde{W}_{x,y}$:

$$\tilde{W}_x = \prod X Z, \quad \tilde{W}_y = \prod X Z^\dagger; \quad (7.20)$$

see Fig. 23. $\tilde{W}_{x,y}$ operators in (7.20) differs from their \mathbb{Z}_2 analogue in two crucial aspects: they cannot be written as a product of $U^{\eta, \bar{\eta}}$ and Ω_p , and do not mutually commute:

$$\tilde{W}_x \tilde{W}_y = \omega^2 \tilde{W}_y \tilde{W}_x.$$

The corresponding t' Hooft operators $\tilde{T}_{x,y}$ are taken to be the same as the ones given in Sec. 7.2.

Due to the non-commutativity of \tilde{W}_x and \tilde{W}_y , passing over to the basis of parafermion occupation number becomes ambiguous. Although one can follow the \mathbb{Z}_2 analogue and define locally τ^η, σ^η in the basis of parafermion occupation (see Sec. 2.2), it is not clear what set of topological operators should be chosen for a complete description of the quasiparticle Hilbert space on a periodic lattice. A way to do this is to construct $\tau_i^\eta \tau_j^{\eta^\dagger}$ operators for cross-boundary pair-creation. It is expected that the result would decompose into a product of the corresponding $U^{\eta, \bar{\eta}}$, e - and η -charge operators σ^e and σ^η , and the topological parity operators. This gives $\tilde{W}_x (\tilde{T}_x^\dagger)^2$ for horizontal motion, while traversing the vertical boundary gives $\tilde{W}_y (\tilde{T}_y)^2$. They do not mutually commute for $N \neq 2$, which is necessary for specifying the Hilbert space. This is due to the aforementioned fact that $\tilde{W}_{x,y}$ cannot be written as products of η -motion and charge operators.

To circumvent this difficulty, we shall consider open boundary conditions only. From the \mathbb{Z}_N lattice we again pass to the Hilbert space of local parafermion occupation numbers with operators τ^η, σ^η . Let us discuss the possibility of constructing parafermion fields using a generalized Jordan-Wigner transformation. To simplify the discussions, we neglect e -particles.

As a first step, we find the mapping from $U_{p_1 p_2}^{\eta, \bar{\eta}}$ to τ^η ; $\tilde{\Omega}_p$ is assumed to map to σ_p^η . This can be done by defining τ^η as $\tau^e \tau^m$ with the prescribed binding convention and use the results in Sec. 7.2. Repeating the derivations given in Sec. 2.2 and note that X, Z and X^\dagger, Z^\dagger are now distinct, we obtain (neglecting the superscript η):

$$\begin{aligned} U_{p_1 p_2}^{\eta, \bar{\eta}} \text{ (horizontal)} &\rightarrow \tau_{p_2}^\dagger \tau_{p_1}; \\ (U_{p_1 p_2}^{\eta, \bar{\eta}})^\dagger \text{ (vertical)} &\rightarrow \omega \left(\prod_{p \in R(p_2)} \sigma_p \right) \left(\prod_{p \in L(p_1)} \sigma_p^\dagger \right) \tau_{p_1}^\dagger \tau_{p_2}, \end{aligned} \quad (7.21)$$

where $L(p)$ and $R(p)$ are all plaquettes to the left and right of and including the given plaquette p on the same row. The plaquettes included in the products of σ and σ^\dagger are shown in Fig. 23. It seems that, due to the presence of both σ_p and σ_p^\dagger terms in (7.21), Eq. (7.21) cannot be mapped to bilinears of parafermions using a \mathbb{Z}_N analogue of Jordan-Wigner transformation. This is because such a transformation for parafermion fields η, η' necessarily has the form:

$$\eta_p = \omega \left(\prod_{p'} \sigma_{p'} \right) \sigma_p \tau_p^\dagger, \quad \eta'_p = \left(\prod_{p'} \sigma_{p'} \right) \tau_p^\dagger, \quad (7.22)$$

so that the horizontal pair-creation can be mapped to $\eta^\dagger \eta'$. But then vertical pair-creation cannot have the parity terms as in Eq. (7.21). However, one can introduce an additional pair of parafermion fields χ, χ' with σ^\dagger instead of σ for plaquettes on the same row as p in (7.22). Then horizontal pair-creation is mapped to $\eta^\dagger \eta'$ or $\chi^\dagger \chi'$, while vertical pair-creation is $\chi^\dagger \eta$. But the introduction of additional fields is not justified.

To conclude, we mention in passing Ref. [92] in which a definition of parafermion fields is given. In our construction here, their results can be derived using (7.22) in one spatial dimension and projection operators P_n given by (7.10). In this case, a bilinear parafermion operator $\Psi_i^\dagger \Psi_j$ that transports a parafermion with charge ω from site j to i is assumed to have the following form:

$$\Psi_i^\dagger \Psi_j = \tau_i \tau_j^\dagger (1 - P_{0,j}) (1 - P_{N-1,i}) = \left[\tau_i^\dagger (1 - P_{0,i}) \right]^\dagger \tau_j^\dagger (1 - P_{0,j}), \quad (7.23)$$

where we have used the identities in (7.11). The projectors annihilate a given initial state if there is no parafermion charge on site j or the charge is ω^{N-1} on site i , and conserve the total charge. The $\tau_i \tau_j^\dagger$ term then changes the parafermion occupation numbers accordingly. It is then possible to define Ψ in terms of η and η' using (7.22) and obtain (7.23); this is given by Eq. (130) in Ref. [92]. For example, for $N = 3$ we have:

$$\Psi_i^\dagger \Psi_{i+1} = \tau_i \tau_{i+1}^\dagger (1 - P_{0,i+1}) (1 - P_{2,i}) = \left[\tau_i^\dagger (1 - P_{0,i}) \right]^\dagger \tau_{i+1}^\dagger (1 - P_{0,i+1}). \quad (7.24)$$

It can be verified that the following definition:

$$\Psi_i = \frac{1}{3} \left(2\eta'_i - \omega \eta_i^\dagger \eta_i^\dagger - \eta_i \right) = \frac{\tau_i^\dagger}{3} \left(2 - \sigma_i^\dagger - \sigma_i \right), \quad (7.25)$$

which is Eqs. (130) in Ref. [92] for $N = 3$, reproduces Eq. (7.24).

In this construction, parafermions with charge ω^k are given by the composite operator $(\Psi)^k$. In particular, the local parafermion occupation number operator [92]:

$$N = \sum_{k=1}^{N-1} \Psi^{\dagger k} \Psi^k = \text{diag}\{0, 1, \dots, N-1\}.$$

Furthermore, N satisfies the commutation relations:

$$[N, \Psi] = -\Psi, \quad [N, \Psi^\dagger] = \Psi^\dagger,$$

which suggests that Ψ indeed annihilates a parafermion.

7.4 Exact Solutions on Periodic Spin Lattices

Despite the apparent difficulty in constructing parafermion operators, it is possible to obtain exact solutions of certain ‘parafermionic’ Hamiltonians on the lattice, the simplest example being the ‘ \mathbb{Z}_N Toric Code’ (7.3). In this subsection we solve the \mathbb{Z}_N generalization of the \mathbb{Z}_2 KW_{*x*} model (5.15):

$$H = -h_x \sum_{p \in \text{horizontal}} U_{p_1 p_2}^{\eta, \bar{\eta}} - \Delta_e \sum_v \tilde{Q}_v + \text{h.c.} \quad (7.26)$$

Despite the ambiguity in interpreting (7.26) in terms of elementary excitations, an exact solution exists on the \mathbb{Z}_N lattice which has many similar properties to the \mathbb{Z}_2 case, i.e. the dependence of ground state degeneracy on lattice size.

The solution is analogous to the one given in Sec. 5.2.3, by finding the constraints between constituent operators in (7.26) and the global topological operator \tilde{W}_x . Before proceeding, we need to designate the other topological operator so that the full Hilbert space is correctly taken into account. As is noted, \tilde{W}_y does not commute with \tilde{W}_x , and cannot be used. As will be shown below, it seems appropriate for this purpose to use \tilde{T}_x , which commutes with all other operators.

The global constraint is, for L_y even:

$$\left(\prod_{v \in \text{odd rows}} \tilde{Q}_v \right) \left(\prod_{p \in \text{odd rows}} U_{p_1 p_2}^{\eta, \bar{\eta}} \right) \left[\prod_{p \in \text{even rows}} (U_{p_1 p_2}^{\eta, \bar{\eta}})^\dagger \right] = 1; \quad (7.27)$$

compare with (5.19). The other global constraint on \tilde{Q}_v is provided by Eq. (7.19), and we have ground state degeneracy $3^2 = 9$.

Comparing with (5.20), the L_y odd case now gives:

$$\left(\prod_{v \in \text{odd rows}}^{L_y-2} \tilde{Q}_v \right) \left(\prod_{p \in \text{odd rows}} U_{p_1 p_2}^{\eta, \bar{\eta}} \right) \left[\prod_{p \in \text{even rows}} (U_{p_1 p_2}^{\eta, \bar{\eta}})^\dagger \right] = \tilde{W}_x^\dagger (\tilde{T}_x)^2. \quad (7.28)$$

On the first line, the first product is taken over all vertices on odd rows up until and including the $(L_y - 2)$ -th row. The next two products are taken over all plaquettes on odd and even rows. We see that \widetilde{W}_x and \widetilde{T}_x are not independent, and there is only one topological operator corresponding to the three-fold ground state degeneracy which is taken to be \widetilde{T}_x .

The degrees of freedom counting can now be summarized as:

operators	degrees of freedom
\widetilde{Q}_v	$L_x L_y - 1$
$U_{p_1 p_2}^{\eta, \bar{\eta}}$ (horizontal)	$L_x L_y - z$
\widetilde{W}_x	z
\widetilde{T}_x	1

$$z = \begin{cases} 1, & L_y \text{ even} \\ 0, & L_y \text{ odd} \end{cases}$$

The ground state degeneracy is then N^{1+z} , where $1+z$ is the number of independent global topological operators.

It is also interesting to study phase transitions in the \mathbb{Z}_N case and consider the following model:

$$H = -h_x \sum_{p \in \text{horizontal}} U_{p_1 p_2}^{\eta, \bar{\eta}} - h_z \sum_p \Omega_p - \Delta_e \sum_v \widetilde{Q}_v + \text{h.c.}, \quad (7.29)$$

which reduces to (7.26) at $|h_x| \gg h_z > 0$, and to the ‘ \mathbb{Z}_N Toric Code’ (7.3) at $|h_x| \ll h_z$. On a torus, as in the \mathbb{Z}_2 case, the dependence of ground state degeneracy on lattice size is qualitatively different in the two limits, and a phase transition must occur at intermediate $|h_x|$. In the \mathbb{Z}_2 case, model (7.29) corresponds to the horizontal axis on the phase diagram Fig. 12 and the critical points are at $h_x = \pm h_z$. For the \mathbb{Z}_N case the following argument suggests that at least the critical point $h_x = h_z$ remains.

We map (7.29) to a model of τ and σ operators of parafermions on an infinite lattice using (7.21); the constraint $\widetilde{Q}_v = 1$ is imposed. This gives:

$$H = -h_x \sum_{p \in \text{horizontal}} \tau_{p_1}^\dagger \tau_{p_2} - h_z \sum_p \sigma_p + \text{h.c.} \quad (7.30)$$

This gives decoupled chains of the \mathbb{Z}_N analogue of the transverse Ising model. At $|h_x| \gg h_z > 0$ and $|h_x| \ll h_z$, the ground states have $\tau_p = 1, \omega, \dots, \omega^{N-1}$ along each chain and $\sigma_p = 1$ respectively [on an infinite lattice the ground state of (7.26) has simply $U_{p_1 p_2}^{\eta, \bar{\eta}} = 1$ which seems to suggest that the ground state is unique instead of N -fold degenerate. This ambiguity is due to taking the infinite limit of an open lattice which has edge zero-modes; see the open lattice analysis below]. The critical point of (7.30) is known to be $h_x = h_z$ from exact solutions [93]. To show this, let m, n be row and column indices starting from the upper-left corner of the lattice and apply an ‘order-disorder’ transformation similar to that of the transverse Ising model:

$$\sigma_{m,n} \rightarrow \tau_{m,n}^\dagger \tau_{m,n+1}, \quad \tau_{m,n} \rightarrow \prod_{k \leq n} \sigma_{m,k}, \quad (7.31)$$

where m, n are row and column indices respectively. As a result, the Hamiltonian (7.30) is mapped to itself but with h_x, h_z exchanged. This indicates that $h_x = h_z$ is indeed a critical point.

On a torus or open lattice, the analysis is more complex. Since the cross-boundary operator is not mapped to $\tau_{m,L_x}^\dagger \tau_{m,1}$ on a torus, the Hamiltonian is not mapped to itself under the transformation (7.31) as on the infinite lattice. If the lattice is finite and open, similar situation occurs because the transformation (7.31) for σ_p on the last column is ill-defined. However, in that case $\tau_{m,n}^\dagger \tau_{m,n+1}$ and σ_p can be mapped to parafermion bilinears $\eta^\dagger \eta'$; c.f. Eq. (7.22) and the discussion that follows. The model (7.29) then maps to decoupled chains of parafermions:

$$H = -h_x \sum_{n,m} \eta_{n,m}^\dagger \eta'_{n,m+1} - h_z \sum_{n,m} \eta_{n,m}^\dagger \eta'_{n,m} + \text{h.c.} \quad (7.32)$$

From this representation it is clear that there are \mathbb{Z}_N edge zero-modes at least at $h_z = 0$. They are given here by $\eta'_{n,1}$ and η_{n,L_x} on each row which do not enter into the Hamiltonian (7.32); see the \mathbb{Z}_2 case in (5.22). \mathbb{Z}_N edge zero-modes in a class of one-dimensional parafermionic chains have been studied in Refs. [94, 95], which includes (7.32) as a particular example. Interestingly, the region in which edge-modes exist inside the phase diagram does not coincide with the phase boundary $h_x = h_z$, contrary to bulk-edge correspondence. In relation to this, we mention another construction in Ref. [96] which shows in an exactly solvable model that parafermionic zero-modes are present at the boundary of ground states with different topological properties. There the zero-modes are found via the Bethe ansatz, and are collective excitations inside solitons of a one-dimensional fermionic model.

To summarize, we have found \mathbb{Z}_N models with topological order and associated ground state degeneracy, even though here it seems that the system cannot be mapped to a Hamiltonian of free elementary excitations as in the \mathbb{Z}_2 case in Sec. 5. It remains unclear if the results in this subsection can be attributed to certain properties of the quasiparticles, or if such a quasiparticle picture exists at all for ‘translation-symmetry-enriched \mathbb{Z}_N topological order’.

8 Conclusions

In this thesis we have considered exact dualities from spin-1/2 operators on infinite, open and periodic square lattices, to field operators of (e, m) and (e, ε) quasiparticles from the Toric Code. In particular, the duality to e, ε offers a systemic framework for studying \mathbb{Z}_2 topologically ordered phases enriched by lattice translation symmetry, and is also relevant for investigating physical properties of candidate Kitaev materials, i.e. α -RuCl₃, on a honeycomb lattice [27].

The dualities are inspired by viewing the Toric Code as a model of static, non-interacting e - and m -particles, and by Ref. [41] which proposed the mapping of spin operators to Majorana bilinears of ε -fermion without e -bosons on an infinite lattice. Thus the dualities are a generalization of these results to allow for quasiparticle dynamics, mutual anyonic statistics and the effect of lattice periodicity. This fact in turn motivates an extension of the Toric Code to m and ε ideal gases, and a series of \mathbb{Z}_2 topologically ordered phases ‘enriched by lattice translation symmetry’, in which ε -fermions acquire dynamics and become superconducting. By rewriting the corresponding Hamiltonians directly in terms of quasiparticle fields, the properties of the underlying \mathbb{Z}_2 topological order can be studied using well-established methods from topological superconductivity and classified in a $\mathbb{Z} \times (\mathbb{Z}_2)^3$ scheme. Thus the duality shows unequivocally the interrelation between \mathbb{Z}_2 topological order and band topology, and the effect of lattice periodicity.

In particular, we find that on a periodic lattice, the ground state degeneracy in these phases may depend on lattice size. This is confirmed explicitly by exact solutions of the spin Hamiltonian in certain limits. However, the quasiparticle picture is applicable to cases where exact solutions on the spin lattice are not possible. This includes phases with non-zero Chern number whose constituent operators in their Hamiltonians are generally non-commuting [87]. Even in the exactly solvable case, the interpretation of results in terms of quasiparticles is much more transparent and physical than on the spin lattice.

The (e, ε) -duality can also be used to study the emergent anyon statistics of e -bosons renormalized by the superconducting vacua. This gives a concrete and general means of numerically computing anyon braiding rules in phases with arbitrary Chern numbers. In this thesis we have considered the simplest phases with $C = \pm 1, 2$ and confirmed the predictions made in Ref. [17]. The computations are considerably simplified using the duality method. By considering a periodic lattice and choosing given super-selection sectors, which also determine the boundary conditions of ε -fermions, Berry phases of specific braiding processes between non-abelian anyons can be separately calculated. Furthermore, the Berry phase of e -bosons from the superconducting background can be computed using this method. The background magnetic flux from the square unit cell is shown numerically to be quantized as 0 or π , depending on $\mathbb{Z} \times (\mathbb{Z}_2)^3$ indices of the underlying \mathbb{Z}_2 topologically ordered phases. Clarifying and proving analytically this relation between \mathbb{Z}_2 topological order and the quantized background flux is therefore a natural extension of current work.

Although the questions addressed in this thesis are mostly theoretical, the (e, ε) -duality can be applied to more physical problems, given its validity also on the honeycomb lattice. Here the quasiparticle degrees of freedom are naturally the Majorana fermions and the

bosonic visons in the Kitaev honeycomb model [17]. This makes the duality also relevant to studying the properties of candidate Kitaev materials such as α - RuCl_3 . For example, Ref. [23] considered the vison dispersion on a generalized honeycomb model due to perturbations that transport visons, in relation to experimentally observed peaks in thermal Hall conductivity. The vison band is also calculated using the present duality [27]. Here the duality provides a general and transparent method for analysing these materials, and can be used to study, for instance, the stability of the spin-liquid ground state with respect to vison motion.

Appendix A Cylindrical lattices and independence of local parity operators

In this Appendix a cylindrical lattice is considered, which has open boundary condition along one direction but is periodic along the other. This gives rise to an interesting admixture of features from the torus and open lattice geometries: even though periodicity along y -axis remains, there are no global parity constraints and single-particle creation operators can be defined, similarly to the open lattice case in Sec. 2. We will then discuss changes to mappings to quasiparticle basis (e, m) and (e, ε) .

Without loss of generality we choose the system to be periodic along the y -direction. To have $2L_x L_y$ total number of independent edges, the edges on the right boundary are removed as shown in Fig. A.24; compare with the open lattice in Sec. 2.

The mapping to e and m quasiparticles are now considered. Operators on the boundary plaquettes with links removed are modified in the same way as the open lattice case. This means A_v and B_p are three-spin operators on the left and right boundaries respectively. It is possible to create, analogous to the open lattice case, e and m quasiparticles as single isolated particles by extending their strings right- and left-ward to the open edges of the cylinder respectively. As is proven in Sec. 2, this fact is related to the mutual independence of A_v and B_p . Therefore, the corresponding TC Hamiltonian (1.1) has a unique ground state in the cylinder and a gap to all excitations. This does not contradict the existence of global topological operators $W_y^{\text{TC}}, T_y^{\text{TC}}$ along the periodic y -direction, which are not independent from A_v and B_p :

$$\begin{aligned} W_y^{\text{TC}} &= \prod_{l \in \gamma_y} X_l = \prod_{v \in \text{lattice}} A_v, \\ T_y^{\text{TC}} &= \prod_{l \in \gamma'_y} Z_l = \prod_{p \in \text{lattice}} B_p. \end{aligned} \tag{A.1}$$

Here γ_y and γ'_y are contours that cross the periodic y -direction associated with transporting m and e quasiparticles. The convention for the above relations is depicted in Fig. A.24. Eq. (A.1) reflects the branch-cut convention for e - and m -bosons, as $W_y^{\text{TC}}, T_y^{\text{TC}}$ corresponds to m - and e -motion across the lattice along the paths that necessarily intersects all branch-cuts.

Thus local occupation numbers of e and m now form a complete basis for the quasiparticle Hilbert space. σ operators are not affected by lattice geometry and has the same form as in Eq. (2.4). τ_v^e and τ_p^m are defined similarly to the open lattice: on a given row, the corresponding strings of Z and X matrices extend from the right and left lattice boundary, and arrives at the site. Note that however, single τ_v^e and τ_p^m operators anti-commute with W_y^{TC} and T_y^{TC} , due to the relation (A.1). This point does not affect pair-creation operators. It can be shown that all pair-creation operators retain their form in Eqs. (2.7) and (2.8) with the same branch-cuts as on the open lattice: each e -boson extends a branch-cut to the right and terminates at the boundary of the same row; branch-cuts for m -bosons go left

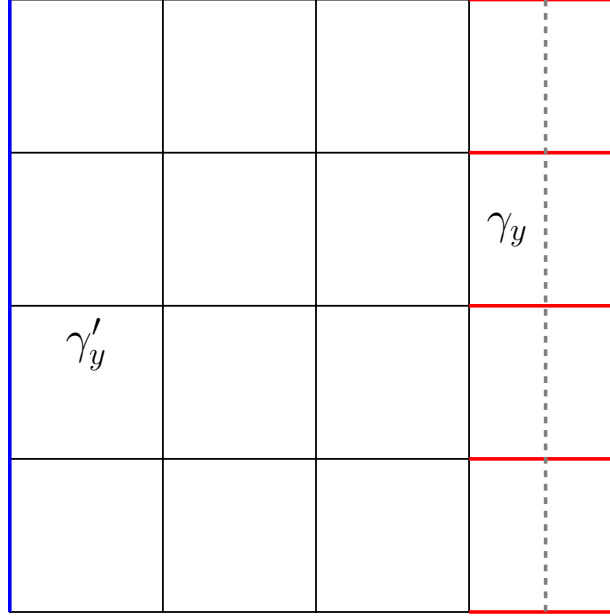


Figure A.24: Cylindrical lattice in which the vertical direction is periodic and the horizontal direction is open. Accordingly the right edge of the lattice is removed. The global topological operators for (e, m) and (e, ε) Hilbert spaces are the same given by (A.2).

and terminate at the left boundary. This is true also for cross-boundary motion, as can be shown in the following way. Since the mapping for single τ operators remain the same as in the open lattice case, $\tau\tau$ terms on the spin lattice also remain the same (there is nothing special with respect to cross-lattice motion under the current τ definition). Therefore, after mapping to hard-core bosons the form of the mapping for pair-creation operators coincide with the open lattice case.

We now turn to the mapping from cylindrical lattices to (e, ε) degrees of freedom.

In this case the global topological operators W_y, T_y are still given by (A.1). As in the case of e, m quasiparticles, the absence of global parity constraints means that W_y and T_y can be expressed in terms of local parity operators:

$$W_y = -\left(\prod_{v \in \text{lattice}} \Gamma_v^e\right) \left(\prod_{p \in \text{lattice}} \Gamma_p^\varepsilon\right), \quad T_y = \left(\prod_{p \in \text{lattice}} \Gamma_p^\varepsilon\right). \quad (\text{A.2})$$

The schematic of these operators is depicted in Fig. A.24. The product of Γ_v^e in W_y and Γ_p^ε in T_y reflect the gauge convention for e -boson and ε -fermion branch-cuts: they extend to the right and left respectively and reach the lattice boundary. The second product of Γ_p^ε in W_y implies, interestingly, that the the boundary condition of ε -fermion along the y -direction depends on its global parity. In particular in the case of no static e -bosons ($\Gamma_v^e = 1$ for all v), the constraint means that for a total odd (even) number of ε -fermions in the cylinder one must necessarily choose periodic (anti-periodic) boundary conditions along its y -direction. In other words, the quasiparticle Hilbert spaces with i.e. periodic y -boundary conditions and an even number of fermions must be discarded as unphysical.

We define single τ^ε and τ^e with the same non-local string conventions as on the open lattice in Sec. 2.2. In this case also, single τ^ε operators anti-commute with both T_y and W_y due to the relation (A.2). The Jordan-Wigner transformation for fermions is also taken to be the same as on the open lattice. Then the bulk mapping from spin to quasiparticles has identical form as on an open lattice given by Eqs. (2.19), (2.22) and (2.23). The situation is different for ε -fermion motion across the vertical lattice boundary, because the Jordan-Wigner transformation (2.18) now gives additional ε -parity terms as γ , γ' are defined on bottom and top rows respectively, similarly to the periodic lattice case. To show this, we write the mapping for vertical $U_{p_1 p_2}^\varepsilon$ in terms of σ and τ , which is the same as on the open lattice in Eq. (2.21):

$$U_{p_1 p_2}^\varepsilon \rightarrow - \left(\prod_{\substack{v \in \\ L(p_1, p_2)}} \sigma_v^e \right) \left(\prod_{\substack{p \in \\ L(p_1), R(p_2)}} \sigma_p^\varepsilon \right) \tau_{p_1}^\varepsilon \tau_{p_2}^\varepsilon.$$

The definitions of $L(p_1, p_2)$, $L(p_1)$ and $R(p_2)$ are given below Eq. (2.21). We then substitute the Jordan-Wigner transformation (2.18) for $\gamma_{p_1}, \gamma'_{p_2}$ with p_1, p_2 at the bottom and top rows respectively. This gives the final mapping:

$$U_{p_1 p_2}^\varepsilon \rightarrow i \gamma_{p_1} \gamma'_{p_2} \left(\prod_{\substack{v \in \\ L(p_1, p_2)}} e^{i\pi b_v^\dagger b_v} \right) \left[- \left(\prod_{\substack{p \in \\ \text{lattice}}} -i \gamma_p \gamma'_p \right) \right], \quad (\text{A.3})$$

which differs from the bulk mapping by the additional total ε -parity factor; see also the derivation of the same expression (2.27) for the torus. The result confirms the conclusion below Eq. (A.2) that the ε -fermion B.C. is determined by the total ε -fermion parity. The branch-cut conventions are the same as the open lattice case.

Appendix B Free electrons in the field of a point vortex

In this Appendix, we calculate the total energy difference (4.16) between a free fermi-gas with and without a point vortex on a large disk. The fermion Hamiltonian is taken parabolic in momentum and isotropic.

First let us determine the energy levels of a particle in the field of a point vortex.

The vortex is placed at the origin. Since we are only concerned with the energy levels, the problem is equivalent to solving for the Hamiltonian with a vector potential \mathbf{A} satisfying the following properties. Outside the origin, the magnetic field $\mathbf{B} = \nabla \times \mathbf{A}$ is zero. But the vortex carries magnetic flux Φ , we then have:

$$\oint \mathbf{A} \cdot d\mathbf{r} = \Phi, \quad (\text{B.1})$$

where the integral is taken over any contour that encircles the origin. The vector potential \mathbf{A} can be chosen as:

$$\mathbf{A} = \frac{\Phi}{2\pi} \nabla \phi,$$

where ϕ is the polar angle of the plane. The left hand side of Eq. (B.1) then gives $(\Delta\phi/2\pi)\Phi$, where $\Delta\phi$ is the change of polar angle after completing the loop. Upon encircling the origin, $\Delta\phi = 2\pi$ and we obtain Eq. (B.1). Moreover, $\nabla \times \mathbf{A}$ always vanishes outside the origin, as \mathbf{A} is the gradient of a scalar function.

The Schrödinger's equation has the form:

$$\frac{1}{2m} \left(\hat{\mathbf{p}} - e\mathbf{A} \right)^2 \Psi = E\Psi. \quad (\text{B.2})$$

We shall solve the problem for a π -vortex: the wave-function receives phase $(e/\hbar) \oint \mathbf{A} \cdot d\mathbf{r} = (e/\hbar)\Phi = \pi$. In the following we use the units $e = \hbar = c = 1$ and consequently $\Phi = \pi$.

Eq. (B.2) is invariant under rotations. Accordingly we seek Ψ in polar coordinates in the form:

$$\Psi = \exp(il\phi)\chi_l(r), \quad (\text{B.3})$$

where l is the integer angular momentum. Substituting (B.3) into (B.2) gives for $\chi_l(r)$:

$$\chi_l'' + \frac{1}{r}\chi_l' + \left[k^2 - \frac{1}{r^2} \left(l - \frac{1}{2} \right)^2 \right] \chi_l = 0, \quad (\text{B.4})$$

with the notation $k^2 = 2mE$ and the prime denotes differentiation with respect to r . Eq. (B.4) needs to be supplemented by certain boundary conditions for χ_l . It is clear that for a sufficiently large system, the precise shape of the boundary is not relevant. Thus for convenience we shall assume the vortex is placed at the origin of a cylindrical infinite potential well of radius R . The boundary conditions are then $\chi_l(R) = 0$ and $\chi_l(0)$ is regular.

The solution to Eq. (B.4) for the n -th energy level satisfying the boundary condition is:

$$\chi_{nl}(r) = \mathcal{C}_{nl} J_{|l-1/2|}(k_{nl}r). \quad (\text{B.5})$$

$J_n(x)$ are Bessel functions of order n and \mathcal{C}_{nl} is a normalization constant. The boundary condition at $r = R$ gives for k_{nl} :

$$k_{nl}R = x_{nl},$$

where x_{nl} is the n -th zero of the Bessel function of order $|l - 1/2|$. Thus the energy is:

$$E_{nl} = \frac{k_{nl}^2}{2m} = \frac{x_{nl}^2}{2mR^2}.$$

Since l includes both positive and negative integers, each energy level E_{nl} is doubly degenerate. As $R \rightarrow \infty$ the energy levels become continuous.

For completeness, we shall also give the solution to (B.2) in the absence of vortices. The wave-functions correspond to a free particle placed inside a large cylinder of radius R , with the same boundary conditions. We then have:

$$\chi_{nl}(r) = \mathcal{C}_{nl} J_{|l|}(k_{nl}r), \quad k_{nl}R = x_{nl}. \quad (\text{B.6})$$

x_{nl} is the n -th zero of the Bessel function of order $|l|$. The energy levels $E_n = x_{nl}^2/(2mR^2)$ are doubly degenerate for $l \neq 0$. All energy levels with $l = 0$ have no degeneracy.

We now compute the same quantities as in Sec. 4.2, and check explicitly that the results at low filling fractions on the square lattice are reproduced. To make correspondence between the two cases, the physical quantities in this Appendix are related to the tight-binding approximation at low filling-fraction as: $\epsilon_F = 2\pi n_\epsilon/m_\epsilon$, n_ϵ is the number density and $m_\epsilon = 1/(2t)$ is the effective mass at low filling from the tight-binding approximation.

To characterize the differences between ground states with and without vortex in the thermodynamic limit, we must first take the limit $T \rightarrow 0$ then $N \rightarrow \infty$. The energy difference between the Fermi gas with and without vortex ($\Phi = 0, \pi$) at constant N and $T = 0$ is shown in Fig. B.25a). We find that the difference approaches a constant value with system size:

$$\lim_{N \rightarrow \infty} \{E(N, \Phi = \pi) - E(N, \Phi = 0)\}_{T=0} = \frac{\epsilon_F}{8}, \quad (\text{B.7})$$

This agrees with the square lattice case at low filling fraction (4.18). Despite strong finite-size fluctuations, the limiting value in Fig. B.25a) is clear and the results are also consistent with the complete deconfinement of the e -boson. The fluctuations arise from the fact that in the above procedure the temperature remains smaller or comparable to the level spacing up to very large system sizes. One can mitigate such fluctuations by taking a slightly different thermodynamic limit in which the zero temperature limit ($T \rightarrow 0$) and large system size limit ($N \rightarrow \infty$) are taken while keeping the temperature larger than the level spacing $\Delta\epsilon \sim \epsilon_F/\sqrt{N}$, namely by keeping $\epsilon_F \gg T \gg \Delta\epsilon$. Fig. B.25b) illustrates this idea by showing that at finite but small temperatures the system approaches the same limit as that in Eq. (B.7) while avoiding the strong finite size fluctuations of the $T = 0$ case. This figure has been obtained by adjusting the chemical potentials of the states with and without vortex ($\Phi = 0, \pi$) to ensure that we always compare systems with the same total N .

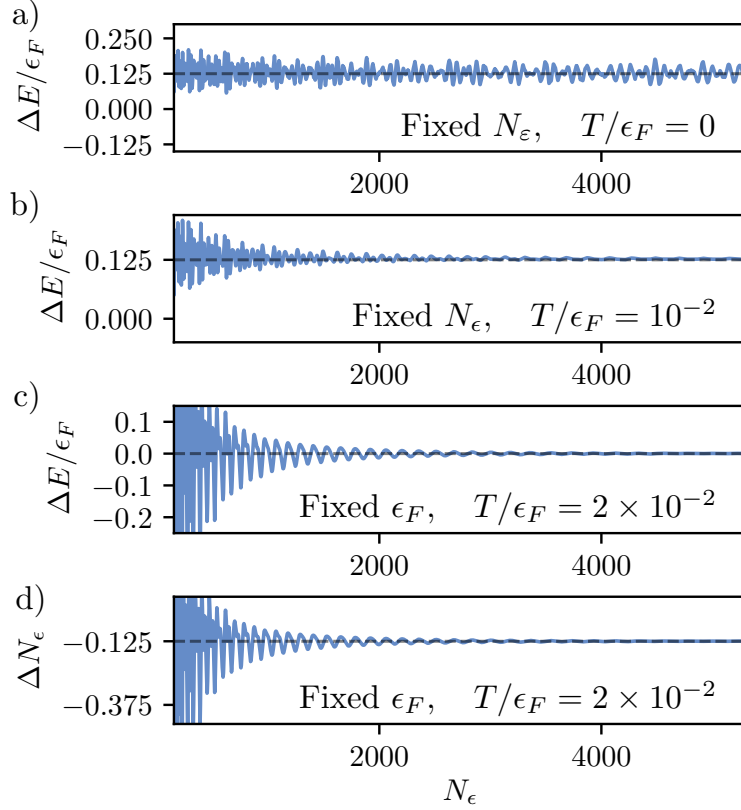


Figure B.25: Energy and particle number differences with and without the π -vortex in the continuum disk model from Eq. (B.2). a) and b) are energy difference fixing the ε particle number at zero and finite temperature respectively. The energy unit is taken to be the Fermi energy of the zero flux configuration. c) and d) are energy and particle number differences fixing the Fermi energy ϵ_F at finite temperature respectively. Here $\epsilon_F \equiv 2\pi n_\varepsilon/m_\varepsilon$, n_ε is the number density and $m_\varepsilon = 1/(2t)$.

In addition, Figs. B.25c) and d) show that in this case we have the following limits:

$$\lim_{T \rightarrow 0} \lim_{R \rightarrow \infty} \{E(\mu, \Phi = \pi, T) - E(\mu, \Phi = 0, T)\} = 0, \quad (\text{B.8})$$

$$\lim_{T \rightarrow 0} \lim_{R \rightarrow \infty} \{N(\mu, \Phi = \pi, T) - N(\mu, \Phi = 0, T)\} = -\frac{1}{8}. \quad (\text{B.9})$$

In particular, the change in the number of particles due to the vortex approaches the same value obtained for the square lattice at small filling fraction as the temperature decreases to zero.

To study the spatial distribution of the screening cloud of ε -fermions surrounding the e -vortex, we compute the change of ε -density as a function of radius r :

$$\rho_\varepsilon(r, \Phi) = \sum_{i=1}^{\infty} n_F[E_i(\Phi), \mu, T] |\Psi_i(r, \Phi)|^2, \quad (\text{B.10})$$

$$\Delta\rho_\varepsilon(r) = \rho_\varepsilon(r, \pi) - \rho_\varepsilon(r, 0). \quad (\text{B.11})$$

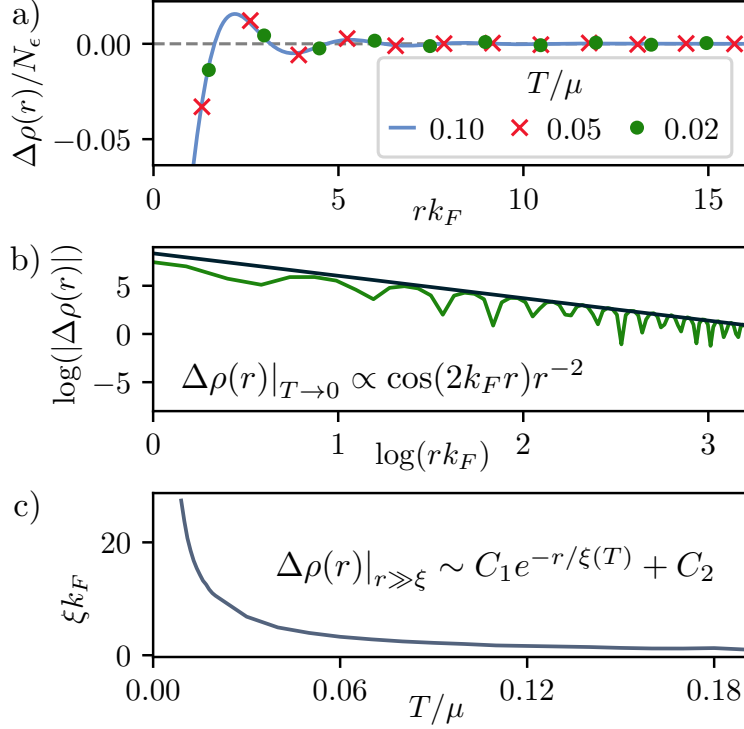


Figure B.26: a) Local ε density difference with and without the π -vortex at fixed chemical potential μ . b) Near the π -vortex core, the density perturbation displays a Friedel-like oscillatory decay with a power that approaches $\alpha = -2$ in the zero temperature limit. The plot shows the envelope fitting for $T/\mu = 0.02$, for which $\alpha = -2.32$. c) At finite temperatures, there exists a correlation length $\xi(T)$ above which the decay becomes exponential. The correlation length diverges in the zero temperature limit. Results are for the continuum model from Eq. (B.2) with disk geometry and fixing the ratio of level spacing ($\Delta\epsilon = \mu/N^{1/2}$) to be $\Delta\epsilon/T = 1/3$.

The results are shown in Fig. B.26. As can be seen from Fig. B.26a), ε -fermion density is modified near the vortex. We have found numerically that the fermion density far from the vortex can be fitted by the following functions:

$$\Delta\rho_\varepsilon(r) \approx A \cos(2k_F r) r^{-\alpha(T)}, \quad r \ll \xi(T) \ll R; \quad (\text{B.12})$$

$$\Delta\rho_\varepsilon(r) \approx B \cos(2k_F r) e^{-r/\xi(T)}, \quad \xi(T) \ll r \ll R. \quad (\text{B.13})$$

Here k_F is the Fermi momentum and $\xi(T)$ is a finite temperature correlation length that separates the two regimes. Near the π -vortex core, the density decays with a power-law as shown in Fig. B.26b), while at scales larger or comparable to the correlation length $\xi(T)$ the decay becomes exponential. The correlation length $\xi(T)$ diverges as $T \rightarrow 0$, as is shown in Fig. B.26c). Therefore, the e -particle (π -vortex) induces an oscillatory corrections to the ε -fermion density which decays with power $\alpha \approx 2$ as $T \rightarrow 0$. The period of the oscillation $2k_F$ resembles 2D Friedel oscillations [97], and indicates the presence of a sharp Fermi surface. Despite that the e -particle induces such a long-range perturbation on the surrounding ε -fermions, its energy cost remains finite. This can be attributed to the gapless excitations of particle-hole pairs infinitesimally close to the Fermi surface.

Appendix C Topological Superconductivity

In this section we review the topological classification of spinless superconductors with inversion symmetry. The Hamiltonian with dispersion $\varepsilon(\mathbf{k})$ and gap function $\Delta(\mathbf{k})$ has the form (5.1) in quasimomentum and particle-hole space:

$$H(\mathbf{k}) = \begin{pmatrix} \varepsilon(\mathbf{k}) & \Delta(\mathbf{k}) \\ \Delta^*(\mathbf{k}) & -\varepsilon(\mathbf{k}) \end{pmatrix},$$

which can be written alternatively as:

$$H(\mathbf{k}) = \boldsymbol{\sigma} \cdot \mathbf{c}(\mathbf{k}); \quad \mathbf{c}(\mathbf{k}) = [\text{Re } \Delta(\mathbf{k}), -\text{Im } \Delta(\mathbf{k}), \varepsilon(\mathbf{k})]. \quad (\text{C.1})$$

Here $\boldsymbol{\sigma}$ is a vector with the i -th Pauli matrix as its i -th component. It will be shown in this section that the Hamiltonian (C.1) can be classified by an integer quantum number (the Chern number C) in combination with three \mathbb{Z}_2 invariants which are related to the ground state fermion number at certain quasimomenta.

Appendix C.1 Classification by Chern Number

To obtain the Chern number classification, we form a three-dimensional unit vector $\mathbf{n}(\mathbf{k}) = \mathbf{c}/|\mathbf{c}|$ from (C.1) defined on the Brillouin zone. This gives a mapping from the square Brillouin zone $T^2 = S^1 \times S^1$ to the two-sphere S^2 defined by $\mathbf{n}^2 = 1$:

$$\mathbf{n} : T^2 \rightarrow S^2, \quad (\text{C.2})$$

as is shown in Fig. C.27. Generally, mappings between two manifolds:

$$f : N \rightarrow M, \quad (\text{C.3})$$

can be classified by equivalent classes $[N, M]$ up to a continuous deformation of the mapping (*homotopy classes*). In the case of Eq. (C.2), the homotopy classes give simultaneously a classification of the eigenstate. Finding the homotopy classes of mappings between two generic manifolds is in general difficult. Nonetheless we shall prove an important result that for $N = T^2$ and any manifold M with trivial fundamental group $\pi_1(M) = 0$, the homotopy classes of the mapping (C.3) can be classified by the homotopy group $\pi_2(M)$.¹¹ For (C.2), $\pi_1(S^2) = 0$ (S^1 is mapped to a closed loop on S^2 which can always be deformed into a point: a constant map) which means that the eigenstates can be classified by:

$$\mathbf{n} : [T^2, S^2] \sim \pi_2(S^2) \cong \mathbb{Z}; \quad \pi_1(S^2) = 0. \quad (\text{C.4})$$

Here \mathbb{Z} is the integer Chern number.

¹¹The n -th homotopy group $\pi_n(M)$ has, as its elements, homotopy classes of mappings $[S^n, M]$. In particular, $\pi_n(M) = 0$ is trivial if all mappings can be continuously deformed to a constant map, i.e. ‘contracted to a point’.

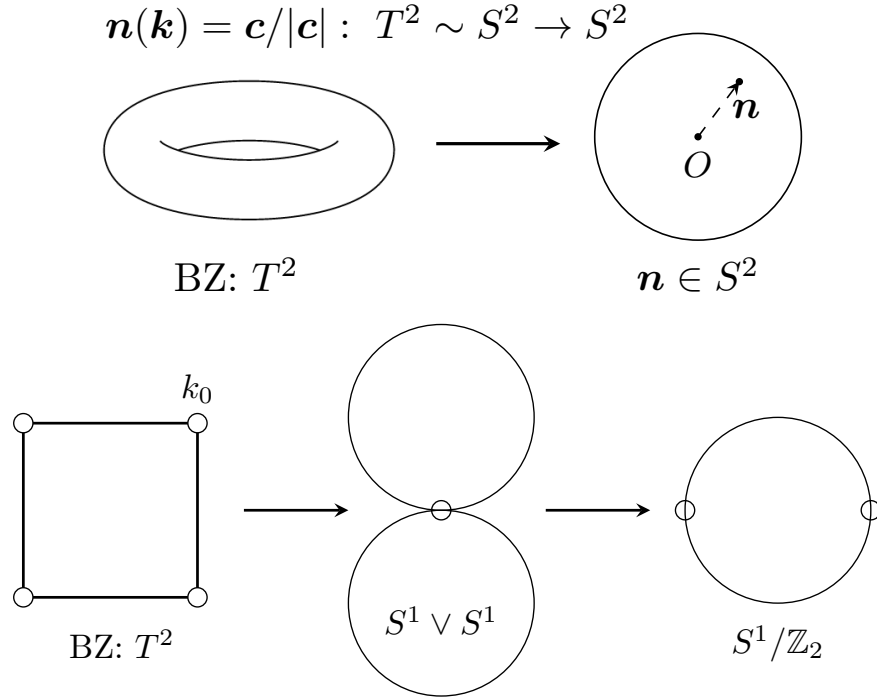


Figure C.27: Top: schematic of mapping from the two-dimensional Brillouin zone to the unit vector \mathbf{n} in (C.2). Bottom: the equivalence of the Brillouin zone boundary to two circles joining at the equivalent corner of the square k_0 , and to a single circle with its two points on the equator regarded as equivalent. Here the white disk denotes k_0 .

We now prove this result. The square Brillouin zone T^2 with lattice constant a can be obtained from a square of side-length $2\pi/a$ by identifying edges on opposite sides as equivalent:

$$(k_x, k_y) \sim (k_x + 2\pi/a, k_y) \sim (k_x, k_y + 2\pi/a).$$

Denoting by k_0 the point at the four (equivalent) corners of the square, the Brillouin zone boundary can be seen as two circles corresponding to the vertical and horizontal sides joining at the point k_0 :

$$\partial T^2 \cong S^1 \vee S^1 \cong S^1/\mathbb{Z}_2,$$

where S^1/\mathbb{Z}_2 is a circle with its equator (two points connected along the diameter) regarded as a point; see Fig. C.27. The two-sphere S^2 is then given by:

$$S^2 \cong T^2/S^1 \vee S^1,$$

by ‘contracting’ the boundary of T^2 to a point. However, $S_i^1 \vee S_j^1$ defines precisely multiplication of group elements of $\pi_1(M)$:

$$\begin{aligned} a_i \in \pi_1(M) &\sim f_i : S_i^1 \rightarrow M; \\ a_j \times a_k &\sim g : S_j^1 \vee S_k^1 \rightarrow M, \quad g(x_i) = f_i, \quad x_i \in S_i^1. \end{aligned}$$

Therefore for $\pi_1(M) = 0$, any mapping from S^1 and by extension $S^1 \vee S^1$ to M can be continuously deformed into a constant map. Applying this procedure to the restriction to the torus boundary $S^1 \vee S^1$ of a given map:

$$f : T^2/S^1 \vee S^1 \rightarrow M,$$

the quotient by $S^1 \vee S^1$ becomes trivial and we obtain:

$$f : [T^2, M] \sim [S^2, M], \quad \pi_1(M) = 0. \quad (\text{C.5})$$

This proves our statement.¹²

Eq. (C.4) has the meaning that by covering completely the manifold T^2 , the region extended by the unit vector \mathbf{n} covers the entire sphere S^2 an integer number of times, which is just the Chern number C . Therefore, we can define C analytically as the solid angle integral on S^2 normalized by 4π (the ‘Gauss map’):

$$C = \frac{1}{4\pi} \int \mathbf{n} \cdot d\mathbf{S}, \quad dS_i = e^{ijk} dn_j dn_k, \quad (\text{C.6})$$

where dS_i is the differential surface area element on S^2 . In quasimomentum space:

$$C = \frac{1}{8\pi} e^{ij} \int_{T^2} \mathbf{n} \cdot \left(\frac{\partial \mathbf{n}}{\partial k_i} \times \frac{\partial \mathbf{n}}{\partial k_j} \right) dk_x dk_y. \quad (\text{C.7})$$

In proving the Chern number classification (C.4), we made use of the fact that the Hamiltonian (C.1) has only two bands. For completeness we shall present another formulation which holds generally for n bands with $n \geq 2$.

The Hamiltonian for a given quasimomentum \mathbf{k} is an $n \times n$ matrix. Each eigenstate is, up to a constant phase factor, given by a complex n -tuple $z = [z_1(\mathbf{k}), \dots, z_n(\mathbf{k})]$ with the normalization condition $\sum_i |z_i(\mathbf{k})|^2 = 1 \rightarrow z \in S^{2n-1}$. This is the definition of the *complex projective space* CP^{n-1} (we assume there are no additional internal symmetries in the Hamiltonian) which has the following structure:

$$CP^{n-1} \cong S^{2n-1}/U(1),$$

¹²An analogous theorem to (C.5) holds, which states that the homotopy classes of mappings from the N -dimensional Brillouin zone, i.e. an N -dimensional torus $T^N = S^1_1 \times \dots \times S^1_N$, to an arbitrary $(N-1)$ -connected manifold M [$\pi_k(M) = 0$, $k < N$] can be classified by $\pi_N(M)$. In this case T^N can be seen as an N -dimensional hypercube I_N with its faces $\{I_{N-1}^i\}$ on opposite sides regarded as equivalent. Each boundary I_{N-1}^i then contains inequivalent boundaries $\{I_{N-2}^{ij}\}$ and so on. The reduction of T^N to S^N can be carried out inductively in the same way as for (C.5) by consecutively deforming its k -boundary (I_k with equivalent faces) into a point. In proving (C.5) this is essentially done for $k = 2$. Now assuming the $(k-1)$ -boundaries ($k \geq 2$) has already been reduced to a point, the mapping f restricted to the k -boundaries $f|_{I_k}$ can be continuously deformed into a mapping from a bouquet of k -spheres equal to the number of inequivalent I_k , joining at the single equivalent corner of the cubes $\vee_i S_i^k$. Again this defines the multiplication of $\pi_k(M)$ elements. Since $\pi_k(M) = 0$, $f|_{I_k}$ can be continuously deformed to a constant map. Repeating this procedure until $k = N-1$, we have reduced the T^N -boundary to a point and T^N to S^N by one-point compactification, which proves the theorem. This theorem might be related to the study of ‘weak’ and ‘strong’ topological systems; see the footnote in Sec. 5.

where the $U(1)$ group corresponds to the global phase. In particular for $n = 2$, $S^3/U(1) \cong S^3/S^1 \cong S^2$. It is known in algebraic topology that for a quotient manifold $M = G/H$, $\pi_i(G) = 0$ and $\pi_{i-1}(G) = 0$ gives $\pi_i(G/H) \cong \pi_{i-1}(H)$; see i.e. Ref. [98]. Since $\pi_i(S^{2n-1}) = 0$ for $0 < i < 2n - 1$, we have for $n \geq 2$:

$$\pi_1(CP^{n-1}) \cong \pi_1[S^{2n-1}/U(1)] \cong \pi_0[U(1)] = 0, \quad \pi_2(CP^{n-1}) \cong \pi_1[U(1)] \cong \mathbb{Z}.$$

Since $\pi_1(CP^{n-1}) = 0$, by (C.5) the n -tuples and therefore the eigenstates can be classified by $\pi_2(CP^{n-1})$. The same Chern number C is now given by the fundamental group $\pi_1[U(1)] \cong \mathbb{Z}$. This has the physical interpretation as the integer multiple of 2π acquired by the phase of each eigenstate as its argument completes a closed-loop motion along the Brillouin zone boundary, i.e. the Berry phase. Thus introducing the Berry connection and curvature:

$$A_j = -\frac{i}{2} [\bar{z}\partial_j z - (\partial_j \bar{z})z], \quad F_{ij} = \partial_i A_j - \partial_j A_i, \quad (\text{C.8})$$

the Chern number is defined in this case as:

$$C = \frac{1}{2\pi} \oint_{\partial T^2} \mathbf{A} \cdot d\mathbf{k} = \frac{1}{4\pi} \int_{T^2} e^{ij} F_{ij} dk_x dk_y.$$

Substituting Eq. (C.8) gives C in terms of z, \bar{z} :

$$C = -\frac{i}{4\pi} e^{ij} \int_{T^2} \sum_{a=1}^2 \frac{\partial \bar{z}_a}{\partial k_i} \frac{\partial z_a}{\partial k_j} dk_x dk_y. \quad (\text{C.9})$$

Let us check that Eq. (C.9) reduces to (C.7) for $n = 2$. Define $\mathbf{n} = \bar{z}\boldsymbol{\sigma}z$ for the conduction band. It can be shown that:

$$(\bar{z}\boldsymbol{\sigma}z) \cdot \boldsymbol{\sigma}z = z,$$

where we have used $\boldsymbol{\sigma}_{\alpha\beta} \cdot \boldsymbol{\sigma}_{\gamma\delta} = 2\delta_{\alpha\delta}\delta_{\beta\gamma} - \delta_{\alpha\beta}\delta_{\gamma\delta}$ and $\bar{z}z = 1$. Hence \mathbf{n} is indeed the unit vector obtained from the Hamiltonian (C.1). To find z , writing:

$$\mathbf{n} = (\sin \theta \cos \phi, \sin \theta \sin \phi, \cos \theta),$$

it can be seen that the parameterization:

$$z_1 = \frac{1}{\sqrt{2}} e^{i(\psi-\phi)/2} \cos\left(\frac{\theta}{2}\right), \quad z_2 = \frac{1}{\sqrt{2}} e^{i(\psi+\phi)/2} \sin\left(\frac{\theta}{2}\right), \quad (\text{C.10})$$

in terms of Euler-angles ϕ, θ, ψ gives the desired form for \mathbf{n} . Substituting (C.10) into (C.9) gives:

$$\frac{1}{4\pi} \int_{T^2} \sin \theta \frac{\partial(\theta, \phi)}{\partial(k_x, k_y)} dk_x dk_y,$$

which is just Eq. (C.6) written in spherical coordinates on S^2 . For the valence band we take $\mathbf{n} = -\bar{z}\boldsymbol{\sigma}z$ which gives an additional minus sign in C .

Appendix C.2 Classification by Ground State Fermion Number

It turns out that C does not completely specify the topological properties of a spinless superconductor. One can define four additional global \mathbb{Z}_2 invariants $\{\zeta_i\}$ for the system [48, 49, 51–53]. Three of the $\{\zeta_i\}$ values together with C completely determine the other \mathbb{Z}_2 invariant, and hence the bulk topology. We shall now review this classification scheme.

On a square lattice, the Brillouin zone contains four high-symmetry quasimomenta points:

$$\mathbf{k}_{0i} = \{(0, 0), (0, \pi), (\pi, 0), (\pi, \pi)\}, \quad (\text{C.11})$$

where $-\mathbf{k}_{0i} \sim \mathbf{k}_{0i}$. For a spinless superconductor, the gap function $\Delta(\mathbf{k})$ vanishes identically at these points since by definition:

$$\Delta(\mathbf{k}) \propto \langle c_{\mathbf{k}} c_{-\mathbf{k}} \rangle, \quad \Delta(-\mathbf{k}_{0i}) = -\Delta(\mathbf{k}_{0i}) = \Delta(\mathbf{k}_{0i}) = 0.$$

Therefore, the quasiparticle dispersion:

$$E(\mathbf{k}) = [\varepsilon(\mathbf{k})^2 + |\Delta(\mathbf{k})|^2]^{1/2},$$

at \mathbf{k}_{0i} is simply $E(\mathbf{k}_{0i}) = \varepsilon(\mathbf{k}_{0i})$. The ground state fermion number at the given quasimomenta is given by the Fermi distribution $n(\mathbf{k})$ in the limit $T \rightarrow 0$. If there are no gapless modes in the system, the only non-zero contribution comes from \mathbf{k}_{0i} and we have:

$$n[\varepsilon(\mathbf{k}_{0i})] = 1, \quad \varepsilon(\mathbf{k}_{0i}) < 0; \quad n[\varepsilon(\mathbf{k}_{0i})] = 0, \quad \varepsilon(\mathbf{k}_{0i}) > 0.$$

Therefore, defining $\zeta_i = 1, 0$ as the ground state fermion number at \mathbf{k}_{0i} :

$$\zeta_i = 1 - \Theta[\varepsilon(\mathbf{k}_{0i})], \quad (\text{C.12})$$

a spinless superconductor can be classified by the 4-tuple $\{\zeta_1, \zeta_2, \zeta_3, \zeta_4\}$ which also determines the ground state fermion parity.

The Chern number C and $\{\zeta_i\}$ are not independent [51, 53]:

$$(-1)^C = \prod_{i=1}^4 (-1)^{\zeta_i}. \quad (\text{C.13})$$

To prove Eq. (C.13), one can consider:

$$(-1)^C = e^{i\pi C} = \exp\left(\frac{i}{2} \oint_{\partial T^2} \mathbf{A} \cdot d\mathbf{k}\right),$$

and compute the integral in the exponent [51, 53]. Eq. (C.13) can also be proven by the following argument: consider our system in a trivial phase ($C = \zeta_i = 0$) in the parameter space for which (C.13) is trivially satisfied. One can in principle obtain any topological phases by changing the parameters and successively crossing critical points in the phase diagram. The trajectory can always be chosen such that the gap closes at only one of the

\mathbf{k}_{0i} at each crossing. On two sides in the vicinity of the critical point, $\varepsilon(\mathbf{k})$ changes sign in the neighbourhood of the given \mathbf{k}_{0i} and the corresponding ζ_i changes by unity. However since the quasiparticle gap is small and $\Delta(\mathbf{k})$ should remain qualitatively the same through the phase transition, the dominant contribution to C in Eq. (C.7) near the neighbourhood of \mathbf{k}_{0i} gives $\pm 1/2$ on two sides of the critical point and, as a result, C also changes by ± 1 . Starting from the trivial phase we see that Eq. (C.13) indeed holds.

Accordingly, the bulk topology of a spinless superconductor is determined by C and three of the four \mathbb{Z}_2 invariants $\{\zeta_i\}$. The remaining $\zeta_i = 0, 1$ is obtained from Eq. (C.13). We have thus obtained the $\mathbb{Z} \times (\mathbb{Z}_2)^3$ classification scheme.

Appendix D KW phases corresponding to diagonal stacking of Kitaev Wires

As mentioned in Sec. 5.2.3, KW_{x+y} phases are stackings of 1D Majorana wires along the diagonal direction. To illustrate their properties, we choose the corresponding Hamiltonian:

$$H = -\Delta_e \sum_v \Gamma_v^e - \Delta_\varepsilon \sum_p \Gamma_{NE(p)}^\varepsilon U_{NE(p),E(p)}^\varepsilon U_{p,E(p)}^\varepsilon, \quad (\text{D.1})$$

where $E(p)$ and $NE(p)$ are plaquettes to the east and north-east of plaquette p . Again assume an infinite lattice and that there are no e -bosons. The two phases $\text{KW}_{x+y,1}$ and $\text{KW}_{x+y,0}$ correspond to $\Delta_\varepsilon \lesseqgtr 0$. In the ground states:

$$\Gamma_v^e = 1; \pm \Gamma_{NE(p)}^\varepsilon U_{NE(p),E(p)}^\varepsilon U_{p,E(p)}^\varepsilon |0\rangle = |0\rangle, \quad \Delta_\varepsilon \lesseqgtr 0. \quad (\text{D.2})$$

Substituting Eqs. (2.19) and (2.22), the second term in (D.1) is mapped into the following fermionic Hamiltonian:

$$H = -i\Delta_\varepsilon \sum_{i,k} \gamma_i \gamma'_k. \quad (\text{D.3})$$

The pairing of Majorana modes is depicted by curved dotted lines in Fig. D.28. The BdG spectrum for Eq. (D.3) has the same form as (5.11) with:

$$\varepsilon(\mathbf{k}) = -2\Delta_\varepsilon \cos(k_x + k_y), \quad \Delta(\mathbf{k}) = -2i\Delta_\varepsilon \sin(k_x + k_y). \quad (\text{D.4})$$

The parity indices are:

$$\text{KW}_{x+y,0} : \{1001\}, \quad \Delta_\varepsilon > 0; \quad \text{KW}_{x+y,1} : \{0110\}, \quad \Delta_\varepsilon < 0.$$

The Chern number C is, of course, zero in both phases.

We now show that there is also ‘weak breaking’ of lattice translation symmetry in these phases: the e -bosons split into two sectors of effective anyons e' and m' in the ground state, and lattice translations along both directions permute them. Here each sublattice is given by vertices along the diagonals of the square unit cell. For example, in Fig. D.28, e -bosons on vertices v_{1-4} become e' , while on v_5 it becomes m' . This is similar to Wen’s plaquette model [68]. To show this, we proceed analogously to Section 6.1, by finding the ‘renormalized’ e -transport operators $\tilde{U}_{v_i v_j}^e$ in the superconducting ground states. Such an operator must commute with the corresponding Majorana bilinear terms in Eq. (D.2). They can be found only for translations between diagonals of a square. For example, in Fig. D.28, translations between v_1, v_2 and v_2, v_3 are

$$\tilde{U}_{v_2 v_1}^e = Z_1 Z_2, \quad \tilde{U}_{v_3 v_2}^e = i(Z_2 Z_3) \times (X_3 Z_4). \quad (\text{D.5})$$

The factor i imposes $\tilde{U}_{v_2 v_3}^e = (\tilde{U}_{v_3 v_2}^e)^\dagger = \tilde{U}_{v_3 v_2}^e$. Eq. (D.5) can be understood intuitively similarly to the horizontal stacking case; see discussions below (6.4) in Sec. 6.1. We draw

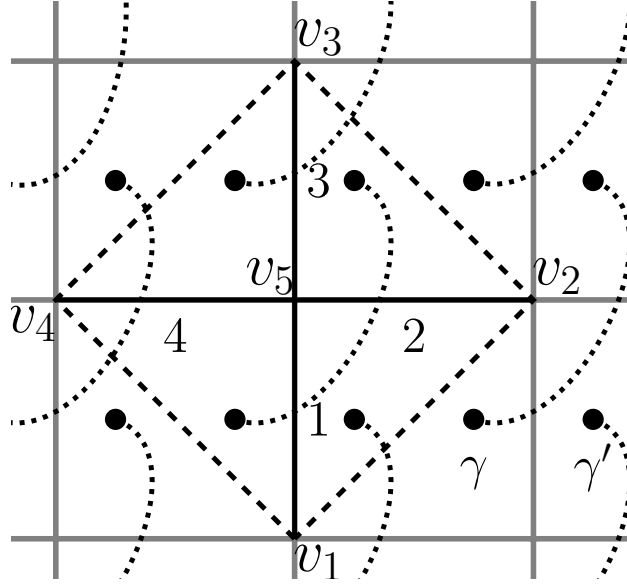


Figure D.28: Graphic representation of the fermionic Hamiltonian (D.3) in KW_{x+y} phases. Couplings between γ', γ are shown as dotted lines. The two sublattices contain vertices v_{1-4} and v_5 respectively. The dashed line shows the transport of an e -boson along a closed loop in one sublattice, which measures the parity of v_5 on the other sublattice enclosed by the loop; see Eq. (D.6).

Majorana pairings with curved lines in the form in Fig. D.28. When an e -boson is transported from v_1 through v_5 to v_2 , it cuts through the same Majorana bond twice, and therefore does not change the ‘fermion parity’ associated with such a pair of Majorana modes. However, going from v_2 through v_5 to v_3 , it cuts through two different bonds, annihilating two Majorana fermions, which are then created by the pair creation operator $X_3 Z_4$. The loop translation operator on the ground state $|0\rangle$ along the dashed line in Fig. D.28 now gives:

$$\tilde{U}_{v_4 v_1}^e \tilde{U}_{v_3 v_4}^e \tilde{U}_{v_2 v_3}^e \tilde{U}_{v_1 v_2}^e |0\rangle = \Gamma_{v_5}^e |0\rangle, \quad (\text{D.6})$$

where we used the ground state identity (D.2) for $\text{KW}_{x,0}$ and $\text{KW}_{x,1}$ respectively; c.f. the derivation leading to (6.5). This illustrates the mutual anyonic statistics of e -bosons in the two sublattices. Here the two sublattices are exchanged by both vertical and horizontal lattice translations.

Appendix E BCS ground state wave-function without translational symmetry

As is discussed in Sec. 6, the computation of Berry phase of e -bosons for $C \neq 0$ phases reduces to calculating matrix elements between parity-even superconducting ground states of ε -fermions. Due to the presence of static e -vortices, the corresponding superconducting Hamiltonians lose translation invariance. In this Appendix, we briefly review the solution of mean-field BdG Hamiltonians without translational symmetry. Namely, we construct the parity-even ground state wave-function in terms of annihilation operators c_i of spinless fermions defined on each (dual) lattice site i .

The BdG Hamiltonian is defined on a finite lattice with N sites as:

$$H = \frac{1}{2} \Psi^\dagger h_{\text{BdG}} \Psi, \quad h_{\text{BdG}} = \begin{pmatrix} \Xi & \Delta \\ \Delta^\dagger & -\Xi^T \end{pmatrix}. \quad (\text{E.1})$$

Here $\Psi = (c_1, \dots, c_N, c_1^\dagger, \dots, c_N^\dagger)^T$. The single-particle hopping matrix Ξ satisfies the hermicity condition: $\Xi^\dagger = \Xi$, while the pairing matrix is anti-symmetric $\Delta^T = -\Delta$.

Due to particle-hole symmetry, Eq. (E.1) can be diagonalized into the following form:

$$H = \frac{1}{2} \tilde{\Psi}^\dagger h_0 \tilde{\Psi} = \sum_{n=1}^N E_n \left(\alpha_n^\dagger \alpha_n - \frac{1}{2} \right); \quad (\text{E.2})$$

$$h_0 = \text{diag}\{E_1, E_2, \dots, -E_1, -E_2, \dots\}, \quad \tilde{\Psi} = (\alpha_1, \dots, \alpha_1^\dagger, \dots)^T.$$

Here $\{E_1, E_2, \dots, -E_1, -E_2, \dots\}$ are the eigenvalues of h_{BdG} , and α_n is the annihilation operator of a Bogoliubov quasiparticle with energy $E_n \geq 0$. α_n is related to c_i by a standard Bogoliubov transformation:

$$\alpha_n = \sum_i \left[u_{in}^* c_i + v_{in}^* c_i^\dagger \right]. \quad (\text{E.3})$$

To find the coefficients u_{in} , v_{in} and energies E_n , we use the equation of motion for α_n^\dagger : $[H, \alpha_n^\dagger] = E_n \alpha_n^\dagger$, and substitute Eqs. (E.1) and (E.3). This gives the following eigenvalue problem for the eigenvector $C_n = (u_{1n}, \dots, u_{Nn}, v_{1n}, \dots, v_{Nn})^T$:

$$h_{\text{BdG}} C_n = E_n C_n. \quad (\text{E.4})$$

The energies E_n and u_{in} , v_{in} can then be found from Eq. (E.4) by exact diagonalization. Due to particle-hole symmetry of h_{BdG} , it can be shown that, for each eigenvector C_n , there exists another eigenvector $C'_n = (v_{1n}^*, \dots, v_{Nn}^*, u_{1n}^*, \dots, u_{Nn}^*)^T$ such that:

$$h_{\text{BdG}} C'_n = -E_n C'_n. \quad (\text{E.5})$$

From Eqs. (E.4) and (E.5), one can obtain the following relations due to orthogonality of eigenvectors:

$$\sum_i \left[u_{in}^* u_{im} + v_{in}^* v_{im} \right] = \delta_{nm}, \quad (\text{E.6a})$$

$$\sum_n \left[u_{in} u_{jn}^* + v_{in}^* v_{jn} \right] = \delta_{ij}, \quad (\text{E.6b})$$

$$\sum_i \left[u_{in} v_{im} + v_{in} u_{im} \right] = 0, \quad (\text{E.6c})$$

$$\sum_n \left[u_{in} v_{jn}^* + v_{in}^* u_{jn} \right] = 0. \quad (\text{E.6d})$$

The first of these identities can also be obtained from the relation: $\{\alpha_n^\dagger, \alpha_m\} = \delta_{nm}$.

We can now construct a ground state wave-function of H_{BdG} taking u_{in} , v_{in} as input. As is well-known, the superconducting ground state of Eq. (E.1) is a condensate of Cooper-pairs of fermions. In systems with translational invariance, the pairing occurs between fermions with opposite momenta $\pm \mathbf{k}$ and the ground state wave-function can be written as:

$$\begin{aligned} |\Omega\rangle &= \prod_{\mathbf{k}} \left[u^*(\mathbf{k}) - v^*(\mathbf{k}) c_{\mathbf{k}}^\dagger c_{-\mathbf{k}}^\dagger \right] |0\rangle \\ &= \mathcal{N} \exp \left[\frac{1}{2} \sum_{\mathbf{k}} f(\mathbf{k}) c_{\mathbf{k}}^\dagger c_{-\mathbf{k}}^\dagger \right] |0\rangle, \end{aligned} \quad (\text{E.7})$$

where $\mathcal{N} = \prod_{\mathbf{k}} u^*(\mathbf{k})$ is a normalization constant, $f(\mathbf{k}) = -f(-\mathbf{k}) = -v^*(\mathbf{k})/u^*(\mathbf{k})$, and $|0\rangle$ is the fermion vacuum state. For a system without translation invariance, we can write the ground state as:

$$|\Omega\rangle = \mathcal{N} \exp \left(\frac{1}{2} \sum_{i,j} f_{ij} c_i^\dagger c_j^\dagger \right) |0\rangle, \quad f_{ij} = -f_{ji}. \quad (\text{E.8})$$

The summation in the exponent is taken over lattice sites. Note that the ground state ansatz Eq. (E.8) has even fermion parity. This may not be true in certain topologically non-trivial phases whose ground states have odd parity. This can be verified by using the expression for total fermion parity of a BCS ground state in terms of BdG Hamiltonian (E.1) derived in [17]; note the different definition of Majorana modes there. Thus, as is discussed in Sec. 5, these parity-odd states are unphysical and will not be used throughout the calculation. However as will be shown in Appendix E.1, in those cases, the first excited state, which is *physical*, can still be described by a pairing ansatz of the form in Eq. (E.8).

To express f_{ij} in terms of u_{in} and v_{in} , we use the identity for the ground state:

$$\alpha_n |\Omega\rangle = 0, \quad (\text{E.9})$$

and substitute Eqs. (E.3) and (E.8). In subsequent calculations, we bring the c_i term in Eq. (E.3) to the right of the exponential in Eq. (E.8). This can be done by expanding the

exponential function and using the identity:

$$\left[c_i, \frac{1}{2} \sum_{j,k} f_{jk} c_j^\dagger c_k^\dagger \right] = \sum_k f_{ik} c_k^\dagger. \quad (\text{E.10})$$

After some algebra, this gives for f_{ij} :

$$\sum_i f_{ij} u_{in}^* = -v_{jn}^*. \quad (\text{E.11})$$

It can be shown that f_{ij} is indeed anti-symmetric. For this purpose we multiply Eq. (E.11) by v_{jn} and sum over n, j . Substituting the orthogonality conditions Eq. (E.6) then gives:

$$\sum_j f_{ij} u_{jn}^* = v_{in}^*, \quad (\text{E.12})$$

which proves our statement. In what follows, we shall represent u_{in} and v_{in} as $N \times N$ matrices and write f_{ij} in matrix notation as:

$$f = v^*(u^*)^{-1}. \quad (\text{E.13})$$

Eq. (E.13) determines f_{ij} in terms of u_{in} and v_{in} obtained from exact diagonalization.

The normalization constant \mathcal{N} can be determined by directly computing $\langle \Omega | \Omega \rangle$. As will be discussed in Appendix F, there is:

$$\mathcal{N} = [\det(1 + f^\dagger f)]^{-1/4}. \quad (\text{E.14})$$

Finally, we comment on a subtlety in exact diagonalization on a finite lattice. In Eq. (E.8), the ‘vacuum’ state $|0\rangle$ into which the Cooper-pairs condense contains no fermions. However, this can be a bad reference state in some cases. Mathematically, this means the matrix u is not invertible and f in Eq. (E.13) becomes ill-defined. For example, consider a Hamiltonian whose ground state is an atomic insulator:

$$H = -\Delta \sum_i c_i^\dagger c_i, \quad \Delta > 0. \quad (\text{E.15})$$

In its ground state, every site is occupied:

$$|0\rangle_h = \prod_i^N c_i^\dagger |0\rangle. \quad (\text{E.16})$$

If one tries to express $|0\rangle_h$ using the BCS ansatz in momentum space in Eq. (E.7), it would correspond to the limit $u(\mathbf{k}) = 0$, and $f(\mathbf{k}) \rightarrow \infty$ as a result. For ground states sufficiently close to $|0\rangle_h$, the matrix u might not be invertible numerically. This problem can be avoided by choosing Eq. (E.16) as the new ‘vacuum’ state and consider a condensation of hole pairs on top of it. Thus the BCS Ansatz in this case is:

$$|\Omega\rangle = \mathcal{N} \exp\left(\frac{1}{2} \sum_{i,j} g_{ij} c_i c_j\right) |0\rangle_h. \quad (\text{E.17})$$

It can be shown that the (hole) Cooper-pair wave-function has $g_{ij} = u^*(v^*)^{-1}$.

Appendix E.1 The first excited state of a BdG Hamiltonian with odd ground state parity

As discussed in the previous section, in certain topologically non-trivial phases, the ground state of a BdG Hamiltonian has odd fermion parity. These states are unphysical and do not belong to the dual space of a periodic spin system. Therefore, the lowest energy physical eigenstate of H_{BdG} will be the first excited state $|\Psi_1\rangle = \alpha_1^\dagger |\Psi_0\rangle$. In this section, we show that $|\Psi_1\rangle$ can be also expressed by an ansatz of the form in Eq. (E.8).

By definition, $|\Psi_1\rangle$ satisfies:

$$\alpha_1^\dagger \alpha_1 |\Psi_1\rangle = |\Psi_1\rangle; \alpha_n |\Psi_1\rangle = 0, \quad n \neq 1. \quad (\text{E.18})$$

$\alpha_n, \alpha_n^\dagger$ are given in Eq. (E.2). For our purpose, it is more convenient to consider another Hamiltonian:

$$H' = \sum_{n=2}^N E_n \left(\alpha_n^\dagger \alpha_n - \frac{1}{2} \right) - E_1 \left(\alpha_1^\dagger \alpha_1 - \frac{1}{2} \right), \quad (\text{E.19})$$

for which $|\Psi_1\rangle$ is the ground state. Obviously, there is:

$$H' = \frac{1}{2} \tilde{\Psi}^\dagger h'_0 \tilde{\Psi} = \frac{1}{2} \Psi^\dagger h'_{\text{BdG}} \Psi. \quad (\text{E.20})$$

where $h'_0 = \text{diag}\{-E_1, E_2, \dots, E_N, E_1, -E_2, \dots, -E_N\}$, which is related to the h_0 through a permutation P :

$$h'_0 = P h_0 P. \quad (\text{E.21})$$

Here $P_{ii} = 1$ for $i \neq 1, N+1$, $P_{1,N+1} = P_{N+1,1} = 1$ and zero otherwise. Using the fact that:

$$\Psi = U \tilde{\Psi}, \quad U = \begin{pmatrix} u & v^* \\ v & u^* \end{pmatrix}, \quad (\text{E.22})$$

one can obtain:

$$\begin{aligned} h'_{\text{BdG}} &= U P h_0 P U^\dagger \\ &= \tilde{U} h_0 \tilde{U}^\dagger, \end{aligned} \quad (\text{E.23})$$

with

$$\tilde{U} = U P \equiv \begin{pmatrix} \tilde{u} & \tilde{v}^* \\ \tilde{v} & \tilde{u}^* \end{pmatrix}. \quad (\text{E.24})$$

Using the ansatz

$$|\Psi_1\rangle = \mathcal{N} \exp \left(\frac{1}{2} \sum_{i,j} \tilde{f}_{ij} c_i^\dagger c_j^\dagger \right) |0\rangle, \quad (\text{E.25})$$

it can be shown that $\tilde{f} = \tilde{v}^* (\tilde{u}^*)^{-1}$.

Appendix F Matrix Elements between BCS ground states

We compute overlaps and matrix elements of ground states (E.8) of BdG Hamiltonians with different e -boson configurations. Since e -bosons act as π -vortices for fermions, each configuration of e corresponds to a different set of matrix elements Ξ , Δ in Eq. (E.1). Therefore, we consider two such BCS ground states:

$$|\Omega_0\rangle = \mathcal{N}_0 |\tilde{\Omega}_0\rangle = \mathcal{N}_0 \exp\left(\frac{1}{2} \sum_{i,j} f_{i,j}^{(0)} c_i^\dagger c_j^\dagger\right) |0\rangle, \quad (\text{F.1a})$$

$$|\Omega_1\rangle = \mathcal{N}_1 |\tilde{\Omega}_1\rangle = \mathcal{N}_1 \exp\left(\frac{1}{2} \sum_{i,j} f_{i,j}^{(1)} c_i^\dagger c_j^\dagger\right) |0\rangle. \quad (\text{F.1b})$$

$\mathcal{N}_{0,1}$ are defined in Eq. (E.14), and $f^{(1)}$, $f^{(2)}$ are given by exact diagonalization of the respective Hamiltonians; see Eq. (E.13). The overlap between the two states has been calculated, for example in Ref. [99] as an integral over anti-commuting fermion fields:

$$\langle \tilde{\Omega}_0 | \tilde{\Omega}_1 \rangle = (-1)^{\frac{N(N+1)}{2}} \text{pf} \left[\begin{pmatrix} f^{(1)} & -I \\ I & f^{(0)\dagger} \end{pmatrix} \right]. \quad (\text{F.2})$$

$\text{pf}(A)$ is the Pfaffian of matrix A . In particular, by taking $|\tilde{\Omega}_0\rangle = |\tilde{\Omega}_1\rangle$, we arrive at Eq. (E.14) for the normalization constant \mathcal{N} . For this thesis to be self-contained, we derive Eq. (F.2) below using functional integration.

The ‘vacuum transition amplitude’ (F.2) can be seen as an averaging of exponential operators over the trivial vacuum $|0\rangle$, which can be written as a functional integral over anti-commuting fields \bar{c}, c with certain statistical weight ρ :

$$\langle 0 | O[c, c^\dagger] | 0 \rangle = \int O[c, \bar{c}] \rho[c, \bar{c}] \prod_i d\bar{c}_i dc_i.$$

In transitioning from Hamiltonian to Lagrangian formalism we have changed the notation $c^\dagger \rightarrow \bar{c}$. To find ρ , note that operators in (F.2) have all c^\dagger to the right and c to the left. Therefore the functional integral should correspond to the ‘anti-normal’ product of c, c^\dagger operators. The averaging over $|0\rangle$ satisfies the following requirements:

$$\langle 0 | c_i c_j^\dagger | 0 \rangle = \delta_{ij}, \quad \langle 0 | 0 \rangle = 1,$$

and by definition Wick’s theorem. This gives for the statistical weight: ¹³

$$\langle 0 | O[c, c^\dagger] | 0 \rangle = \int O[c, \bar{c}] \exp\left(-\sum_{i=1}^N \bar{c}_i c_i\right) \prod_{i=1}^N d\bar{c}_i dc_i.$$

¹³The convention for integration over anti-commuting variables θ is as follows:

$$\int \theta d\theta = 1, \quad \int d\theta = 0, \quad \int \theta_1 \theta_2 d\theta_1 d\theta_2 = -\int \theta_1 d\theta_1 \int \theta_2 d\theta_2 = -1, \quad \int f(\theta) d\theta = f'(0);$$

see i.e. Ref. [100]. Note that the differential $d\theta$ is also anti-commuting.

Thus introducing the notation $\Psi = (\bar{c}_1, \dots, \bar{c}_N, c_1, \dots, c_N)^T$, Eq. (F.2) can be re-written as:

$$\langle \Omega_0 | \Omega_1 \rangle = N_0 N_1 \int \exp \left(\frac{1}{2} \Psi M_0 \Psi \right) \prod_{i=1}^N d\bar{c}_i dc_i, \quad M_0 = \begin{pmatrix} f^{(1)} & -I \\ I & f^{(0)\dagger} \end{pmatrix}. \quad (\text{F.3})$$

Note that M_0 is anti-symmetric. Eq. (F.3) is the same expression as in Ref. [99]. Before proceeding, we rearrange the integral measure by moving all $d\bar{c}_i$ to the left, consistent with the definition of Ψ . Starting from $i = 2$, each term $d\bar{c}_i$ moves past $\prod_{k=1}^{i-1} dc_k$ which gives $(-1)^{i-1}$. Adding the powers together gives $\sum_{i=2}^N (i-1) = N(N-1)/2$ and we get:

$$\prod_{i=1}^N d\bar{c}_i dc_i = (-1)^{N(N-1)/2} \left(\prod_{i=1}^N d\bar{c}_i \right) \left(\prod_{i=1}^N dc_i \right) = (-1)^{N(N-1)/2} \prod_i^{2N} d\Psi_i.$$

The integral (F.3) can now be computed as follows. By an orthogonal transformation U any even-dimensional anti-symmetric matrix A can be diagonalized into block diagonal form with the 2×2 blocks:

$$\begin{pmatrix} 0 & \lambda_i \\ -\lambda_i & 0 \end{pmatrix}, \quad \prod_{i=1}^N \lambda_i = \text{pf}(U^T A U) = \det U \times \text{pf}(A).$$

Then in (F.3) we effect a change of variables $\theta_i = (U^{-1})_{ij} \Psi_j$. The integration gives:

$$\frac{1}{\det U} \int \exp \left(\sum_{k=1}^{2N} \lambda_k \theta_{2k-1} \theta_{2k} \right) \prod_{i=1}^{2N} d\theta_i = \frac{1}{\det U} \prod_k^N (-\lambda_k) = (-1)^N \text{pf}(M_0), \quad (\text{F.4})$$

and we return to Eq. (F.2). In deriving (F.4), we have used the following identity for change of variables in fermion field integration:

$$\int \prod_i d\Psi_i = (\det U)^{-1} \int \prod_i d\theta_i.$$

We shall also calculate matrix elements between two BCS ground states. First we consider a product of fermion parity operators $\prod_p \Gamma_p^\varepsilon = \exp(-i\pi \sum_p c_p^\dagger c_p)$ between two BCS ground states. Its matrix elements can be expressed in a similar form to Eq. (F.2). For simplicity, first consider the matrix element for a single plaquette p :

$$\langle \Omega_1 | \Gamma_p^\varepsilon | \Omega_0 \rangle = \mathcal{N}_1 \mathcal{N}_0 \langle 0 | \exp \left(\frac{1}{2} \sum_{i,j} f_{i,j}^{(1)*} c_j c_i \right) \Gamma_p^\varepsilon \exp \left(\frac{1}{2} \sum_{i,j} f_{i,j}^{(0)} c_i^\dagger c_j^\dagger \right) | 0 \rangle. \quad (\text{F.5})$$

In Eq. (F.5) we insert on the RHS the identity $(\Gamma_p^\varepsilon)^2 = 1$:

$$\mathcal{N}_1 \mathcal{N}_0 \langle 0 | \exp \left(\frac{1}{2} \sum_{i,j} f_{i,j}^{(1)*} c_j c_i \right) \Gamma_p^\varepsilon \exp \left(\frac{1}{2} \sum_{i,j} f_{i,j}^{(0)} c_i^\dagger c_j^\dagger \right) \Gamma_p^\varepsilon | 0 \rangle. \quad (\text{F.6})$$

To evaluate the matrix exponential, we use the following identity (remember that Γ_p^ε is hermitian):¹⁴

$$\Gamma_p^\varepsilon c_i^\dagger \Gamma_p^\varepsilon = e^{i\pi c_p^\dagger c_p} c_i^\dagger e^{-i\pi c_p^\dagger c_p} = c_i^\dagger \exp(i\pi \delta_{ip}) = (-1)^{\delta_{ip}} c_i^\dagger. \quad (\text{F.7})$$

From Eq. (F.7) and that $\Gamma_p^\varepsilon |0\rangle = |0\rangle$, Eq. (F.6) becomes:

$$\mathcal{N}_1 \mathcal{N}_0 \langle 0 | \exp\left(\frac{1}{2} \sum_{i,j} f_{i,j}^{(1)*} c_j c_i\right) \exp\left(\frac{1}{2} \sum_{i,j} \tilde{f}_{i,j}^{(0)} c_i^\dagger c_j^\dagger\right) |0\rangle; \quad \tilde{f}_{ij} = (-1)^{\delta_{ip}} f_{ij} (-1)^{\delta_{jp}}. \quad (\text{F.8})$$

Above can be immediately generalized to matrix elements of a product of fermion parity operators:

$$\langle \Omega_1 | \prod_p \Gamma_p^\varepsilon | \Omega_0 \rangle = \mathcal{N}_1 \mathcal{N}_0 \langle 0 | \exp\left(\frac{1}{2} \sum_{i,j} f_{i,j}^{(1)*} c_j c_i\right) \exp\left(\frac{1}{2} \sum_{i,j} \tilde{f}_{i,j}^{(0)} c_i^\dagger c_j^\dagger\right) |0\rangle. \quad (\text{F.9})$$

Now \tilde{f}_{ij} satisfies:

$$\tilde{f}_{ij} = (-1)^{\sum_p \delta_{ip}} f_{ij} (-1)^{\sum_p \delta_{jp}}, \quad (\text{F.10})$$

where the summation is taken over plaquettes of the fermion parity operators. In matrix notation, Eq. (F.10) can be written as:

$$\tilde{f} = \left(\prod_p I_p \right) f \left(\prod_p I_p \right), \quad (\text{F.11})$$

where $(I_p)_{ij} = \delta_{ij} (-1)^{\delta_{ip}}$ is a diagonal matrix with elements unity apart from the p -th diagonal, which has element -1 . Eqs. (F.9), (F.10) together with Eqs. (F.2) and (E.14) determine the matrix elements of fermion parities.

For reference purposes we shall also present formulae for matrix elements of fermion fields on different plaquettes of the form: $\langle c_i c_j \rangle$, $\langle c_i c_j^\dagger \rangle$ and $\langle c_i^\dagger c_j^\dagger \rangle$. Here it is important that $i \neq j$ so that the operators can be always brought to ‘anti-normal’ ordering. To compute these elements it is convenient to define a ‘generating functional’ of the form (F.3) but with an arbitrary $2N \times 2N$ anti-symmetric matrix M :

$$Z[M] = (-1)^{\frac{N(N+1)}{2}} \int \exp\left(\frac{1}{2} \Psi M \Psi\right) \prod_i^{2N} d\Psi_i = (-1)^{\frac{N(N+1)}{2}} \text{pf}(M). \quad (\text{F.12})$$

Then averages of the form $\langle \bar{c}_i \bar{c}_j \rangle$ can be obtained as:

$$\langle \Omega_0 | \bar{c}_i \bar{c}_j | \Omega_1 \rangle = 2N_0 N_1 \left. \frac{\delta Z[M]}{\delta M_{ij}} \right|_{M=M_0} = 2N_0 N_1 (-1)^{\frac{N(N+1)}{2}} \left. \frac{\delta}{\delta M_{ij}} \text{pf}(M) \right|_{M=M_0}. \quad (\text{F.13})$$

¹⁴Eq. (F.7) can be obtained by noting that $\exp(-i\pi c_p^\dagger c_p)$ is formally a single-particle time evolution operator with energy $\varepsilon_p = 1$ and time $t = \pi$, and $c_p^\dagger \rightarrow c_p^\dagger \exp(i\varepsilon_p t)$ under such a transformation.

Similarly there is:

$$\begin{aligned}\langle \Omega_0 | c_i \bar{c}_j | \Omega_1 \rangle &= 2N_0 N_1 \left. \frac{\delta Z[M]}{\delta M_{N+i,j}} \right|_{M=M_0}; \\ \langle \Omega_0 | c_i c_j | \Omega_1 \rangle &= 2N_0 N_1 \left. \frac{\delta Z[M]}{\delta M_{N+i,N+j}} \right|_{M=M_0}.\end{aligned}\tag{F.14}$$

We now calculate Eq. (F.13). Using the identity:

$$\text{pf}(M)^2 = \det M \rightarrow \log \text{pf}(M) = \frac{1}{2} \log \det M = \frac{1}{2} \text{Tr} \log M,$$

there is:

$$\delta \log \text{pf}(M) = \frac{1}{\text{pf}(M)} \delta \text{pf}(M) = \frac{1}{2} \text{Tr} (M^{-1} \delta M); \quad \frac{\delta M_{ij}}{\delta M_{kl}} = \delta_{ik} \delta_{jl}.\tag{F.15}$$

Substituting (F.15) in (F.13) gives:

$$\langle \Omega_0 | \bar{c}_i \bar{c}_j | \Omega_1 \rangle = (-1) N_0 N_1 (-1)^{\frac{N(N+1)}{2}} \text{pf}(M_0) (M_0^{-1})_{ij},\tag{F.16}$$

since M_0^{-1} is also anti-symmetric. For other types of averages we obtain:

$$\begin{aligned}\langle \Omega_0 | c_i \bar{c}_j | \Omega_1 \rangle &= -N_0 N_1 (-1)^{\frac{N(N+1)}{2}} \text{pf}(M_0) (M_0^{-1})_{N+i,j}; \\ \langle \Omega_0 | c_i c_j | \Omega_1 \rangle &= -N_0 N_1 (-1)^{\frac{N(N+1)}{2}} \text{pf}(M_0) (M_0^{-1})_{N+i,N+j}.\end{aligned}\tag{F.17}$$

References

- [1] L. D. Landau, E. M. Lifshitz, *Statistical Physics Part I*, 3rd Edition, Pergamon Press, 1980.
- [2] L. D. Landau, E. M. Lifshitz, L. P. Pitaevskii, *Statistical Physics Part II*, Pergamon Press, 1980.
- [3] E. Fradkin, *Field Theories of Condensed Matter Physics*, 2nd Edition, Cambridge University Press, 2013. doi:10.1017/CB09781139015509.
- [4] A. Patashinskii, V. Pokrovskii, *Fluctuation Theory of Phase Transitions*, Pergamon Press, 1979.
- [5] X. G. Wen, Q. Niu, Ground-state degeneracy of the fractional quantum hall states in the presence of a random potential and on high-genus riemann surfaces, *Phys. Rev. B* 41 (1990) 9377–9396. doi:10.1103/PhysRevB.41.9377.
URL <https://link.aps.org/doi/10.1103/PhysRevB.41.9377>
- [6] X. G. Wen, Vacuum degeneracy of chiral spin states in compactified space, *Phys. Rev. B* 40 (1989) 7387–7390. doi:10.1103/PhysRevB.40.7387.
URL <https://link.aps.org/doi/10.1103/PhysRevB.40.7387>
- [7] X. G. Wen, Topological orders in rigid states, *International Journal of Modern Physics B* 04 (02) (1990) 239–271. arXiv:<https://doi.org/10.1142/S0217979290000139>, doi:10.1142/S0217979290000139.
URL <https://doi.org/10.1142/S0217979290000139>
- [8] X.-G. Wen, Colloquium: Zoo of quantum-topological phases of matter, *Rev. Mod. Phys.* 89 (2017) 041004. doi:10.1103/RevModPhys.89.041004.
URL <https://link.aps.org/doi/10.1103/RevModPhys.89.041004>
- [9] A. Kitaev, J. Preskill, Topological entanglement entropy, *Phys. Rev. Lett.* 96 (2006) 110404. doi:10.1103/PhysRevLett.96.110404.
URL <https://link.aps.org/doi/10.1103/PhysRevLett.96.110404>
- [10] M. Levin, X.-G. Wen, Detecting topological order in a ground state wave function, *Phys. Rev. Lett.* 96 (2006) 110405. doi:10.1103/PhysRevLett.96.110405.
URL <https://link.aps.org/doi/10.1103/PhysRevLett.96.110405>
- [11] N. Read, B. Chakraborty, Statistics of the excitations of the resonating-valence-bond state, *Phys. Rev. B Condens. Matter* 40 (10) (1989) 7133–7140.
URL <https://link.aps.org/doi/10.1103/PhysRevB.40.7133>
- [12] X. G. Wen, Mean-field theory of spin-liquid states with finite energy gap and topological orders, *Phys. Rev. B* 44 (1991) 2664–2672. doi:10.1103/PhysRevB.44.2664.
URL <https://link.aps.org/doi/10.1103/PhysRevB.44.2664>
- [13] A. Y. Kitaev, Fault-tolerant quantum computation by anyons, *Ann. Phys.* 303 (1) (2003) 2–30.
URL <https://www.sciencedirect.com/science/article/pii/S0003491602000180>
- [14] X. Chen, Z.-C. Gu, Z.-X. Liu, X.-G. Wen, Symmetry protected topological orders and the group cohomology of their symmetry group, *Phys. Rev. B* 87 (2013) 155114. doi:10.1103/PhysRevB.87.155114.
URL <https://link.aps.org/doi/10.1103/PhysRevB.87.155114>
- [15] E. Witten, Quantum field theory and the jones polynomial, *Communications in Mathematical Physics* 121 (3) (1989) 351–399. doi:10.1007/BF01217730.
- [16] X.-G. Wen, *Quantum Field Theory of Many-Body Systems: From the Origin of Sound to an Origin of Light and Electrons*, Oxford University Press, 2007. doi:10.1093/acprof:oso/9780199227259.001.0001.
URL <https://doi.org/10.1093/acprof:oso/9780199227259.001.0001>
- [17] A. Kitaev, Anyons in an exactly solved model and beyond, *Ann. Phys.* 321 (1) (2006) 2–111.
URL <http://dx.doi.org/10.1016/j.aop.2005.10.005>
- [18] J. Knolle, D. L. Kovrizhin, J. T. Chalker, R. Moessner, Dynamics of a two-dimensional quantum spin liquid: Signatures of emergent majorana fermions and fluxes, *Phys. Rev. Lett.* 112 (2014) 207203. doi:10.1103/PhysRevLett.112.207203.
URL <https://link.aps.org/doi/10.1103/PhysRevLett.112.207203>

- [19] A. Banerjee, P. Lampen-Kelley, J. Knolle, C. Balz, A. A. Aczel, B. Winn, Y. Liu, D. Pajerowski, J. Yan, C. A. Bridges, A. T. Savici, B. C. Chakoumakos, M. D. Lumsden, D. A. Tennant, R. Moessner, D. G. Mandrus, S. E. Nagler, Excitations in the field-induced quantum spin liquid state of α -RuCl₃, *npj Quantum Materials* 3 (1) (2018) 8. doi:10.1038/s41535-018-0079-2.
- [20] M. Yamashita, J. Gouchi, Y. Uwatoko, N. Kurita, H. Tanaka, Sample dependence of half-integer quantized thermal hall effect in the kitaev spin-liquid candidate α -RuCl₃, *Phys. Rev. B* 102 (2020) 220404. doi:10.1103/PhysRevB.102.220404.
URL <https://link.aps.org/doi/10.1103/PhysRevB.102.220404>
- [21] Y. Motome, J. Nasu, Hunting majorana fermions in kitaev magnets, *Journal of the Physical Society of Japan* 89 (1) (2020) 012002. arXiv:<https://doi.org/10.7566/JPSJ.89.012002>, doi:10.7566/JPSJ.89.012002.
URL <https://doi.org/10.7566/JPSJ.89.012002>
- [22] P. Czajka, T. Gao, M. Hirschberger, P. Lampen-Kelley, A. Banerjee, J. Yan, D. G. Mandrus, S. E. Nagler, N. P. Ong, Oscillations of the thermal conductivity in the spin-liquid state of α -RuCl₃, *Nature Physics* 17 (8) (2021) 915–919. doi:10.1038/s41567-021-01243-x.
- [23] A. P. Joy, A. Rosch, Dynamics of visons and thermal hall effect in perturbed kitaev models (2022). arXiv:2109.00250.
- [24] T. Minakawa, Y. Murakami, A. Koga, J. Nasu, Majorana-mediated spin transport in kitaev quantum spin liquids, *Phys. Rev. Lett.* 125 (2020) 047204. doi:10.1103/PhysRevLett.125.047204.
URL <https://link.aps.org/doi/10.1103/PhysRevLett.125.047204>
- [25] J. Feldmeier, W. Natori, M. Knap, J. Knolle, Local probes for charge-neutral edge states in two-dimensional quantum magnets, *Phys. Rev. B* 102 (2020) 134423. doi:10.1103/PhysRevB.102.134423.
URL <https://link.aps.org/doi/10.1103/PhysRevB.102.134423>
- [26] R. G. Pereira, R. Egger, Electrical access to ising anyons in kitaev spin liquids, *Phys. Rev. Lett.* 125 (2020) 227202. doi:10.1103/PhysRevLett.125.227202.
URL <https://link.aps.org/doi/10.1103/PhysRevLett.125.227202>
- [27] C. Chen, I. S. Villadiego, The nature of visons in the perturbed ferromagnetic and antiferromagnetic kitaev honeycomb models (2022). doi:10.48550/ARXIV.2207.09492.
URL <https://arxiv.org/abs/2207.09492>
- [28] S. Trebst, C. Hickey, Kitaev materials, *Physics Reports* 950 (2022) 1–37, kitaev materials. doi:10.1016/j.physrep.2021.11.003.
URL <https://www.sciencedirect.com/science/article/pii/S0370157321004051>
- [29] A. A. Abrikosov, Electron scattering on magnetic impurities in metals and anomalous resistivity effects, *Physics Physique Fizika* 2 (1965) 5–20. doi:10.1103/PhysicsPhysiqueFizika.2.5.
URL <https://link.aps.org/doi/10.1103/PhysicsPhysiqueFizika.2.5>
- [30] X.-G. Wen, Quantum orders and symmetric spin liquids, *Phys. Rev. B* 65 (2002) 165113. doi:10.1103/PhysRevB.65.165113.
URL <https://link.aps.org/doi/10.1103/PhysRevB.65.165113>
- [31] H.-D. Chen, J. Hu, Exact mapping between classical and topological orders in two-dimensional spin systems, *Phys. Rev. B* 76 (2007) 193101. doi:10.1103/PhysRevB.76.193101.
URL <https://link.aps.org/doi/10.1103/PhysRevB.76.193101>
- [32] H.-D. Chen, Z. Nussinov, Exact results of the kitaev model on a hexagonal lattice: spin states, string and brane correlators, and anyonic excitations, *Journal of Physics A: Mathematical and Theoretical* 41 (7) (2008) 075001. doi:10.1088/1751-8113/41/7/075001.
URL <https://doi.org/10.1088/1751-8113/41/7/075001>
- [33] E. Cobanera, G. Ortiz, Z. Nussinov, Unified approach to quantum and classical dualities, *Phys. Rev. Lett.* 104 (2010) 020402. doi:10.1103/PhysRevLett.104.020402.
URL <https://link.aps.org/doi/10.1103/PhysRevLett.104.020402>
- [34] E. Cobanera, G. Ortiz, Z. Nussinov, The bond-algebraic approach to dualities, *Advances in Physics* 60 (5) (2011) 679–798. doi:10.1080/00018732.2011.619814.

- URL <https://doi.org/10.1080/00018732.2011.619814>
- [35] Z. Nussinov, G. Ortiz, E. Cobanera, Arbitrary dimensional majorana dualities and architectures for topological matter, *Phys. Rev. B* 86 (2012) 085415. doi:10.1103/PhysRevB.86.085415.
URL <https://link.aps.org/doi/10.1103/PhysRevB.86.085415>
- [36] S. B. Bravyi, A. Y. Kitaev, Fermionic quantum computation, *Annals of Physics* 298 (1) (2002) 210–226. doi:10.1006/aphy.2002.6254.
URL <https://www.sciencedirect.com/science/article/pii/S0003491602962548>
- [37] M. Levin, X.-G. Wen, Fermions, strings, and gauge fields in lattice spin models, *Phys. Rev. B* 67 (24) (2003) 245316.
URL <https://link.aps.org/doi/10.1103/PhysRevB.67.245316>
- [38] F. Verstraete, J. I. Cirac, Mapping local hamiltonians of fermions to local hamiltonians of spins, *Journal of Statistical Mechanics: Theory and Experiment* 2005 (09) (2005) P09012–P09012. doi:10.1088/1742-5468/2005/09/p09012.
URL <https://doi.org/10.1088/1742-5468/2005/09/p09012>
- [39] R. C. Ball, Fermions without fermion fields, *Phys. Rev. Lett.* 95 (2005) 176407. doi:10.1103/PhysRevLett.95.176407.
URL <https://link.aps.org/doi/10.1103/PhysRevLett.95.176407>
- [40] D. Gaiotto, A. Kapustin, Spin tqfts and fermionic phases of matter, *International Journal of Modern Physics A* 31 (28n29) (2016) 1645044. arXiv:<https://doi.org/10.1142/S0217751X16450445>, doi:10.1142/S0217751X16450445.
URL <https://doi.org/10.1142/S0217751X16450445>
- [41] Y.-A. Chen, A. Kapustin, Đ. Radičević, Exact bosonization in two spatial dimensions and a new class of lattice gauge theories, *Ann. Phys.* 393 (2018) 234–253.
URL <https://linkinghub.elsevier.com/retrieve/pii/S0003491618300873>
- [42] D. Radicevic, Spin structures and exact dualities in low dimensions (2018). doi:10.48550/ARXIV.1809.07757.
URL <https://arxiv.org/abs/1809.07757>
- [43] Y.-A. Chen, Exact bosonization in arbitrary dimensions, *Phys. Rev. Research* 2 (2020) 033527. doi:10.1103/PhysRevResearch.2.033527.
URL <https://link.aps.org/doi/10.1103/PhysRevResearch.2.033527>
- [44] U. Borla, B. Jeevanesan, F. Pollmann, S. Moroz, Quantum phases of two-dimensional \mathbb{Z}_2 gauge theory coupled to single-component fermion matter, *Phys. Rev. B* 105 (2022) 075132. doi:10.1103/PhysRevB.105.075132.
URL <https://link.aps.org/doi/10.1103/PhysRevB.105.075132>
- [45] A. Mesaros, Y. Ran, Classification of symmetry enriched topological phases with exactly solvable models, *Phys. Rev. B* 87 (2013) 155115. doi:10.1103/PhysRevB.87.155115.
URL <https://link.aps.org/doi/10.1103/PhysRevB.87.155115>
- [46] P. Rao, I. Sodemann, Theory of weak symmetry breaking of translations in \mathbb{Z}_2 topologically ordered states and its relation to topological superconductivity from an exact lattice \mathbb{Z}_2 charge-flux attachment, *Phys. Rev. Research* 3 (2) (2021) 023120.
URL <https://link.aps.org/doi/10.1103/PhysRevResearch.3.023120>
- [47] X.-Y. Song, T. Senthil, Translation-enriched \mathbb{Z}_2 spin liquids and topological vison bands: Possible application to α - RuCl_3 (2022). doi:10.48550/ARXIV.2206.14197.
URL <https://arxiv.org/abs/2206.14197>
- [48] S.-P. Kou, M. Levin, X.-G. Wen, Mutual chern-simons theory for \mathbb{Z}_2 topological order, *Phys. Rev. B* 78 (2008) 155134. doi:10.1103/PhysRevB.78.155134.
URL <https://link.aps.org/doi/10.1103/PhysRevB.78.155134>
- [49] S.-P. Kou, X.-G. Wen, Translation-symmetry-protected topological orders in quantum spin systems, *Phys. Rev. B* 80 (2009) 224406. doi:10.1103/PhysRevB.80.224406.
URL <https://link.aps.org/doi/10.1103/PhysRevB.80.224406>
- [50] S. Ryu, A. P. Schnyder, A. Furusaki, A. W. W. Ludwig, Topological insulators and superconductors:

- tenfold way and dimensional hierarchy, *New Journal of Physics* 12 (6) (2010) 065010. doi:10.1088/1367-2630/12/6/065010.
 URL <https://doi.org/10.1088/1367-2630/12/6/065010>
- [51] M. Sato, S. Fujimoto, Existence of majorana fermions and topological order in nodal superconductors with spin-orbit interactions in external magnetic fields, *Phys. Rev. Lett.* 105 (2010) 217001. doi:10.1103/PhysRevLett.105.217001.
 URL <https://link.aps.org/doi/10.1103/PhysRevLett.105.217001>
- [52] S.-P. Kou, X.-G. Wen, Translation-invariant topological superconductors on a lattice, *Phys. Rev. B* 82 (2010) 144501. doi:10.1103/PhysRevB.82.144501.
 URL <https://link.aps.org/doi/10.1103/PhysRevB.82.144501>
- [53] M. Sato, Topological odd-parity superconductors, *Phys. Rev. B* 81 (2010) 220504. doi:10.1103/PhysRevB.81.220504.
 URL <https://link.aps.org/doi/10.1103/PhysRevB.81.220504>
- [54] A. M. Essin, M. Hermele, Classifying fractionalization: Symmetry classification of gapped \mathbb{Z}_2 spin liquids in two dimensions, *Phys. Rev. B* 87 (2013) 104406. doi:10.1103/PhysRevB.87.104406.
 URL <https://link.aps.org/doi/10.1103/PhysRevB.87.104406>
- [55] X.-L. Qi, A new class of $(2 + 1)$ -dimensional topological superconductors with \mathbb{Z}_8 topological classification, *New Journal of Physics* 15 (6) (2013) 065002. doi:10.1088/1367-2630/15/6/065002.
 URL <https://doi.org/10.1088/1367-2630/15/6/065002>
- [56] H. Yao, S. Ryu, Interaction effect on topological classification of superconductors in two dimensions, *Phys. Rev. B* 88 (2013) 064507. doi:10.1103/PhysRevB.88.064507.
 URL <https://link.aps.org/doi/10.1103/PhysRevB.88.064507>
- [57] C. Wang, T. Senthil, Interacting fermionic topological insulators/superconductors in three dimensions, *Phys. Rev. B* 89 (2014) 195124. doi:10.1103/PhysRevB.89.195124.
 URL <https://link.aps.org/doi/10.1103/PhysRevB.89.195124>
- [58] M. A. Metlitski, L. Fidkowski, X. Chen, A. Vishwanath, Interaction effects on 3d topological superconductors: surface topological order from vortex condensation, the 16 fold way and fermionic kramers doublets (2014). doi:10.48550/ARXIV.1406.3032.
 URL <https://arxiv.org/abs/1406.3032>
- [59] S. Ono, H. C. Po, H. Watanabe, Refined symmetry indicators for topological superconductors in all space groups, *Science Advances* 6 (18) (2020) eaaz8367. doi:10.1126/sciadv.aaz8367.
 URL <https://www.science.org/doi/abs/10.1126/sciadv.aaz8367>
- [60] M. Geier, P. W. Brouwer, L. Trifunovic, Symmetry-based indicators for topological bogoliubov–de gennes hamiltonians, *Phys. Rev. B* 101 (2020) 245128. doi:10.1103/PhysRevB.101.245128.
 URL <https://link.aps.org/doi/10.1103/PhysRevB.101.245128>
- [61] S. Ono, H. C. Po, K. Shiozaki, \mathbb{Z}_2 -enriched symmetry indicators for topological superconductors in the 1651 magnetic space groups, *Phys. Rev. Research* 3 (2021) 023086. doi:10.1103/PhysRevResearch.3.023086.
 URL <https://link.aps.org/doi/10.1103/PhysRevResearch.3.023086>
- [62] S. C. Zhang, T. H. Hansson, S. Kivelson, Effective-field-theory model for the fractional quantum hall effect, *Phys. Rev. Lett.* 62 (1989) 82–85. doi:10.1103/PhysRevLett.62.82.
 URL <https://link.aps.org/doi/10.1103/PhysRevLett.62.82>
- [63] N. Read, Order parameter and ginzburg-landau theory for the fractional quantum hall effect, *Phys. Rev. Lett.* 62 (1989) 86–89. doi:10.1103/PhysRevLett.62.86.
 URL <https://link.aps.org/doi/10.1103/PhysRevLett.62.86>
- [64] Z. F. Ezawa, A. Iwazaki, Chern-simons gauge theories for the fractional-quantum-hall-effect hierarchy and anyon superconductivity, *Phys. Rev. B* 43 (1991) 2637–2641. doi:10.1103/PhysRevB.43.2637.
 URL <https://link.aps.org/doi/10.1103/PhysRevB.43.2637>
- [65] E. Witten, Three lectures on topological phases of matter, *La Rivista del Nuovo Cimento* 39 (7) (2016) 313–370. doi:10.1393/ncr/i2016-10125-3.
- [66] C. Chen, P. Rao, I. Sodemann, Berry phases of vison transport in F_2 topologically ordered states

- from exact fermion-flux lattice dualities, *Phys. Rev. Research* 4 (2022) 043003. doi:10.1103/PhysRevResearch.4.043003.
URL <https://link.aps.org/doi/10.1103/PhysRevResearch.4.043003>
- [67] O. Pozo, P. Rao, C. Chen, I. Sodemann, Anatomy of \mathbb{Z}_2 fluxes in anyon fermi liquids and bose condensates, *Phys. Rev. B* 103 (3) (2021) 035145.
URL <https://link.aps.org/doi/10.1103/PhysRevB.103.035145>
- [68] X.-G. Wen, Quantum orders in an exact soluble model, *Phys. Rev. Lett.* 90 (2003) 016803. doi:10.1103/PhysRevLett.90.016803.
URL <https://link.aps.org/doi/10.1103/PhysRevLett.90.016803>
- [69] H. Bombin, Topological order with a twist: Ising anyons from an abelian model, *Phys. Rev. Lett.* 105 (2010) 030403. doi:10.1103/PhysRevLett.105.030403.
URL <https://link.aps.org/doi/10.1103/PhysRevLett.105.030403>
- [70] G. Y. Cho, Y.-M. Lu, J. E. Moore, Gapless edge states of background field theory and translation-symmetric \mathbb{Z}_2 spin liquids, *Phys. Rev. B* 86 (2012) 125101. doi:10.1103/PhysRevB.86.125101.
URL <https://link.aps.org/doi/10.1103/PhysRevB.86.125101>
- [71] J. Yu, X.-H. Zhang, S.-P. Kou, Majorana edge states for \mathbb{Z}_2 topological orders of the wen plaquette and toric code models, *Phys. Rev. B* 87 (2013) 184402. doi:10.1103/PhysRevB.87.184402.
URL <https://link.aps.org/doi/10.1103/PhysRevB.87.184402>
- [72] P. M. Tam, C. L. Kane, Nondiagonal anisotropic quantum hall states, *Phys. Rev. B* 103 (2021) 035142. doi:10.1103/PhysRevB.103.035142.
URL <https://link.aps.org/doi/10.1103/PhysRevB.103.035142>
- [73] A. A. Abrikosov, On the Magnetic properties of superconductors of the second group, *Sov. Phys. JETP* 5 (1957) 1174–1182.
- [74] V. L. Berezinskii, Destruction of Long-range Order in One-dimensional and Two-dimensional Systems having a Continuous Symmetry Group I. Classical Systems, *Sov. Phys. JETP* 32 (1971) 493.
- [75] V. L. Berezinskii, Destruction of Long-range Order in One-dimensional and Two-dimensional Systems Possessing a Continuous Symmetry Group. II. Quantum Systems, *Sov. Phys. JETP* 34 (1972) 610.
- [76] J. M. Kosterlitz, D. J. Thouless, Ordering, metastability and phase transitions in two-dimensional systems, *Journal of Physics C: Solid State Physics* 6 (7) (1973) 1181–1203. doi:10.1088/0022-3719/6/7/010.
URL <https://doi.org/10.1088/0022-3719/6/7/010>
- [77] L. Fidkowski, A. Kitaev, Effects of interactions on the topological classification of free fermion systems, *Phys. Rev. B* 81 (2010) 134509. doi:10.1103/PhysRevB.81.134509.
URL <https://link.aps.org/doi/10.1103/PhysRevB.81.134509>
- [78] A. M. Turner, F. Pollmann, E. Berg, Topological phases of one-dimensional fermions: An entanglement point of view, *Phys. Rev. B* 83 (2011) 075102. doi:10.1103/PhysRevB.83.075102.
URL <https://link.aps.org/doi/10.1103/PhysRevB.83.075102>
- [79] L. Fidkowski, A. Kitaev, Topological phases of fermions in one dimension, *Phys. Rev. B* 83 (2011) 075103. doi:10.1103/PhysRevB.83.075103.
URL <https://link.aps.org/doi/10.1103/PhysRevB.83.075103>
- [80] Y.-Z. You, Z. Wang, J. Oon, C. Xu, Topological number and fermion green’s function for strongly interacting topological superconductors, *Phys. Rev. B* 90 (2014) 060502. doi:10.1103/PhysRevB.90.060502.
URL <https://link.aps.org/doi/10.1103/PhysRevB.90.060502>
- [81] S. Ryu, S.-C. Zhang, Interacting topological phases and modular invariance, *Phys. Rev. B* 85 (2012) 245132. doi:10.1103/PhysRevB.85.245132.
URL <https://link.aps.org/doi/10.1103/PhysRevB.85.245132>
- [82] Z.-C. Gu, M. Levin, Effect of interactions on two-dimensional fermionic symmetry-protected topological phases with \mathbb{Z}_2 symmetry, *Phys. Rev. B* 89 (2014) 201113. doi:10.1103/PhysRevB.89.201113.
URL <https://link.aps.org/doi/10.1103/PhysRevB.89.201113>
- [83] Y.-M. Lu, A. Vishwanath, Classification and properties of symmetry-enriched topological phases:

- Chern-simons approach with applications to \mathbb{Z}_2 spin liquids, *Phys. Rev. B* 93 (2016) 155121. doi:10.1103/PhysRevB.93.155121.
 URL <https://link.aps.org/doi/10.1103/PhysRevB.93.155121>
- [84] R. S. K. Mong, J. H. Bardarson, J. E. Moore, Quantum transport and two-parameter scaling at the surface of a weak topological insulator, *Phys. Rev. Lett.* 108 (2012) 076804. doi:10.1103/PhysRevLett.108.076804.
 URL <https://link.aps.org/doi/10.1103/PhysRevLett.108.076804>
- [85] Z. Ringel, Y. E. Kraus, A. Stern, Strong side of weak topological insulators, *Phys. Rev. B* 86 (2012) 045102. doi:10.1103/PhysRevB.86.045102.
 URL <https://link.aps.org/doi/10.1103/PhysRevB.86.045102>
- [86] T. Morimoto, A. Furusaki, Stability of surface states of weak \mathbb{Z}_2 topological insulators and superconductors, *Phys. Rev. B* 89 (2014) 035117. doi:10.1103/PhysRevB.89.035117.
 URL <https://link.aps.org/doi/10.1103/PhysRevB.89.035117>
- [87] A. Kapustin, L. Fidkowski, Local commuting projector hamiltonians and the quantum hall effect, *Commun. Math. Phys.* 373 (2) (2020) 763–769.
 URL <https://doi.org/10.1007/s00220-019-03444-1>
- [88] D. A. Ivanov, Non-abelian statistics of half-quantum vortices in p -wave superconductors, *Phys. Rev. Lett.* 86 (2001) 268–271. doi:10.1103/PhysRevLett.86.268.
 URL <https://link.aps.org/doi/10.1103/PhysRevLett.86.268>
- [89] G. E. Volovik, *The Universe in a Helium Droplet*, Oxford University Press, 2009. doi:10.1093/acprof:oso/9780199564842.001.0001.
 URL <https://doi.org/10.1093/acprof:oso/9780199564842.001.0001>
- [90] K. Kawagoe, M. Levin, Microscopic definitions of anyon data, *Phys. Rev. B* 101 (11) (2020) 115113.
 URL <https://link.aps.org/doi/10.1103/PhysRevB.101.115113>
- [91] P. Fendley, Free parafermions, *Journal of Physics A: Mathematical and Theoretical* 47 (7) (2014) 075001. doi:10.1088/1751-8113/47/7/075001.
 URL <https://doi.org/10.1088/1751-8113/47/7/075001>
- [92] E. Cobanera, G. Ortiz, Fock parafermions and self-dual representations of the braid group, *Phys. Rev. A* 89 (2014) 012328. doi:10.1103/PhysRevA.89.012328.
 URL <https://link.aps.org/doi/10.1103/PhysRevA.89.012328>
- [93] H. N. V. Temperley, E. H. Lieb, S. F. Edwards, Relations between the ‘percolation’ and ‘colouring’ problem and other graph-theoretical problems associated with regular planar lattices: some exact results for the ‘percolation’ problem, *Proceedings of the Royal Society of London. A. Mathematical and Physical Sciences* 322 (1549) (1971) 251–280. arXiv:<https://royalsocietypublishing.org/doi/pdf/10.1098/rspa.1971.0067>, doi:10.1098/rspa.1971.0067.
 URL <https://royalsocietypublishing.org/doi/abs/10.1098/rspa.1971.0067>
- [94] P. Fendley, Parafermionic edge zero modes in \mathbb{Z}_n -invariant spin chains, *Journal of Statistical Mechanics: Theory and Experiment* 2012 (11) (2012) P11020. doi:10.1088/1742-5468/2012/11/p11020.
 URL <https://doi.org/10.1088/1742-5468/2012/11/p11020>
- [95] A. S. Jermyn, R. S. K. Mong, J. Alicea, P. Fendley, Stability of zero modes in parafermion chains, *Phys. Rev. B* 90 (2014) 165106. doi:10.1103/PhysRevB.90.165106.
 URL <https://link.aps.org/doi/10.1103/PhysRevB.90.165106>
- [96] A. M. Tsvelik, Integrable model with parafermion zero energy modes, *Phys. Rev. Lett.* 113 (2014) 066401. doi:10.1103/PhysRevLett.113.066401.
 URL <https://link.aps.org/doi/10.1103/PhysRevLett.113.066401>
- [97] G. Giuliani, G. Vignale, *Quantum theory of the electron liquid*, Cambridge university press, 2005.
- [98] B. Dubrovin, A. Fomenko, S. Novikov, *Modern Geometry— Methods and Applications: Part II: The Geometry and Topology of Manifolds*, Graduate Texts in Mathematics, Springer New York, 1985.
- [99] L. M. Robledo, Sign of the overlap of hartree-fock-bogoliubov wave functions, *Phys. Rev. C* 79 (2009) 021302. doi:10.1103/PhysRevC.79.021302.
 URL <https://link.aps.org/doi/10.1103/PhysRevC.79.021302>

[100] F. Berezin, The Method of Second Quantization, Academic Press, 1966.

Versicherung

Hiermit versichere ich, Peng Rao, dass ich die vorliegende Arbeit ohne unzulässige Hilfe Dritter und ohne Benutzung anderer als der angegebenen Hilfsmittel angefertigt habe; die aus fremden Quellen direkt oder indirekt übernommenen Gedanken sind als solche kenntlich gemacht. Die Arbeit wurde bisher weder im Inland noch im Ausland in gleicher oder ähnlicher Form einer anderen Prüfungsbehörde vorgelegt. Diese Arbeit wurde unter der wissenschaftlichen Betreuung von Prof. Inti Sodemann am Max-Planck- Institut für Physik komplexer Systeme in Dresden angefertigt. Ich erkläre hiermit, dass keine früheren erfolgreichen Promotionsverfahren stattgefunden haben. Ich erkenne die Promotionsordnung der Bereich Mathematik und Naturwissenschaften der Technische Universität Dresden an.

Unterschrift

Dresden, September 2022.